A COMPUTATIONAL IMPLEMENTATION OF DESIGN SENSITIVITY ANALYSIS AND STRUCTURAL OPTIMISATION

A dissertation submitted
to

The Department of
MATHEMATICS and APPLIED MATHEMATICS
of
the University of Cape Town

in fulfillment of the requirements for the degree
of

MASTER OF SCIENCE

in

APPLIED MATHEMATICS

By
André Smith Bothma
March 1996

Summary

In the field of computational mechanics, increases in computing power and enhancements in material and kinematic models have enhanced the feasibility of performing structural design optimisation for a wide range of applications. The work presented here was motivated by the current groundswell of research effort in computational optimisation.

Design Sensitivity Analysis (DSA) crucially underpins much of structural optimisation and, as such, is focussed on more intently than the optimisation theory itself: various approaches to the Direct Differentiation Method (DDM) DSA procedure are investigated and computationally implemented. The procedures implemented were chosen so as to involve a range of important issues in computational sensitivity analysis, particularly

- Shape and non-shape sensitivity analysis,
- Total and Updated Lagrange-based DSA,
- DSA of displacement and non-displacement based response functionals,
- Multiparameter DSA.
- DSA for large strain behaviour

The primary objectives of this thesis are:

I. Development of a design sensitivity formulation which, when discretised, resembles the standard displacement based kinematic element formulation, thus enabling the implementation of design sensitivity analysis in established Finite Element Analysis (FEA) codes as a 'pseudo'-element routine.

II. Implemention of several design sensitivity formulations and structural optimisation into the FEA code ABAQUS as a verification of the first objective.

Numerical results provided in this work demonstrate the successful completion of the above-mentioned objectives. The *discretised* DSA formulations presented, as

well as the 'pseudo'-element approach adopted, particularly in the case of *shape* DSA, are entirely original. To the best of the author's knowledge, DSA and DSA-based structural optimisation had never before been attempted with ABAQUS. The research conducted here lays the foundation for potentially very fruitful future work.

Acknowledgements

With any time consuming and labourious endeavour one inevitably accrues debts, financial and otherwise, for support provided. It is with full understanding of the complex set of conditions which have to be maintained in order to make work like this possible that I wish to express my gratitude

- To Dr. Jacek Ronda (Dr.Sc.) for supervising this thesis.
- To the FRD (Foundation for Research Development) and CERECAM (FRD / UCT Centre for Research into Computational and Applied Mechanics) for the provision of financial support and computational facilities.
- To all the people who made the system work the way it should in times of need, particularly Mike Eastman and Prof. B.D. Reddy.
- To colleagues, comrades-in-arms and friends in the Mathematics and Applied Mathematics department, too numerous to mention: the last couple of years have been the most memorable yet.
- Finally, to Pam, for everything.

Contents

1 Introduction **1**

2 Structural Analysis **15**

2.1 Variational Formulation 15

2.1.1 First Principles: The displacement-based equilibrium formulation 15

2.1.2 Kinematic Nonlinearity 18

2.2 Discretisation 25

3 Design Sensitivity Analysis **34**

3.1 Variational Formulation 34

3.1.1 General Ideas on the formulation of Design Sensitivity Analysis 34

3.1.2 'Intuitive' Approach 38

3.1.3 'Rigorous' Approach 38

3.1.4 Stress Sensitivity Analysis 42

3.2 Discretisation 43

3.2.1 'Intuitive' Non-shape DSA 43

3.2.2 'Rigorous' Non-shape DSA 44

3.2.3 'Rigorous' Shape DSA 45

3.2.4 Stress DSA 47

4 Structural Optimisation 51

4.1 Structural Optimisation, Design Sensitivity and Finite Element Analysis 51

4.1.1 Structural Optimisation with the PLBA RQP 52

4.1.2 The PLBA RQP method algorithm 58

5 Implementing DSA and Optimisation into ABAQUS 59

6 Numerical Results 67

6.1 The 3-bar truss 67

6.2 The 10-bar truss 75

6.3 The 200-bar truss 84

6.4 The 25-bar pylon truss 95

6.5 Optimising the 25-bar pylon truss 109

7 Conclusion 114

7.1 Research Achievements 114

7.2 Results Discussion 115

7.2.1 Design Sensitivity Analysis 115

7.2.2 Structural Optimisation 116

7.3 Future Research 117

Nomenclature

Abbreviation	Definition	First Defined
AVM/ASM	Adjoint Variable/System Method	p. 6
BEM	Boundary Element Method	p. 2
BFGS	Broyden-Fletcher-Goldfarb-Shanno solution procedure	p. 53
DDM	Direct Differentiation Method	p. 1
DSA	Design Sensitivity Analysis	p. 1
DSC	Design Sensitivity Coefficient	p. 4
FDM	Finite Difference Method	p. 6
FEA	Finite Element Analysis	p. 1
FEM	Finite Element Method	p. 1
MP	Mathematical Programming	p. 9
NEL	Number of Elements	p. 111
NF	Number of Function calls	p. 110
NI	Number of Iterations	p. 110
NLP	Nonlinear Programming	p. 11
N-R	Newton-Raphson iterative solution procedure	p. 21
PLBA	Pshenichny-Lim-Belegundu-Arora	p. 2
QP	Quadratic Programming	p. 53
QPP	Quadratic Programming Problem	p. 53
RQP	Recursive Quadratic Programming	p. 2
SQP	Successive Quadratic Programming	p. 11
TL	Total Lagrange	p. 13
UL	Updated Lagrange	p. 13

In generating results for structural analysis, DSA and design optimisation, the units employed for the various example problems correspond to that employed in the *source* literature. The following table provides the conversion factors.

Imperial Unit	Definition	Converted to SI
1 kip	1000 lbf	4.4482×10^{3} N
1 ksi	1000 psi	6.8948×10^{3} kPa
1 inch		2.5400×10^{-2} m

Symbol and Definition		First Defined/Used
${}^{r}\square$	Value of quantity $\square$ defined i.t.o. the parent frame C_r	p. 26
${}^{t}\square$	Value of quantity $\square$ at time $\boldsymbol{t}$, defined i.t.o. frame ${}^{t}C$	p. 18
${}_{t}\square$	Incremental quantity $\square$ defined i.t.o. frame ${}^{t}C$	p. 19
${}_{t}^{t+\Delta t}\square$	Quantity $\square$ at $\boldsymbol{t}+\boldsymbol{\Delta t}$, defined i.t.o. frame ${}^{t}C$	p. 19
$\square'$	Quantity $\square$ defined i.t.o. frame C_0'	p. 26
$\square^{\star}$	Quantity $\square$ defined i.t.o. frame $C_0^{\star}$	p. 41
$\hat{\square}$	Quantity $\square$ is *shape* design parameter, $\boldsymbol{h}$, dependent	p. 41
$\square^{(k)}$	k^{th} iterative estimate of quantity $\square$	p. 21
$\square_{xx}$	$\equiv \square_{11}$	p. 25
$\square_I$	I^{th} element discretisation of quantity $\square$	p. 37
$\nabla_A \square$	Gradient of quantity $\square$ w.r.t. cross-sectional area A	p. 43
$\delta\square$	Variation of expression $\square$	p. 17
$\overline{\delta}\square$	Full design parameter differentiation operator	p. 36
$\overline{\overline{\delta}}\square$	Explicit design parameter differentiation operator	p. 36
$\tilde{\delta}\square$	Implicit design parameter differentiation operator	p. 36
A	Truss cross-sectional area	p. 28
α	Stepsize parameter	p. 55
C_0'	Local, or principal, frame	p. 26
C_r	Natural, or parent, frame	p. 26
${}^{t}C$, C_t	Configuration/frame at time $\boldsymbol{t}$	p. 19
$C_0^{\star}$	*Unperturbed* 'initial' global frame, cf. shape DSA	p. 41
E	Young's modulus	p. 25
f	Cost, or objective, functional	p. 34
$F(\boldsymbol{u},\boldsymbol{b})$	Equilibrium expression	p. 36
φ	Rotation angle defined in Fig.[2.4]	p. 27
$\hat{\varphi}$	Iterative rotation angle	p. 31
Φ	Rotational multiplicative factor	p. 32
Γ_u	Surface of prescribed displacement	p. 16
Γ_t	Surface of prescribed traction	p. 16
I_1, I_2	Constraint sets	p. 53
I_ε	*Active* constraints set	p. 53
J, J_Γ	Jacobian integration factors	p. 26
L	Truss element length	p. 26
$P(\boldsymbol{b},\boldsymbol{\mu})$	Unconstrained Lagrange function	p. 52
$Q(\boldsymbol{u},\boldsymbol{b})$	Internal load expression	p. 36
θ	Rotation angle defined in Fig.[2.4]	p. 27
$\hat{\theta}$	Iterative rotation angle	p. 31
$\Re$	External load expression	p. 18
ρ	Material density	p. 16
S	Body surface area	p. 16
t	Time	p. 18
V	Body volume	p. 17
Ψ	General design parameter dependent functional	p. 34

Symbol and Definition		First Defined/Used
a	Linear acceleration vector	p. 16
b	Design parameter vector	p. 27
$\overline{b}$	Optimal design parameter vector	p. 55
C	Material constitutive tensor	p. 20
d	Global truss nodal displacement vector	p. 28
e	Infinitesimal strain tensor/vector	p. 17
ϵ	Green-Lagrange strain tensor/vector	p. 18
f	Body force vector	p. 16
g	Constraint functions vector	p. 34
G^0, G^i	Cost and constraint function sensitivity vectors	p. 54
h	*Shape* design parameter vector	p. 41
η	Nonlinear part of Green-Lagrange strain tensor/vector	p. 20
K	Stiffness matrix	p. 29
K'	'Pseudo'-stiffness matrix	p. 44
$\mathcal{K}$	TL local frame internal load matrix	p. 29
$\overline{\mathcal{K}}$	$\equiv \nabla_{0_A} \mathcal{K}$	p. 43
$\mathcal{L}$	UL local frame internal load matrix	p. 33
$\overline{\mathcal{L}}$	$\equiv \nabla_{0_A} \mathcal{L}$	p. 43
μ	Lagrange multipliers	p. 55
n	Body normal vector	p. 16
N	Shape function matrix	p. 27
$N_{\square,\square}$	Shape function derivative vector	p. 28
$\aleph$	Shape function derivative factor	p. 28
$\dot{\aleph}$	Shape function derivative factor	p. 28
$\ddot{\aleph}$	Shape function derivative factor	p. 29
$\overline{\aleph}$	Shape function derivative factor	p. 32
p	Vector direction of design parameter change	p. 53
R'	'Pseudo'-external load vector	p. 44
S	2^{nd} Piola-Kirchhoff stress tensor/vector	p. 18
t	Traction load vector	p. 16
T	Coordinate transformation matrix	p. 27
$\mathcal{T}$	Transformation matrix component	p. 27
τ	Cauchy stress tensor/vector	p. 16
u	Displacement vector	p. 17
W	Hessian matrix for P	p. 57
x	Coordinate vector	p. 16
${}^{t+\Delta t}_{t}x_{i,j}$	$\equiv \frac{\partial^{t+\Delta t}x_i}{\partial^t x_j}$	p. 19
X	Global nodal coordinate vector of a truss element	p. 27
$\mathcal{X}$	Coordinate transformation factor	p. 47
X'	Local nodal coordinate vector of a truss element	p. 27
ξ	Natural, or parent, frame coordinate vector	p. 26

Chapter 1

Introduction

Background

In industry and manufacturing, structural design specifications commonly demand some manner of optimisation, e.g. for the purposes of material cost reduction or mass minimisation. The optimisation procedure is usually constrained in terms of structural response limits[1] imposed for a whole range of realistic loading conditions.

The range of approaches to the solution of Structural Optimisation problems, both computational and analytical, are many and varied. In the research presented here a computational structural optimisation procedure is formulated and implemented in conjunction with the Finite Element Analysis (FEA) code ABAQUS; the procedure consists of three discrete components:

- The kinematic and material formulation describes the structural behaviour subject to loads and boundary conditions. The Finite Element Method (FEM) is adopted as a numerical solution procedure.
- Design Sensitivity Analysis (DSA) solves for the sensitivity matrices

$$\nabla_{\boldsymbol{b}} \boldsymbol{\tau} \equiv \frac{d\boldsymbol{\tau}}{d\boldsymbol{b}}, \nabla_{\boldsymbol{b}} \boldsymbol{\varepsilon} \equiv \frac{d\boldsymbol{\varepsilon}}{d\boldsymbol{b}} \text{ and } \nabla_{\boldsymbol{b}} \boldsymbol{u} \equiv \frac{d\boldsymbol{u}}{d\boldsymbol{b}},$$

  which express the influence of design parameters $\boldsymbol{b}$ on structural response. Most optimisation procedures rely crucially on the sensitivity matrices in order to obtain an optimal value. Various approaches to the Direct Differentiation Method (DDM) are utilised to perform both *shape* and *non-shape* sensitivity analysis.

[1] Defined in terms of displacement, strain and stress.

- A nonlinear optimisation model, designed to interface with ABAQUS, utilises the sensitivity matrices to iteratively calculate improved optimal values of the design parameters $\boldsymbol{b}$, subject to the constraints imposed. The Pshenichny-Lim-Belegundu-Arora recursive quadratic programming (PLBA RQP) method is employed for this purpose.

Although computational structural optimisation is still in its infancy, innovation in computer technology and recent developments in computational mechanics are rapidly enabling the analysis and structural optimisation of complex large-scale applications.

Mechanics, DSA and Structural Optimisation

Research focused on the optimisation of linear structures, as a specific field of interest in engineering mechanics, span almost thirty years. The majority of linear optimisation problems could be solved purely analytically or with relatively simple computational procedures. For the analysis of applications with nonlinearity, however, the computational approach is vastly more efficient. With the introduction of high-speed, affordable computing power in the early 1970's numerical optimisation of complex structures with nonlinear behavior started becoming increasingly viable.

From the start of the 1980's researchers [15] took advantage of the advances made in computational structural analysis and proceeded to implement structural optimisation in conjunction with various discrete (numerical) procedures, e.g. Rayleigh-Ritz, Galerkin, the FEM and the BEM. The isoparametric formulation (FEM) is especially convenient for the purposes of performing DSA as the interval of integration is independent of the design variable [14], i.e. even for *shape* DSA the parent element formulation is independent of the design parameters. Yang and Botkin[40] demonstrated the equivalence of the FEM and variational description of DSA for linear problems; this equivalence can also be demonstrated for nonlinear problems [35].

The initial applications of the FEM to structural optimisation were somewhat unrealistic: only non-shape DSA was utilised and the kinematic and material models were mostly linear with no provision being made for more sophisticated path-dependent material behaviour. Later the investigation of DSA and structural optimisation in conjunction with FEM methodologies capable of dealing with full material and kinematic nonlinearity started gaining ground. Thus, in contrast to the wealth of literature available for structural optimisation of linearly behaved structures, research in the domain of nonlinearity - particularly for material nonlinearity - is relatively young and not characterised by a lack of controversy.

The increasing application of DSA and structural optimisation to a wide variety of large scale real-world problems necessitated the development of optimisation models

capable of more accurate behavior. Much of this development is focused on more complex nonlinear material models which include path-dependent, and often also rate-dependent, behavior. Additionally, a substantial portion of the literature now exclusively focuses on large deformation scenarios, i.e. kinematic nonlinearity with dynamic and static constraints.

Due to the sheer complexity of issues relating to kinematic and material nonlinearity, sensitivity analysis and optimisation, research on the subject has been somewhat incremental. Ohsaki[28] presents a partial review of contemporary developments, particularly in regard to material nonlinearity:

- DSA for nonlinear elasticity was extended to idealised materials with perfectly plastic behavior; Kaneko and Maier[21] discussed the optimum design problem of plastic structures with strain hardening where only monotonic loading was considered.
- Path-independent methods of elasto-plasticity, using only monotonic loading, were investigated by Bendsøe and Sokolowski[6]; no allowance was made for geometric nonlinearity.
- Employing a relatively straightforward piecewise linear constitutive model, Ray et al.[30] pointed out that the yield time of elastic-plastic constitutive models depends on the design parameters.
- Tsay and Arora[35] developed a method which successfully dealt with both path-dependent elastic-plastic material behavior and geometric nonlinearity, with good results.

Considering the effect of the path dependent solution process on DSA is vital in enabling the implementation of materially nonlinear optimisation models. Originally this issue was side-stepped by using nonlinear elasticity or elasto-plasticity without cyclic loading.[2] As a result the DSA formulation for problems with path dependent response is also path dependent. For path independent problems the DSA of the final configuration does not require sensitivity coefficients at any other increment during the load cycle [35][28][36].

A further complexity resulting from the DSA of path-dependent nonlinearity involves the treatment of hardening and the attendant radial-return solution procedures. Kaneko and Maier[21] dealt with the optimal design for linear hardening or non-hardening plastic structures under proportional loading where constitutive law is reversible and path independent. Application to distributed parameter structures with kinematic and/or isotropic hardening using the Von Mises yield condition and

[2]When the material goes into the inelastic range and unloading and reloading of the structure occurs (cyclic loading), the response variables are loading path dependent, i.e. the state of stress in the body depends on the full history of the state variables.

the elastic predictor radial-return method is discussed in [28]. Although isotropic hardening behavior is amenable to DSA, much controversy surrounds the application of DSA to material models involving kinematic hardening.

Rate-dependent material models add substantial complication to the implementation of DSA. The expansiveness of this subject field means that a fixed body of theory for DSA applied to rate-dependent models is not likely to evolve soon. Yet a couple of standard approaches have been successfully applied to rate-dependent inelasticity, viscoelasticity and viscoplasticity. The preferred methods are based on implicit integration schemes. Additionally, some authors have enlisted novel material models in order to simplify the sensitivity analysis process, e.g. the endochronic constitutive model[20].

Performing a non-linear dynamic analysis as part of an automated design procedure, for a material with rate-dependent response, requires efficient techniques for calculating the sensitivity of the non-linear dynamic response to variations in the design variables [24]. For structural analysis, explicit (forward Euler) solution procedures are usually faster than the implicit approach, while definitely lagging in accuracy. In determining the design sensitivity coefficients (DSC's) for applications involving both material and geometrical non-linearities, however, implicit solution procedures are more accurate and efficient [25]. This is a consequence of the fact that for DSA the explicit procedure has to use a small step-size to maintain accuracy and stability.

The implicit solution procedure is based on objective schemes that employ the Jaumann and Green-Naghdi stress rates so as to ensure accurate integration of the constitutive laws. The implicit method, with objective integration, has been applied to a wide range of problems, including hypoelastic and viscoplastic materials [25]. Vidal et al.[37] and Vidal and Haber[36] used implicit schemes to obtain sensitivity coefficients for creep and elasto-plastic materials.

In working with material models with path and time dependency the issue of *consistent* linearisation and its implication for DSA has been voiced by several authors. Vidal[37] mentioned the consistent tangent operator as a requirement for the accurate implementation of creep in order to achieve enhanced accuracy. It has been demonstrated that, should direct differentiation DSA be performed, then an accurate formulation of the DSA procedure demands the use of the consistent tangent modulus, **regardless** of whether the analysis model uses it or not.

Due to the computational costs attendant in implementing a full structural optimisation procedure, especially for complex material nonlinearity cases, the majority of structures considered in literature are composed of one dimensional truss or bar elements. Some work has, however, been done with higher order elements:

- Rodrigues et al.[29] investigated the optimal design of a 2-D linear-elastic solid subject to thermal loads.

- Kulkarni et al.[24] performed material and viscoplastic parameter DSA on the viscoplastic response of thin plate structures subject to in-plane dynamic loading.

Although a wide range of sophisticated DSA and structural optimisation software has been developed in recent years, most of these codes are purpose-built. That is, very specific application orientated preprocessor and solver routines were designed and implemented to support the DSA and optimisation routines. Several authors have investigated the incorporation of sensitivity analysis and structural optimisation into established, usually FEM-based, commercial analysis codes. The implementation of design sensitivity analysis into the FEA code ADINA was investigated by Haririan et al.[14] and Arora et al.[1], amongst others: as is the case with ABAQUS, structural optimisation cannot be included directly into the analysis package - the optimisation module operates in conjunction with the analysis module, i.e. the ADINA solver. The advantages of this approach are obvious: specialised features and facilities included with the analysis codes, e.g. contact procedures, wavefront optimisation and solver routines, do not have to be developed.

Nonlinear kinematic models and sophisticated material behavior, accounting for path and rate dependence, subject to cyclic loading and hardening represents the current state of the art in DSA and structural optimisation literature:

- A DSA method for structures with non-linear piecewise continuously differentiable constitutive equations subject to cyclic loading conditions was presented in [28] by Ohsaki and Arora. Yield time is considered to be a function of design variables. Application to distributed parameter structures with kinematic and/or isotropic hardening is discussed using the Von Mises yield condition and the elastic-predictor radial-return method; geometric nonlinearity is assumed. Large variations in the sensitivity results, and therefore optimal values, result when loads are increased and yield occurs first at different points. Geometric nonlinearity was shown to have a negligible influence. Additionally, path-dependent material behavior causes DSA to be path-dependent, i.e. the DSA model is required to incorporate sensitivity estimates from all the previous time steps.

- Vidal[36] extended previous research done on the sensitivity analysis of systems with creep behavior and time-independent elastoplasticity. The treatment of algorithmic constitutive models is based on implicit integration strategies and return mappings associated with the elastoplastic consistency conditions. Consistent linearisation ensured that the system matrix appearing in the incremental sensitivity equations is identical to the consistent tangent stiffness matrix from the final equilibrium iteration of the time step.

Fundamentals of DSA and Structural Optimisation

Design Sensitivity Analysis

The last 20 years of active research into sensitivity analysis and structural optimisation has produced two primary *analytical* sensitivity analysis methods to the fore, namely the DDM (direct differentiation method) and the AVM/ASM (adjoint variable/system method). Various other methods, e.g. the control volume and material derivative approaches, have been developed but do not appear to have gained the popularity of the ASM or DDM, particularly when used in conjunction with the FEM.

For exceedingly simple structural optimisation problems the FDM (finite difference method) may also be attempted: the FDM is a *numerical* DSA procedure and estimates structural response sensitivities by systematically performing perturbations of the design parameters and observing the changes in the response variables. This method is extremely inefficient when applied to realistic large-scale engineering systems, in addition to becoming significantly inaccurate for a whole range of nonlinear applications. The FDM does, however, fulfill a useful role in enabling a relative straightforward verification of the actual analytical model.

The DDM involves taking variations of the continuum equilibrium equation with regard to the design variables. Often the stiffness matrix of the analysis phase can be used as part of the DDM DSA procedure, thereby greatly increasing the efficiency of the sensitivity analysis phase; this technique is here referred to as the 'intuitive' approach. It has been pointed out in the literature that should the material model require consistent linearisation, then the DDM procedure should utilise the consistent tangent modulus. As mentioned by Kleiber [22], one of the characteristics of the DDM is that the DSA expression is linear in displacement sensitivity and **no** incremental solution procedure is therefore necessary. This holds true for the ASM as well.

The ASM defines adjoint structures whose solutions permit explicit evaluation of the desired sensitivities. Adjoint sensitivity methods have been derived from virtual work methods, techniques based on reciprocal theorems, mutual energy methods and Lagrangian (weighted residual) methods [37]. In practice the ASM is only of benefit in path-independent problems for which the number of design variables is greater than the number of constraints. Therefore the choice between the two approaches depends on the ratio of active constraints and design variables, as well as the relative difficulty in obtaining the adjoint solutions vs. the sensitivity solutions [35]. The ASM is competitive against the DDM for path-independent problems only [22].

The main differences between the ASM and DDM are:

- The DDM is conceptually simpler, and easier to implement, than the ASM. In most instances it is also more efficient.
- The DDM automatically generates sensitivity data for the response fields at every point in the continuum; the information thus obtained enables the generation of sensitivities for any number of performance functionals. In contrast the AVM only generates sensitivity information for an a priori specified set of performance functionals [37]. This difference is crucial for path-dependent problems since the history of calculated sensitivity vectors for every load level needs to be kept in order to calculate the sensitivity at a specific load level - this makes the ASM very tedious to use [35]. Adjoint methods are generally not very well suited for forward-marching, step-by-step methods.

Some work has been done towards formally establishing the theoretical premises for the discretisation of the general DDM and ASM variational formulations [2]. Systematic proofs have been delivered to demonstrate the correctness of the numerical DSA formulations for linear and nonlinear problems.

Calculating the response sensitivities for transient dynamic problems can be shown to be equivalent to the process undertaken in obtaining the sensitivities for path dependent problems - the time history of the sensitivities of the state variables are required in order to calculate sensitivities at a further time t. Ray et al.[30] calculated the derivatives of transient dynamic response variables as a special problem.

Certain optimisation procedures can take advantage of second order sensitivity information so as to accelerate the optimisation process. To this end variational approaches which calculate the first and second order sensitivities of nonlinear systems were investigated in various publications, notably by Mróz, Dems, Haftka and Haug.

Design sensitivity analysis procedures can be categorised depending on the design parameter with regard to which the response variable sensitivities are obtained: shape design parameters refer to variables which affect or determine the design of a structure, e.g. the base area of a pylon, whereas topological design parameters refer to the number of nodes, the types of elements, etc. Material parameters, e.g. Young's modulus and the Poisson ratio, belong to the category of non-shape design parameters. Although the conceptual difference is straightforward to assimilate, the sensitivity analysis procedures for the various categories are radically different.

A popular, 'unified' shape and non-shape DSA formulation based on the mutual Hu-Washizu principle and an Euler-Lagrangian kinematic description was presented by Haber[16]. The 'unified' approach depends crucially on the reference volume concept, thus requiring a Total Lagrangian analysis formulation. This method enables a straightforward integration of the shape DSA procedure into a commercial FEM code. For modeling design optimisation problems the concept of the refer-

ence volume is shown to be equivalent to, and therefore compatible with, the FEM notion of a parent element that is invariant subject to changes in design [8]: the parent element used in the isoparametric mapping can be considered a reference volume. Alternative procedures, eg. domain parametrization and the material derivative approach, have been employed by some authors to perform *shape* sensitivity analysis.

Topological sensitivity analysis is substantially more complex than shape or non-shape DSA and has only recently been rendered practical with the application of the homogenisation method by Bendsøe and Kikuchi[7]. They proposed a generalisation of the topology DSA problem via the introduction of a material distribution model based on a porous medium with periodic microstructure: at every point in space the topological DSA procedure determines the presence (or not) of material. This model allows for the variation in the number and type of the elements used to model the microstructure. The material (homogenised) properties - elastic and thermal expansion coefficients - are computed using the homogenisation method [29]. The model has application to plate and shell reinforcement, natural frequencies control and multiload problems, to mention but a few.

Utilising the basic methodologies described above, variant forms of sensitivity analysis have been applied to problems diversely involving elasto-statics and elasto-dynamics, eigenvalue and natural frequency analysis of beams and plates [37][12], thermal and thermo-mechanical effects, path-dependence, time-dependence, buckling, etc. Generally authors report sizable differences between sensitivity results with and without nonlinear effects.

In addition to applications focused purely on structural optimisation, design sensitivity analysis also plays an important role in a range of other engineering applications, some of which are very rapidly gaining prominence. These applications include reliability analysis, inverse problems and parameter identification problems:

- Sensitivity information gathered from the DSA model may be used to assess the effect of uncertainties in the mathematical model and to predict response variations due to experimental inaccuracies in the design parameters. Research into these aspects extends the sensitivity analysis procedure via the introduction of probability theory and stochastic models; this forms the basis for reliability analysis. Deterministic and stochastic DSA for static and dynamic problems were investigated by Kleiber, Hien and others [18][19][24][17] employing displacement-based FE modelling and a stochastic Hamilton's variational principle.

  For deterministic systems the gradient of the response functional with respect to the design variables is evaluated, whereas the subject of stochastic structural sensitivity analysis is the estimation of probabilistic distributions of this gradient. As a result of the research in [17] a FE code was developed for the

deterministic and stochastic analysis of statics; minimum-weight optimisation; buckling load, eigenpair, forced-vibration and eigenvalue sensitivity analysis; obtaining static and dynamic response sensitivities for truss, beam or shell structures.

- Inverse problems [27] are concerned with the identification of structural parameters. The structural parameters are identified by presetting response variables on the structure boundaries in accordance with data obtained from experimental observations. The objective functional to be minimised is then formulated to be the difference between predicted and measured values of state fields.

Structural Optimisation

The aim of the standard structural optimisation procedures is to optimise a performance functional subject to constraints on stresses and displacements; the structure may be subjected to static or dynamic, monotonic or cyclic loads. Applications include diverse problems in mechanical systems design, kinematic synthesis, shape determination and optimal control systems [34]. Rather than having to laboriously alter and reanalyse structural designs until the structural response matches the design constraints, structural optimisation seeks to automate the process.

Satisfactory structural optimisation crucially depends on four issues [9]:

i. The proper formulation of the optimisation problem.

ii. The robustness, efficiency and accuracy of the optimisation algorithm.

iii. The realism of the structural model that is used.

iv. Efficient structural and sensitivity analysis.

Mathematical programming has been widely adopted as the primary vehicle for structural optimisation [4][9]. Much work has been done in developing design optimisation models based on the standard mathematical programming (MP) techniques. Most of the problems in the MP literature, however, are formulated in terms of explicit functions, are of small size, do not possess a large number of local minima and do not require much effort for function and gradient evaluation, **unlike** optimal structure design applications. In consequence an entire field of optimisation research has come into being, focused on optimisation problems specific to structural design. Design sensitivity analysis is one of the most important bodies of theory developed specifically for the purposes of performing structural optimisation.

Important features in the study of optimal structure design problems are [4]:

- The problems are general - no restriction is placed on the form of the cost and constraint functions.
- The cost and constraint functions usually have an implicit dependence on the design variables.
- Cost and constraint functions evaluation is usually expensive.
- The optimal design problem is usually highly nonlinear and, in general, also non-convex. As a result it can have multiple local minima; globally convergent optimisation procedure are critically important in enabling structural optimisation.
- The problems are typically large; n=50 cost functionals and m=500 constraints is not uncommon.

The iterative approach to structural optimisation has matured since the 1960's and currently considerable research effort is being focused on the optimisation of nonlinear structures - structural optimisation based on nonlinear formulations produces substantially different results to models which employ linearity. Integrating structural optimisation with commercial analysis packages, like ADINA [14], is an additional goal in a significant portion of the publications.

Research has shown that the optimal calculation depends heavily on the number of load increments. Load increment size has a considerable influence on the accuracy of the sensitivity coefficients - the DSC's are on average more sensitive to the size of the load increments than the response variables. Response variables that are good enough for convergence of the analysis procedure may not be accurate enough to serve as sensitivity coefficients.

The methods used in structural optimisation can be broadly categorised into [4]

1. Primal methods, which include recursive quadratic programming (RQP), gradient projection, the reduced gradient method, the method of Bard and Greenstadt, the feasible directions method, an optimality criteria method, sequential linear programming and projection methods.
2. Transformation methods, which include sequential unconstrained minimisation techniques (penalty and barrier functions) and multiplier (or augmented Lagrangian) methods.

An extensive comparative study of nonlinear programming methods for structural optimisation was presented by Belegundu and Arora[32]. In [32] multiplier (i.e.

transformation) methods were argued to be less efficient than direct linearisation (i.e. primal) methods. Enhanced multiplier procedures, like the trust region method, have been introduced to increase the efficiency of the unconstrained optimisation process.

The efficiency and robustness of the quadratic programming methods contribute to the general appeal of the currently popular SQP/RQP (successive/recursive quadratic programming) procedures in the structural optimisation literature. The efficiency and robustness of the SQP/RQP methods hinges on the superlinear and global convergence characteristics of some of the formulations available.[3] The SQP methods are based on a theorem which states that the optimum is the global minimum of a Lagrange function in the subspace of vectors orthogonal to the active constraint gradients or the tangent subspace. The Hessian of the Lagrange function is not calculated explicitly, rather an algorithmic approximation procedure is constructed to update the Hessian of the Lagrange function.

The SQP methods all have the following qualities [34]:

- Global convergence.
- Superlinear convergence of the iterative process near the solution point if step length is unity.
- Use of only first order information.
- Natural suitability to equality and inequality constraints.

Differences which exist between the various SQP techniques are generally a consequence of variations in the definition of the QP subproblem solved at each iteration and the Lagrange descent function used during step-size determination. The performance of the optimisation algorithm can be radically influenced depending on the appropriateness of the SQP method used. Infeasibilty of the QP subproblem and the loss of the local superlinear rate of convergence are some of the major problems faced with the SQP problems.

A particularly efficient and robust method is the PLBA (Pshenichny-Lim-Belegundu-Arora) RQP. The PLBA is based on Pshenichny's descent function, preferred to other standard descent functions like the augmented Lagrangian function used by Schittkowski or a L1 penalty function. The PLBA has the robustness qualities of the Pshenichny method, with increased efficiency: the PLBA is globally convergent,

[3]The SQP/RQP superlinearly convergent solution techniques, employed to solve nonlinear programming (NLP) problems, belong to the class of procedures variously referred to as superlinearly convergent recursive quadratic programming (RQP), projected Lagrangian, successive quadratic programming (SQP) or constrained variable metric (CVM) methods [34]. The SQP methods in general require fewer function and gradient evaluations than the standard quadratic programming algorithms.

uses an active set strategy and superlinearity is achieved via a BFGS acceleration of the Hessian of the Lagrange functional.

Thesis Focus

As mentioned, the main aims of this thesis are:

- Obtaining a DSA formulation which could be discretised and, in theory, be implemented as a 'pseudo'-element in any established FEA code.
- Implementing structural optimisation in conjunction with ABAQUS to validate the success of the 'pseudo'-element approach.

These aims were formulated so as to lay the foundation for further research into structural optimisation, specifically with ABAQUS.

In order to make the range of tractable optimisation problems[4] as wide as possible, more emphasis has been placed on sensitivity analysis, as opposed to optimisation.

A large portion of the effort invested in this work has focussed on the integration of DSA into ABAQUS and implementing an optimisation model capable of interfacing with ABAQUS. As described in Chapter 5, the user element routine UEL was developed so as to allow alternate execution of structural and sensitivity analysis increments - the discretisation of the DSA formulation as a 'pseudo'-element ensures that the native ABAQUS solver interprets the DSA increment as a structural analysis step. Though not as complex, implementing optimisation in conjunction with ABAQUS is more labourious, requiring the development of various script files and utility programs to manage the interface between ABAQUS and the optimisation model.

In order to curb computational cost and to maintain the focus of this research, the nonlinear kinematic formulations employed are simplified: several assumptions are introduced and a *linear elastic* truss/bar element discretisation is used consistently.

Only *shape* (geometric) and *non-shape* DSA is investigated and implemented (cf. Section 3.1.1): possible response variable dependence on load and boundary conditions, as well as topological characteristics[5], is not considered. For the sake of convenience, the truss/bar element cross-section is consistently used as a non-shape design parameter, while Fig.[6.4.3] defines the shape design parameter used in Section 6.4.

[4]Shape and non-shape optimisation; multi-parameters DSA; stress-based DSA; etc.
[5]Number of nodes, elements, connections.

In order to keep the structural optimisation procedure as simple as possible, and to enable compatability with ABAQUS, the DSA formulations utilised are all based on the Direct Differentiation Method (DDM). In brief, the three main DDM formulations are:

- The *'intuitive' non-shape* approach which utilises the stiffness matrix $\boldsymbol{K}$, generated during the analysis phase, to obtain *approximate* sensitivity estimates. For the purposes of this research the 'intuitive' approach incorporates *only* the Updated Lagrange (UL) kinematic formulation, although the Total Lagrange (TL) formulation is equally well suited.

- The *'rigorous' non-shape* approach which, unlike the 'intuitive' approach, applies the **complete** DDM analytical procedure to the kinematic formulation. In this work the TL formulation is preferred to the UL to ensure a more accurate *large* strain sensitivity response. Although more accurate than the 'intuitive' approach, the 'rigorous' procedure is substantially more complex, in theory and implementation.

- *Shape* DSA, employing the TL-based 'rigorous' approach. The infeasibility of UL-based shape sensitivity analysis follows from the formulation for shape DSA in Chapter 3[6].

In conclusion, the PLBA RQP optimisation procedure was implemented to work in tandem with ABAQUS to obtain the optimal structural design configuration. Due to the emphasis of this research on DSA and the refinement of the PLBA, the optimisation routine is utilised as presented in [26], with minimum modification.

Sectional Outline

The rest of this thesis is constituted as follows:

- Chapter 2 is concerned with a review of fundamental kinematic theory, an introduction to the terminology and notation used in the ensuing chapters and a discussion of the nonlinear kinematic solution procedures. The discretisation of the various kinematic formulations is also provided.

- Chapter 3 introduces the concepts and theory employed in the formulation of Design Sensitivity Analysis: the variational formulations for the 'intuitive' and 'rigorous' non-shape DSA approaches are presented; the same is done for *shape* and stress-based DSA. Once again the variational expressions are discretised.

[6]Refer to Fig.[3.1].

- Chapter 4 discusses and summarises the structural optimisation procedure implemented in this research, namely the Pshenichny-Lim-Belegundu-Arora recursive quadratic programming (PLBA RQP) method.
- Chapter 5 describes the integration of the kinematic and DSA formulations into the ABAQUS user element subroutine UEL. In addition, the structural optimisation process, implemented in conjunction with ABAQUS, is detailed.
- Chapter 6 presents numerical results for several structures, demonstrating the successful application of the theory introduced in Chapters 2 to 4.
- Chapter 7 concludes the thesis.

Chapter 2

Structural Analysis

2.1 Variational Formulation

The computational implementation of Design Sensitivity Analysis (DSA), and consequently most numerical Structural Optimisation procedures, requires extensive analytical manipulation of the classical equation of motion[1] in variational form. In the ensuing chapters and sections, familiarity with the standard variational formulations and notations will be assumed. For the sake of clarity, a brief review of the fundamentals of the standard displacement based variational formulation, as well as kinematic nonlinearity, will be presented.

2.1.1 First Principles: The displacement-based equilibrium formulation

The increasing availability of affordable computational power has not only enabled more complex structural analyses to be performed, but has also made computational design sensitivity analysis, and thus structural optimisation, more feasible for a wide range of applications. Substantial research effort has, in addition, been focussed on producing variational balance laws which result in less expensive computational implementations.

From this perspective the specific variational description employed to model the equilibrium state is crucial in maximising computational efficiency, especially in the case of material or kinematic nonlinearity. Although promising alternative element formulations exist, eg. the *three-field* [2] (Hu-Washizu) based enhanced assumed strain

[1] Also: governing or equilibrium equation

[2] Three variational equilibrium equations are solved simultaneously for three different response

approach, the standard quasi-static *one-field* displacement-based formulation is adopted throughout this work due to its relative simplicity, particularly for nonlinear behaviour, albeit with some loss of computational efficiency.

For a static or quasi-static[3] body, the linear momentum equilibrium equation[33]

$$\frac{\partial \tau_{ij}}{\partial x_i} + \rho f_j = \rho a_j$$

simplifies to:

$$\frac{\partial \tau_{ij}}{\partial x_i} + \rho f_j = 0 \tag{2.1}$$

(or $\nabla \cdot \boldsymbol{\tau} + \boldsymbol{f} = \mathbf{0}$ in vector notation).

The traction boundary condition on the surface[4]. , S, of a static or quasi-static body, is generally expressed in the following manner:

$$\tau_{ij} n_j - t_i = 0 \tag{2.2}$$

(or $\boldsymbol{\tau} \cdot \boldsymbol{n} - \boldsymbol{t} = \mathbf{0}$ in vector notation).

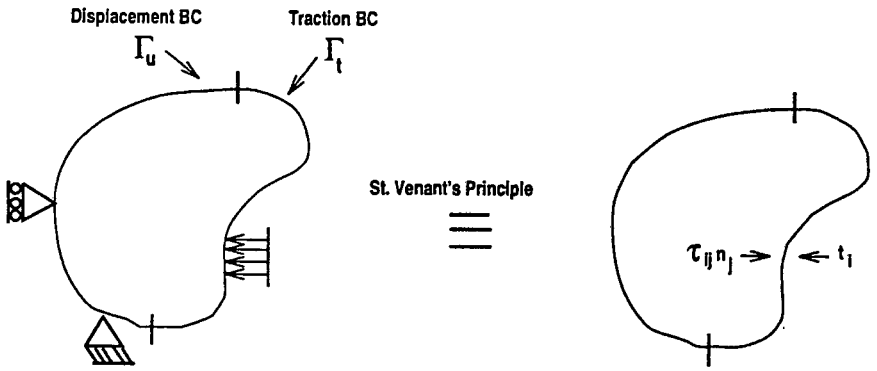

Figure 2.1: Static or Quasi-static body with Boundary Conditions

Applying the principle of virtual work[5]. to (2.1) and (2.2), and combining them, the standard displacement-based *variational* formulation is obtained. The variational form of the governing equation, in conjunction with the essential boundary condition, ie. prescribed displacement $\mathbf{u}$ on Γ_u, fully describes the problem.

variables [39].

[3]Incremental loading is applied in a fashion such that linear acceleration remains negligibly small.

[4]S can be divided into the surface of prescribed displacement Γ_u (Essential BC), and the surface of prescribed traction Γ_t (Natural BC)

[5]A variation on the general Lagrange Multiplier method [39], as opposed to taking the Frechét/Gateaux derivative of the Total Potential Energy [9]

The virtual work form of expression (2.1) is

$$\int_V \left(\frac{\partial \tau_{ij}}{\partial x_j} + \rho f_i \right) \delta u_i \, dV = 0$$

$$\Rightarrow \int_V \frac{\partial \tau_{ij}}{\partial x_j} \delta u_i \, dV = - \int_V \rho f_i \, \delta u_i \, dV \tag{2.3}$$

and applying a similar procedure to (2.2), the following relation is obtained:

$$\int_S (\tau_{ij} n_j - t_i) \, \delta u_i \, dS = 0$$

$$\Rightarrow \int_V \frac{\partial}{\partial x_j} (\tau_{ij} \delta u_i) \, dV = \int_S t_i \, \delta u_i \, dS$$

$$\Rightarrow \int_V \frac{\partial \tau_{ij}}{\partial x_j} \delta u_i \, dV + \int_V \tau_{ij} \frac{\partial \delta u_i}{\partial x_j} \, dV = \int_S t_i \, \delta u_i \, dS \, . \tag{2.4}$$

Consequently, combining (2.3) and (2.4) produces

$$\int_V \tau_{ij} \frac{\partial \delta u_i}{\partial x_j} \, dV - \int_V \rho f_i \, \delta u_i \, dV = \int_S t_i \, \delta u_i \, dS$$

$$\text{i.e.} \int_V \tau_{ij} \, \delta e_{ij} \, dV - \int_V \rho f_i \, \delta u_i \, dV = \int_S t_i \, \delta u_i \, dS \tag{2.5}$$

and, more specifically, for a *displacement* based formulation

$$\int_S t_i \, \delta u_i dS \equiv \int_{\Gamma_t} t_i \, \delta u_i \, d\Gamma_t$$

or, using vector notation:

$$\int_V \boldsymbol{\tau}^{\mathsf{T}} \cdot \delta \mathbf{e} \, dV - \int_V \rho \mathbf{f}^{\mathsf{T}} \cdot \delta \mathbf{e} \, dV = \int_{\Gamma_t} \mathbf{t}^{\mathsf{T}} \delta \mathbf{u} \, d\Gamma_t \, , \tag{2.6}$$

where the Cauchy[6] stress *vector* is

$$\boldsymbol{\tau}^{\mathsf{T}} = \left[\begin{array}{cccccc} \tau_{11} & \tau_{22} & \tau_{33} & \tau_{12} & \tau_{13} & \tau_{23} \end{array} \right] ,$$

and the infinitesimal strain *vector* is

$$\mathbf{e}^{\mathsf{T}} = \left[\begin{array}{cccccc} e_{11} & e_{22} & e_{33} & \gamma_{12} & \gamma_{13} & \gamma_{23} \end{array} \right] .$$

For the *infinitesimal* displacement domain the formulation (2.6) is quite satisfactory. When applied for the purposes of solving problems involving large deformation, however, especially when accompanied by large strain response, the infinitesimal strain formulation (2.6) expressed in terms of Cauchy stress (τ_{ij}) and *infinitesinal* strain (e_{ij}) is no longer adequate.

Most of the research performed here focuses on *finite* displacement applications, therefore requiring a kinematically nonlinear formulation. Two nonlinear formulations capable of correctly modelling large deformation behaviour, specifically the Total (TL) and Updated Lagrangian (UL) procedures, are discussed in the next section.

[6] Utilising Cauchy stress is justified by assuming a static or quasi-static body.

2.1.2 Kinematic Nonlinearity

Assuming equilibrium at time t, (2.5) is restated more conveniently as

$$\int_{{}^tV} {}^t\tau_{ij}\ \delta {}^te_{ij}\ {}^tdV - \int_{{}^tV} {}^t\rho\ {}^tf_i\ \delta {}^tu_i\ {}^tdV - \int_{{}^t\Gamma_t} {}^tt_i\ \delta {}^tu_i\ {}^td\Gamma_t = 0$$

for a *small* rotation and displacement problem. The variational formulation for a further time $t + \Delta t$, ie. for altered loading conditions ${}^{t+\Delta t}\Re$, is expressed as:

$$\int_{{}^{t+\Delta t}V} {}^{t+\Delta t}\tau_{ij}\ \delta {}^{t+\Delta t}e_{ij}\ {}^{t+\Delta t}dV = {}^{t+\Delta t}\Re \tag{2.7}$$

with the external loads ${}^{t+\Delta t}\Re$ formulated as:

$${}^{t+\Delta t}\Re = \int_{{}^{t+\Delta t}V} {}^{t+\Delta t}\rho\ {}^{t+\Delta t}f_i\ \delta {}^{t+\Delta t}u_i\ {}^{t+\Delta t}dV + \int_{{}^{t+\Delta t}\Gamma_t} {}^{t+\Delta t}t_i\ \delta {}^{t+\Delta t}u_i\ {}^{t+\Delta t}d\Gamma_t .$$

In the event of *large* rotations and/or displacements, that is, kinematic nonlinearity, the equilibrium state at time $t + \Delta t$ is formulated in terms of the material reference state at time $t = 0$, employing the Total Lagrangian (TL) procedure, or the material configuration at time t, utilising the Updated Lagrangian (UL)[7] approach.

The strain energy measure $\tau_{ij}\,\delta e_{ij}$, in the *small* displacement/rotation variational formulation, is invariant to frame transformation and can therefore not be used to adequately model the equilibrium state at time $t + \Delta t$ in terms of either of the frames C_0 or C_t.

The *energetically conjugate*[8] , *frame invariant*[9] 2^{nd} Piola-Kirchhoff stress S_{ij} and Green-Lagrange strain ε_{ij} tensors respectively replace Cauchy stress and infinitesimal strain in both the TL and UL formulations.

In the work presented here, *both* the TL and UL are employed and consequently both formulations will be presented. The notational conventions introduced by Bathe [3] are used consistently in the ensuing sections.

---

[7] Refer to Figs.[2.2-2.3].

[8] Energy conjugacy $\Rightarrow \int_{{}^{t+\Delta t}V} {}^{t+\Delta t}S_{ij}\ \delta {}^{t+\Delta t}\varepsilon_{ij}\ {}^{t+\Delta t}dV = \int_{{}^{t+\Delta t}V} {}^{t+\Delta t}\tau_{ij}\ \delta {}^{t+\Delta t}e_{ij}\ {}^{t+\Delta t}dV$

[9] Frame invariance implies that for any two frames $T^{(1)}$ and $T^{(2)}$, where either frame can be obtained by a frame transformation of the other, the following relation holds true
$\int_{T^{(1)}V} {}^{T^{(1)}}S_{ij}\ \delta {}^{T^{(1)}}\varepsilon_{ij}\ {}^{T^{(1)}}dV = \int_{T^{(2)}V} {}^{T^{(2)}}S_{ij}\ \delta {}^{T^{(2)}}\varepsilon_{ij}\ {}^{T^{(2)}}dV$

The Total Lagrange kinematically nonlinear formulation

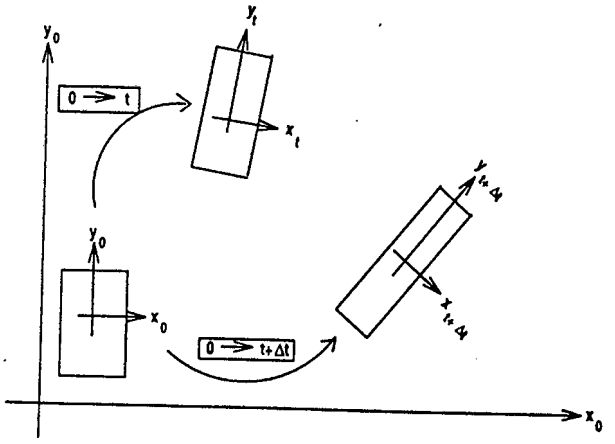

Figure 2.2: The Total Lagrangian (TL) formulation.

In the Total Lagrangian[10] variational formulation, the equilibrium state (2.7) at time $t + \Delta t$ is expressed in terms of quantities defined in the 'initial' frame[11] C_0

$$\int_{{}_0V} {}^{t+\Delta t}_{0}S_{ij}\ \delta^{t+\Delta t}_{0}\varepsilon_{ij}\ {}^{0}dV = {}^{t+\Delta t}\Re \tag{2.8}$$

$$\begin{aligned}
\text{where}\quad {}^{t+\Delta t}\Re &= \int_{{}_0V} {}^{t+\Delta t}_{0}\rho\ {}^{t+\Delta t}_{0}f_i\ \delta^{t+\Delta t}_{0}u_i\ {}^{0}dV \\
&\quad + \int_{{}_0\Gamma_t} {}^{t+\Delta t}_{0}t_i\ \delta^{t+\Delta t}_{0}u_i\ {}^{0}d\Gamma_t \\
\text{and}\quad {}^{t+\Delta t}_{0}S_{ij} &= \det\left(\left[{}^{t+\Delta t}_{0}x_{k,l}\right]\right)\ {}^{0}_{t+\Delta t}x_{i,m}\ {}^{t+\Delta t}\tau_{mn}\ {}^{0}_{t+\Delta t}x_{j,n} \\
\delta^{t+\Delta t}_{0}\varepsilon_{ij} &= {}^{t+\Delta t}_{0}x_{m,i}\ \delta^{t+\Delta t}e_{mn}\ {}^{t+\Delta t}_{0}x_{n,j}\,.
\end{aligned} \tag{2.9}$$

In order to determine the response variables, eg. stress, at time $t + \Delta t$, (2.9) is solved for the incremental displacement ${}_{t+\Delta t}u_i$ whence ${}^{t+\Delta t}_{0}u_i = {}^{t}_{0}u_i + {}_0u_i$ is obtained. The displacement ${}^{t}_{0}u_i$ is found from the solution of the equilibrium state at time t

$$\int_{{}_0V} {}^{t}_{0}S_{ij}\ \delta^{t}_{0}\varepsilon_{ij}\ {}^{0}dV = \int_{{}_0V} {}^{t}_{0}\rho\ {}^{t}_{0}f_i\ \delta^{t}_{0}u_i\ {}^{0}dV + \int_{{}_0\Gamma_t} {}^{t}_{0}t_i\ \delta^{t}_{0}u_i\ {}^{0}d\Gamma_t\,.$$

[10] Refer to Fig.[2.2].

[11] Note:

- '[ ]' indicates a 2nd Order Tensor.
- As a consequence of Conservation of Mass[33], $\det\left(\left[{}^{t+\Delta t}_{0}x_{k,l}\right]\right) = \frac{{}^{0}\rho}{{}^{t+\Delta t}\rho}$.
- Assuming an incompressible material or rigid body displacement, $\det\left(\left[{}^{t+\Delta t}_{0}x_{k,l}\right]\right) = 1$.

Assuming that the body and traction forces are not 'follower forces'[12] , ${}^{t+\Delta t}\Re$ is utilised in the form (2.9), for both TL and UL.

In order to solve the nonlinear TL equation for the displacement increments ${}_0u_i$, (2.8) can be written as

$$\begin{aligned} &\int_{{}_0V} {}_0C_{ijrs}\, {}_0e_{rs}\, \delta_0 e_{ij}\, {}^0dV + \int_{{}_0V} {}^t_0S_{ij}\, \delta_0\eta_{ij}\, {}^0dV \\ \approx\ & {}^{t+\Delta t}\Re - \int_{{}_0V} {}^t_0S_{ij}\, \delta_0 e_{ij}\, {}^0dV \end{aligned} \tag{2.10}$$

using the set of simplifications and linearisations introduced below[13] .

- Displacement and strain increments:
  - The displacement and strain increments in TL refer to the 'initial' reference frame

$$\begin{aligned} {}^{t+\Delta t}_0u_i &= {}^t_0u_i + {}_0u_i \\ {}^{t+\Delta t}_0\varepsilon_{ij} &= {}^t_0\varepsilon_{ij} + {}_0\varepsilon_{ij} \end{aligned}$$

    where

$${}^t_0\varepsilon_{ij} = \tfrac{1}{2}\left({}^t_0u_{i,j} + {}^t_0u_{j,i} + {}^t_0u_{k,i}\, {}^t_0u_{k,j}\right).$$

- Simplifications:
  - The incremental form of the standard response variables at $t+\Delta t$ is[14]

$$\begin{aligned} \delta^{t+\Delta t}_0u_i &= \delta_0u_i \equiv \delta u_i \\ \delta^{t+\Delta t}_0\varepsilon_{ij} &= \delta\left({}^t_0\varepsilon_{ij} + {}_0\varepsilon_{ij}\right) = \delta_0\varepsilon_{ij} \end{aligned}$$

    where $\quad {}_0\varepsilon_{ij} = {}_0e_{ij} + {}_0\eta_{ij}$

    and $\quad {}_0e_{ij} = \tfrac{1}{2}\left({}_0u_{i,j} + {}_0u_{j,i}\right)$

$${}_0\eta_{ij} = \tfrac{1}{2}\left({}^t_0u_{k,i}\, {}_0u_{k,j} + {}^t_0u_{k,j}\, {}_0u_{k,i} + {}_0u_{k,i}\, {}_0u_{k,j}\right)$$

    for which the variational formulation is

$$\delta_0\varepsilon_{ij} = \delta_0e_{ij} + \delta_0\eta_{ij} \tag{2.11}$$

$$\begin{aligned} \text{with}\quad \delta_0e_{ij} &= \tfrac{1}{2}\left(\delta_0u_{i,j} + \delta_0u_{j,i}\right) \\ \delta_0\eta_{ij} &= \tfrac{1}{2}\left({}^t_0u_{k,i}\, \delta_0u_{k,j} + {}^t_0u_{k,j}\, \delta_0u_{k,i} \right. \\ &\quad \left. + \delta_0u_{k,i}\, {}_0u_{k,j} + {}_0u_{k,i}\, \delta_0u_{k,j}\right). \end{aligned} \tag{2.12}$$

---

[12] ${}^{t+\Delta t}\Re$ in (2.9) is subject to the assumption that the body f_i and traction forces t_i are not dependent on the process of deformation, ie. they have no dependency on ${}^{t+\Delta t}_0u_i$.

[13] All variations are taken with respect to ${}_0u_i$: $\delta \equiv \delta_{{}_0u_i}$.

[14] The incremental form of the response variables in some instances differs radically for the UL formulation.

- A further simplification is usually introduced by eliminating some of the terms in[15] $\delta_0\eta_{ij}$

$$\delta_0\eta_{ij} \approx \tfrac{1}{2}(\ \delta_0 u_{k,i}\ {}_0u_{k,j} + \ {}_0u_{k,i}\ \delta_0 u_{k,j})^{16}\,.$$

In order to achieve a higher degree of accuracy in the TL formulation, $\delta_0\eta_{ij}$ is used as introduced in (2.12) in the research presented here.

- Linearisations:

  - The nonlinear term of (2.8), ie. containing the incremental 2nd Piola-Kirchhoff stress ${}_0S_{ij}$, is linearised by replacing the variation of the Green-Lagrange strain $\delta\varepsilon_{ij}$ with the variation of infinitesimal strain δe_{ij}.

$$\int_{{}_0V} {}_0S_{ij}\ \delta_0\varepsilon_{ij}\ {}^0dV \approx \int_{{}_0V} {}_0S_{ij}\ \delta_0 e_{ij}\ {}^0dV$$

  - ${}_0S_{ij}$ is itself linearised[17] :

$$\begin{aligned} {}^{t+\Delta t}_{0}S_{ij} &= {}^{t}_{0}S_{ij} + {}_0S_{ij} = {}^{t}_{0}S_{ij} + {}_0C_{ijrs}\ {}_0\varepsilon_{ij} \\ &\approx {}^{t}_{0}S_{ij} + {}_0C_{ijrs}\ {}_0e_{rs}\,. \end{aligned}$$

In addition to calculating the response variables (stress, strain), the displacement response ${}^{t+\Delta t}_{0}u_i$ also plays a critical role during the sensitivity analysis phase, whence the sensitivity vectors are obtained to eventually be used in the structural optimisation procedure. The numerical procedure employed to solve for ${}^{t+\Delta t}_{0}u_i$ is based on the straightforward Newton-Raphson approach:

- The linearised TL formulation represents a 'predictor' stage in the process of determining ${}^{t+\Delta t}_{0}u_i$. Errors occur in the estimate of ${}^{t+\Delta t}_{0}u_i$ due to the linearisations introduced into the formulation of the TL equilibrium equation.

$$Error = {}^{t+\Delta t}\Re - \int_{{}_0V} {}^{t+\Delta t}_{0}S^{(1)}_{ij}\ \delta^{t+\Delta t}_{0}\varepsilon^{(1)}_{ij}\ {}^0dV$$

- An iterative Newton-Raphson (N-R) 'corrector' method is employed by the solver to calculate a succession of better estimates for ${}^{t+\Delta t}_{0}u_i$[3]

$$\begin{aligned} &\int_{{}_0V} {}_0C_{ijrs}\Delta_0 e^{(k)}_{rs}\ \delta_0 e_{ij}\ {}^0dV + \int_{{}_0V} {}^{t}_{0}S_{ij}\delta\Delta_0\eta^{(k)}_{ij}\ {}^0dV \\ = \ &{}^{t+\Delta t}\Re - \int_{{}_0V} {}^{t+\Delta t}_{0}S^{(k-1)}_{ij}\ \delta^{t+\Delta t}_{0}\varepsilon^{(k-1)}_{ij}\ {}^0dV \end{aligned}$$

[15]Thus ensuring that the stiffness matrix $\boldsymbol{K}$ produced during discretisation remains symmetric in the kinematically nonlinear regime, thereby reducing computational cost.

[17]Assuming linear elasticity

which in the canonical vector form is simply

$$\int_{{}_0V} {}_0\boldsymbol{C}\,\delta_0\boldsymbol{e}^{\mathsf{T}}\cdot\Delta_0\boldsymbol{e}^{(k)}\,{}^0dV + \int_{{}_0V}\delta\Delta_0\boldsymbol{\eta}^{\mathsf{T}(k)}\cdot{}^t_0\boldsymbol{S}\,{}^0dV$$
$$= {}^{t+\Delta t}\Re - \int_{{}_0V}\delta^{t+\Delta t}_0\boldsymbol{\varepsilon}^{\mathsf{T}(k-1)}\cdot{}^{t+\Delta t}_0\boldsymbol{S}^{(k-1)}\,{}^0dV\,. \qquad (2.13)$$

It has to be pointed out at this stage that the entire preceding analysis procedure pre-supposes an incompressible material **or** a material with very high values of Young's modulus (ie. essentially a rigid body), where effectively ${}^{t+\Delta t}_0\rho = {}^t_0\rho = {}^0\rho$.

The Updated Lagrange kinematically nonlinear formulation

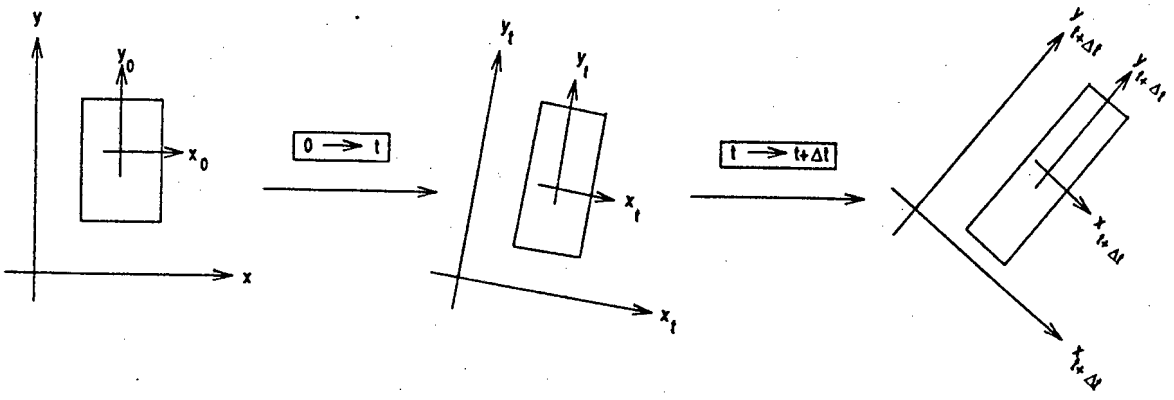

Figure 2.3: The Updated Lagrangian (UL) formulation.

The TL formulation is preferred to the UL[18] , as the former can be integrated more naturally into the ABAQUS user element routine. The TL is, furthermore, more accurate than the UL for large strain behaviour, as well as being more straightforward to implement for geometric (shape) design sensitivity analysis. Notwithstanding these facts, the UL is nevertheless extensively utilised due to its relatively simple formulation, as well as for comparative purposes.

Equilibrium for the UL formulation is succinctly expressed as

$$\int_{{}_tV} {}^{t+\Delta t}_t S_{ij}\,\delta^{t+\Delta t}_t\varepsilon_{ij}\,{}^t dV = {}^{t+\Delta t}\Re$$

$$\text{with}\quad {}^{t+\Delta t}_t S_{ij} = \det\left(\left[{}^{t+\Delta t}_t x_{k,l}\right]\right)\,{}^t_{t+\Delta t}x_{i,m}\,{}^{t+\Delta t}\tau_{mn}\,{}^t_{t+\Delta t}x_{j,n}$$
$$\delta^{t+\Delta t}_t\varepsilon_{ij} = {}^{t+\Delta t}_t x_{m,i}\,\delta^{t+\Delta t}e_{mn}\,{}^{t+\Delta t}_t x_{n,j} \qquad (2.14)$$

[18]Refer to Fig.[2.3].

with all expressions, except ${}^{t+\Delta t}\Re$, referring to the 'current' (time t) material configuration frame. The term ${}^{t+\Delta t}\Re$ remains unchanged from (2.9), assuming deformation independent loading.

The linearisation of the UL formulation in (2.14) is obtained as

$$\begin{aligned} & \int_{{}^tV} {}_tC_{ijrs}\, {}_te_{rs}\, \delta_t e_{ij}\, {}^tdV + \int_{{}^tV} {}^t\tau_{ij}\, \delta_t\eta_{ij}\, {}^tdV \\ \approx\ & {}^{t+\Delta t}\Re - \int_{{}^tV} {}^t\tau_{ij}\, \delta_t e_{ij}\, {}^tdV \end{aligned} \tag{2.15}$$

derived by imposing a series of simplifications and linearisations, as discussed below. The process of reduction of the nonlinear equilibrium expression (2.14) to (2.15) proceeds in a similar manner to what was done in the case of the TL formulation:

- Displacement and strain increments:
  - The displacement and strain increments in UL refer to the 'current' material configuration frame at time t, ie. the last time increment for which a convergent solution was obtained.

$$\begin{aligned} {}^{t+\Delta t}_t u_i &= {}_tu_i\,, \\ {}^{t+\Delta t}_t \varepsilon_{ij} &= {}_t\varepsilon_{ij}\,, \end{aligned}$$

  where

$${}_t\varepsilon_{ij} = \tfrac{1}{2}\left({}_tu_{i,j} + {}_tu_{j,i} + {}_tu_{k,i}\, {}_tu_{k,j}\right).$$

- Simplifications:
  - The incremental form of the deformation measures at $t + \Delta t$ is

$$\begin{aligned} {}_t\varepsilon_{ij} &= {}_te_{ij} + {}_t\eta_{ij}\,, \\ \text{where}\quad {}_te_{ij} &= \tfrac{1}{2}\left({}_tu_{i,j} + {}_tu_{j,i}\right). \\ {}_t\eta_{ij} &= \tfrac{1}{2}\left({}_tu_{k,i}\, {}_tu_{k,j}\right). \end{aligned}$$

  the variations of which may be stated as

$$\delta_t\varepsilon_{ij} = \delta_t e_{ij} + \delta_t\eta_{ij}\,,$$

$$\begin{aligned} \text{with}\quad \delta_t e_{ij} &= \tfrac{1}{2}\left(\delta_t u_{i,j} + \delta_t u_{j,i}\right) \\ \delta_t\eta_{ij} &= \tfrac{1}{2}\left(\delta_t u_{k,i}\, {}_tu_{k,j} + {}_tu_{k,i}\, \delta_t u_{k,j}\right) \end{aligned}$$

- Linearisations:

  - The LHS term of (2.14) containing the incremental stress ${}_tS_{ij}$ is linearised by approximating $\delta_t\varepsilon_{ij} \approx \delta_t e_{ij}$ so that

$$\int_{{}_tV} {}_tS_{ij}\ \delta_t\varepsilon_{ij}\ {}^tdV \approx \int_{{}_tV} {}_tS_{ij}\ \delta_t e_{ij}\ {}^tdV\,.$$

  - A further linearisation is imposed by assuming linear elasticity in the incremental stress ${}_tS_{ij}$

$$\begin{aligned} {}^{t+\Delta t}_{t}S_{ij} &= {}^t_tS_{ij} + {}_tS_{ij} = {}^t\tau_{ij} + {}_tC_{ijrs}\ {}_t\varepsilon_{rs} \\ &\approx {}^t\tau_{ij} + {}_tC_{ijrs}\ {}_te_{rs}\,. \end{aligned}$$

Finally, in a process analogous to that adopted for the TL formulation, the iterative form of (2.15) is found to be

$$\begin{aligned} &\int_{{}_tV} {}_tC_{ijrs}\Delta_t e^{(k)}_{rs}\ \delta_t e_{ij}\ {}^tdV + \int_{{}_tV} {}^t\tau_{ij}\ \delta\Delta_t\eta^{(k)}_{ij}\ {}^tdV \\ = \ &{}^{t+\Delta t}\Re - \int_{{}^{t+\Delta t}V^{(k-1)}} {}^{t+\Delta t}\tau^{(k-1)}_{ij}\ \delta_{t+\Delta t}e_{ij}{}^{(k-1)}\ {}^{t+\Delta t}dV\,, \end{aligned}$$

which in the canonical vector form becomes

$$\begin{aligned} &\int_{{}_tV} {}_t\boldsymbol{C}\ \delta_t\boldsymbol{e}^{\mathsf{T}}\cdot\Delta_t\boldsymbol{e}^{(k)}\ {}^tdV + \int_{{}_tV} \delta\Delta_t\boldsymbol{\eta}^{\mathsf{T}(k)}\cdot{}^t\boldsymbol{\tau}\ {}^tdV \\ = \ &{}^{t+\Delta t}\Re - \int_{{}^{t+\Delta t}V^{(k-1)}} \delta_{t+\Delta t}\boldsymbol{e}^{\mathsf{T}(k-1)}\cdot{}^{t+\Delta t}\boldsymbol{\tau}^{(k-1)}\ {}^{t+\Delta t}dV\,. \end{aligned} \tag{2.16}$$

2.2 Discretisation

Both the Total Lagrangian and Updated Lagrangian formulations are numerically solved by means of the Finite Element Method (FEM); the TL and UL procedures are both discretised in preparation for computational implementation as part of the FE analysis code ABAQUS' user element routine UEL.

The generality of the element discretisations employed in the work presented here is limited by a series of assumptions, as well as the specific area of focus:

- The majority of physical problems to which structural optimisation is applied involve truss structures and, consequently, the bulk of the current literature in this subject field focuses on the FE discretisation and implementation of truss, or *bar* elements[19] ; consequently the research presented here is limited to the utilisation of bar elements exclusively.
- In the general variational formulation for the TL and UL the loading forces (traction and body forces) are assumed to be deformation independent, i.e. they are 'non-follower' forces.
- The material model is chosen to be *linearly elastic.*
- In a significant further assumption for the truss structures investigated, the self-weight of the trusses is considered negligible in comparison with the applied traction forces. Although this assumption does **not** model the majority of physical applications very realistically, it does simplify the DSA formulation without compromising the conceptual basis of the sensitivity calculation[20] .

By eliminating body force in the variational formulation, ${}^{t+\Delta t}\Re$ simplifies to

$$ {}^{t+\Delta t}\Re = \int_{{}^0\Gamma_t} {}^{t+\Delta t}_{0}t_i \; \delta_0 u_i \; {}^0d\Gamma_t \, . $$

The discretised Total Lagrangian formulation

For a truss element implementation the iterative linearised TL equation (2.13) is restated, in the *global* 'initial' frame[21] C_0, as:

$$ \int_{{}^0V} E \; \delta_0 e_{xx} \; \Delta\delta_0 e^{(k)}_{xx} \; {}^0dV + \int_{{}^0V} \delta\Delta_0 \eta^{(k)}_{xx} \; {}^t_0 S_{xx} \; {}^0dV $$

[19]In order to avoid confusion with *truss structures* these elements are consistently referred to as **bar** elements.

[20]The body force term is treated similarly to the traction force term, assuming material incompressibility, and its presence in the variational formulation therefore doesn't contribute significantly towards gaining further insight into the computational implementation of design sensitivity analysis.

[21]Refer to Fig. (2.4).

$$= \int_{{}^0\Gamma_t} \delta_0 u^\top \cdot {}^{t+\Delta t}_0 t \; {}^0 d\Gamma_t - \int_{{}^0V} \delta_0 \varepsilon^{(k-1)}_{xx} \; {}^{t+\Delta t}_0 S^{(k-1)}_{xx} \; {}^0 dV \, .$$

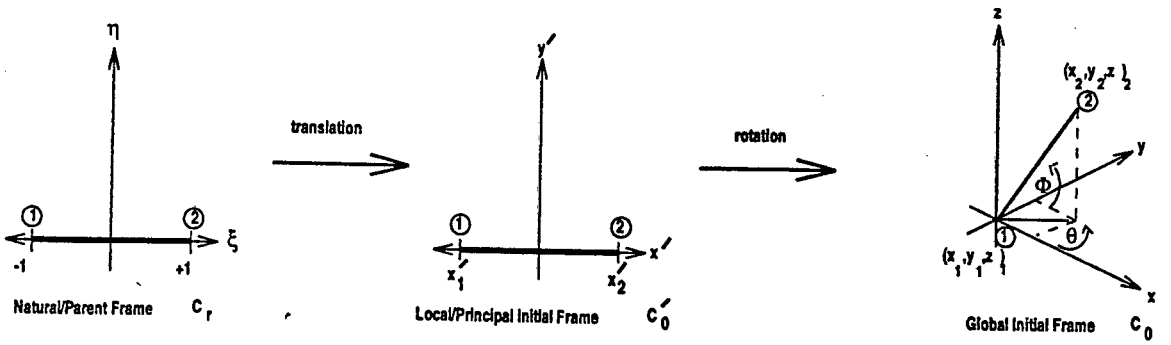

Figure 2.4: Isoparametric mapping.

The discretisation is substantially more straightforward to perform when the preceding expression is formulated in the *local* 'initial' frame C_0' , which is defined to be the *princial frame* of a particular element, ie. C_0' is a frame in which both nodes of the element are mapped onto the *local* ${}^0x'$ axis:

$$\begin{aligned} &\int_{{}^{0'}V} E \; \delta_{0'} e_{xx} \; \Delta\delta_{0'} e^{(k)}_{xx} \; {}^{0'} dV + \int_{{}^{0'}V} \delta\Delta_{0'} \eta^{(k)}_{xx} \; {}^t_{0'} S_{xx} \; {}^{0'} dV \\ = \; &\int_{{}^{0'}\Gamma_t} \delta_{0'} u^\top \cdot {}^{t+\Delta t}_{0'} t \; {}^{0'} d\Gamma_t - \int_{{}^{0'}V} \delta_{0'} \varepsilon^{(k-1)}_{xx} \; {}^{t+\Delta t}_{0'} S^{(k-1)}_{xx} \; {}^{0'} dV \, . \end{aligned} \tag{2.17}$$

Implementing the FEM, discretisation proceeds in the usual fashion by first introducing the standard isoparametric mapping from the 'natural' (or 'parent') frame C_r to the *local/principal* 'initial' reference frame C_0', so that (2.17) is restated as

$$\begin{aligned} &\int_{{}^rV} E \; \delta_{0'} e_{xx} \; \Delta\delta_{0'} e^{(k)}_{xx} \; J \; {}^r dV + \int_{{}^rV} \delta\Delta_{0'} \eta^{(k)}_{xx} \; {}^t_{0'} S_{xx} \; J \; {}^r dV \\ = \; &\int_{{}^r\Gamma_t} \delta_{0'} u^\top \cdot {}^{t+\Delta t}_{0'} t \; J_\Gamma \; {}^r d\Gamma_t - \int_{{}^rV} \delta_{0'} \varepsilon^{(k-1)}_{xx} \; {}^{t+\Delta t}_{0'} S^{(k-1)}_{xx} \; J \; {}^r dV \, , \end{aligned} \tag{2.18}$$

where 'r' refers to the 'natural' configuration C_r, with the Jacobian coefficients J, J_Γ defined as

$$\begin{aligned} J &\equiv \det\left(\left[{}^{0'}_r x_{i,j} \right] \right) = \frac{{}^0 L}{2} \\ J_\Gamma &\equiv \| \left[{}^{0'}_r x_{i,j} n_j \right] \| \end{aligned}$$

The isoparametric mapping $C_r \rightarrow C_0'$ is represented by a transformation operation from a coordinate system in ξ to a system in ${}^0x'$, which can be written as

$${}^0x' \equiv {}^0x'(\xi) \text{ where } {}^0x' = \begin{pmatrix} {}^0x' \\ {}^0y' \\ {}^0z' \end{pmatrix}, \; \xi = \begin{pmatrix} \xi \\ \eta \end{pmatrix}, \tag{2.19}$$

utilising the shape functions, $N_1 = \frac{1-\xi}{2}$ and $N_2 = \frac{1+\xi}{2}$, so that ${}^0\boldsymbol{x}'$ is simply defined, in terms of the nodal coordinates $\boldsymbol{X}'$, as

$$ {}^0\boldsymbol{x}' = N^\top \cdot \boldsymbol{X}' \quad \text{where} \quad N^\top = \begin{bmatrix} N_1 & 0 & 0 & N_2 & 0 & 0 \\ 0 & N_1 & 0 & 0 & N_2 & 0 \\ 0 & 0 & N_1 & 0 & 0 & N_2 \end{bmatrix} $$
$$ \text{and} \quad \boldsymbol{X}'^\top = \begin{bmatrix} X_1' & Y_1' & Z_1' & X_2' & Y_2' & Z_2' \end{bmatrix} . \tag{2.20} $$

Hence, ${}^0\boldsymbol{x}'$ is a vector of first order continuous functions based on the interpolated nodal coordinates $\boldsymbol{X}'$ of the truss element in the *local* 'initial' frame C_0'. From ${}^0\boldsymbol{x}'$ the orientation ${}^0\boldsymbol{x}$ of the element in the *global* 'initial' frame C_0 is obtained as

$$ {}^0\boldsymbol{x} = {}^0\boldsymbol{T}^\top \cdot {}^0\boldsymbol{x}' \tag{2.21} $$

by applying the frame transformation

$$ {}^0\boldsymbol{T}^\top = \left[{}^0_{0'}x_{i,j} \right] \equiv \left[\frac{\partial\, {}^0x_i}{\partial\, {}^0x_j'} \right] $$

where the transformation ${}^0\boldsymbol{T}^\top$ is expressed[22] in terms of θ and ϕ as

$$ {}^0\boldsymbol{T}^\top = \begin{bmatrix} \mathcal{T} & 0_{3\times3} \\ 0_{3\times3} & \mathcal{T} \end{bmatrix} $$

with

$$ \mathcal{T} = \begin{bmatrix} \cos\phi\cos\theta & -\sin\theta & -\sin\phi\cos\theta \\ \cos\phi\sin\theta & \cos\theta & -\sin\phi\sin\theta \\ \sin\phi & 0 & \cos\phi \end{bmatrix} . $$

Referring to (2.20), $\boldsymbol{X}'$ is found by mapping the truss element nodal coordinates $\boldsymbol{X}$ from the *global* 'initial' frame into C_0' in a procedure analogous to (2.21):

$$ \boldsymbol{X}' = {}^0\boldsymbol{T} \cdot \boldsymbol{X} . \tag{2.22} $$

Consequently, the localisation and isoparametric mapping processes in (2.20) and (2.22) may be combined as

$$ {}^0\boldsymbol{x}' = N^\top \cdot {}^0\boldsymbol{T} \cdot \boldsymbol{X} . \tag{2.23} $$

As will become apparent in the section on *shape* DSA, the role fulfilled by the *localising* transformation matrix[23]

$$ \hat{\boldsymbol{T}} = \underset{\sim}{T}(\boldsymbol{b} = \hat{\boldsymbol{h}}) \tag{2.24} $$

in the discretised TL formulation is of considerable importance. The definition of $\hat{\boldsymbol{T}}$ and its dependence on structural configuration are further examined in the relevant section.

[22] Refer to Fig. (2.4).

[23] $\boldsymbol{h} \equiv$ **shape** design parameters.

The isoparametric $C_r \rightarrow C_0$ (with $\boldsymbol{N}^{\mathsf{T}}$) and localising $C_0 \rightarrow C_0{}'$ (with ${}^0\boldsymbol{T}$) mappings are employed to express the incremental displacements ${}^0\boldsymbol{u}'$ as interpolating functions of the *global* nodal incremental displacements $\boldsymbol{d}$ in the same manner that ${}^0\boldsymbol{x}'$ is expressed in terms of $\boldsymbol{X}$ in (2.23):

$$\begin{aligned} {}^0\boldsymbol{u}' &= \boldsymbol{N}^{\mathsf{T}} \cdot \boldsymbol{d}' \\ &= \boldsymbol{N}^{\mathsf{T}} \cdot {}^0\boldsymbol{T} \cdot \boldsymbol{d} \end{aligned}$$

$$ {}^0\boldsymbol{u} = {}^0\boldsymbol{T}^{\mathsf{T}} \cdot {}^0\boldsymbol{u}' $$

with

$$\begin{aligned} \boldsymbol{d}'^{\mathsf{T}} &= \left[\begin{array}{cccccc} u_1' & v_1' & w_1' & u_2' & v_2' & w_2' \end{array} \right] \\ \boldsymbol{d}^{\mathsf{T}} &= \left[\begin{array}{cccccc} u_1 & v_1 & w_1 & u_2 & v_2 & w_2 \end{array} \right] \end{aligned} \tag{2.25}$$

where ${}^0\boldsymbol{u}$ and $\boldsymbol{d}$ are, respectively, the interpolated incremental displacement and nodal incremental displacement vectors in the *global* 'initial' frame C_0.

Finally, the FEM discretisation of (2.17) is completed by introducing (2.19)-(2.25) into (2.18):

$$\begin{aligned} & \delta_{0'}\boldsymbol{u}^{\mathsf{T}} \cdot \left(\left\{ {}^0A\, {}^0L\, E\, {}^0\boldsymbol{N}_{x,x} \otimes {}^0\boldsymbol{N}_{x,x}{}^{\mathsf{T}} \right\} + \left\{ {}^0A\, {}^0L\, {}_0^t S_{xx}\, {}^0\aleph \right\} \right) \cdot \Delta\delta_{0'}\boldsymbol{u}^{(k)} \\ = \; & \delta_{0'}\boldsymbol{u}^{\mathsf{T}} \cdot \left(\left\{ \int_{{}^r\Gamma_t} {}^0\aleph \otimes {}^0\aleph^{\mathsf{T}}\, {}_{0'}^{t+\Delta t}\boldsymbol{t}_\delta\, {}^r d\Gamma_t \right\} - \left\{ {}^0A\, {}^0L\, {}^0\tilde{\aleph}^{(k-1)}\, {}_0^{t+\Delta t} S_{xx}{}^{(k-1)} \right\} \right) \end{aligned} \tag{2.26}$$

where the symbols used in (2.26) are defined as:

$$\begin{aligned} {}_0^t S_{xx} &\equiv {}_{0'}^t S_{xx} \\ {}^0L &\equiv {}^{0'}L = \text{ truss length} \\ {}^0A &\equiv {}^{0'}A = \text{ truss cross-section} \\ E &\equiv \text{Young's modulus} \end{aligned}$$

$$\begin{aligned} {}^0\boldsymbol{N}^{\mathsf{T}}{}_{x,x} &= \frac{1}{{}^0L} \left[\begin{array}{cccccc} -1 & 0 & 0 & 1 & 0 & 0 \end{array} \right] \\ {}^0\boldsymbol{N}^{\mathsf{T}}{}_{y,x} &= \frac{1}{{}^0L} \left[\begin{array}{cccccc} 0 & -1 & 0 & 0 & 1 & 0 \end{array} \right] \\ {}^0\boldsymbol{N}^{\mathsf{T}}{}_{z,x} &= \frac{1}{{}^0L} \left[\begin{array}{cccccc} 0 & 0 & -1 & 0 & 0 & 1 \end{array} \right] \end{aligned}$$

$$\begin{aligned} {}^0\aleph &= {}^0\boldsymbol{N}_{x,x} \otimes {}^0\boldsymbol{N}^{\mathsf{T}}{}_{x,x} + {}^0\boldsymbol{N}_{y,x} \otimes {}^0\boldsymbol{N}^{\mathsf{T}}{}_{y,x} + {}^0\boldsymbol{N}_{z,x} \otimes {}^0\boldsymbol{N}^{\mathsf{T}}{}_{z,x} \\ {}^0\tilde{\aleph}^{(k-1)} &= {}^0\boldsymbol{N}_{x,x} + {}^0\aleph \cdot {}^0\boldsymbol{T} \cdot {}_0^{t+\Delta t}\boldsymbol{u}'^{(k-1)} \end{aligned}$$

$$ {}_0^{t+\Delta t} S_{xx}{}^{(k-1)} = {}_0^t S_{xx} + E \left[{}^0\tilde{\aleph}^{\mathsf{T}(k-1)} - \tfrac{1}{2}\, {}_0^t\boldsymbol{u}^{\mathsf{T}(k-1)} \cdot {}^0\boldsymbol{T}^{\mathsf{T}} \cdot {}^0\boldsymbol{T} \cdot {}_0\boldsymbol{u}^{(k-1)} \right] \tag{2.27}$$

and ${}^{t+\Delta t}_{0'}\boldsymbol{t}_\delta$ is a delta function describing the traction force distribution such that

$$ {}^{t+\Delta t}_{0'}\boldsymbol{t}_\delta = {}^{t+\Delta t}_{0'}\boldsymbol{t}_1\, \delta\left({}^{0'}\boldsymbol{x} - {}^{0'}\boldsymbol{x}_1\right) + {}^{t+\Delta t}_{0'}\boldsymbol{t}_2\, \delta\left({}^{0'}\boldsymbol{x} - {}^{0'}\boldsymbol{x}_2\right) $$

with ${}^{0'}\boldsymbol{x}_i = {}^{0'}\boldsymbol{x}|_{(node\,=\,i)}$ and

$$ \begin{aligned} {}^{t+\Delta t}_{0'}\boldsymbol{t}_1{}^{\mathsf{T}} &= \left[\, t'_{1x} \;\; t'_{1y} \;\; t'_{1z} \;\; 0 \;\; 0 \;\; 0 \,\right]_{node\,=\,1} \\ {}^{t+\Delta t}_{0'}\boldsymbol{t}_2{}^{\mathsf{T}} &= \left[\, 0 \;\; 0 \;\; 0 \;\; t'_{2x} \;\; t'_{2y} \;\; t'_{2z} \,\right]_{node\,=\,2}. \end{aligned} $$

In preparation for implementation of the ABAQUS user element routine UEL, the discretised formulation (2.26) is expressed in the *global* 'initial' frame and simplified by expanding ${}^{t}_{0}S_{xx} \equiv E\,{}^{t}_{0}\varepsilon_{xx}$:

$$ \begin{aligned} &\underbrace{\left[{}^{0}\boldsymbol{T}^{\mathsf{T}} \cdot {}^{0}A\,{}^{0}L \left(\left\{E\,{}^{0}\boldsymbol{N}_{x,x} \otimes {}^{0}\boldsymbol{N}^{\mathsf{T}}{}_{x,x}\right\} + \left\{{}^{t}_{0}S_{xx}\,{}^{0}\aleph\right\}\right) \cdot {}^{0}\boldsymbol{T}\right]}_{{}^{t}_{0}\boldsymbol{K}} \cdot \Delta_0\boldsymbol{u}^{(k)} \\ &= {}^{t+\Delta t}_{0}\boldsymbol{t} - \left[{}^{0}\boldsymbol{T}^{\mathsf{T}} \cdot \boldsymbol{\mathcal{K}} \cdot {}^{0}\boldsymbol{T} \cdot {}^{t+\Delta t}_{0}\boldsymbol{u}^{(k-1)}\right], \end{aligned} \tag{2.28} $$

where

$$ \begin{aligned} {}^{t+\Delta t}_{0}\boldsymbol{t}^{\mathsf{T}} &= \left[\, t_{1x} \;\; t_{1y} \;\; t_{1z} \;\; t_{2x} \;\; t_{2y} \;\; t_{2z} \,\right], \\ \boldsymbol{\mathcal{K}} &= \left({}^{0}A\,{}^{0}L\,E\right) {}^{0}\tilde{\aleph}^{(k-1)} \cdot {}^{0}\tilde{\aleph}^{\mathsf{T}(k-1)}, \end{aligned} \tag{2.29} $$

for

$$ {}^{0}\tilde{\aleph}^{(k-1)} \equiv {}^{0}\boldsymbol{N}_{x,x} + \tfrac{1}{2}\,{}^{0}\aleph \cdot {}^{0}\boldsymbol{T} \cdot {}^{t+\Delta t}_{0}\boldsymbol{u}^{(k-1)}. \tag{2.30} $$

From (2.28) it is evident that the $(k-1)^{th}$ iterative estimate for stress ${}^{t+\Delta t}_{0}S_{xx}{}^{(k-1)}$ becomes

$$ {}^{t+\Delta t}_{0}S_{xx}{}^{(k-1)} \equiv E\,{}^{0}\tilde{\aleph}^{\mathsf{T}(k-1)} \cdot {}^{0}\boldsymbol{T} \cdot {}^{t+\Delta t}_{0}\boldsymbol{u}^{(k-1)}. \tag{2.31} $$

The discretised equilibrium expression (2.28) is easily rewritten in the standard quasi Newton-Raphson iterative form

$$ \underbrace{{}^{t}_{0}\boldsymbol{K} \cdot \Delta_0\boldsymbol{u}^{(k)}}_{{}_0\boldsymbol{Q}^{(k)}} = {}^{t+\Delta t}_{0}\boldsymbol{\Re} - {}^{t+\Delta t}_{0}\boldsymbol{Q}^{(k-1)}. \tag{2.32} $$

The discretised Updated Lagrangian formulation

The truss element implementation of the linearised UL equation (2.16) is expressed in the *global* 'current' frame C_t in a procedure similar to that used for the TL

formulation in the previous section:

$$\int_{{}_tV} E\ \delta_t e_{xx}\ \Delta\delta_t e_{xx}^{(k)}\ {}^tdV + \int_{{}_tV} \delta\Delta_t \eta_{xx}^{(k)}\ {}^t\tau_{xx}\ {}^tdV$$
$$= \int_{{}_0\Gamma_t} \delta_0\boldsymbol{u}^{\mathsf{T}} \cdot {}_0^{t+\Delta t}\boldsymbol{t}\ {}^0d\Gamma_t - \int_{t+\Delta t V^{(k-1)}} \delta_{t+\Delta t} e_{xx}{}^{(k-1)}\ {}^{t+\Delta t}\tau_{xx}^{(k-1)}\ {}^{t+\Delta t}dV^{(k-1)}.$$

In *localising* the variational expression (2.33), the UL formulation is dealt with in a significantly different manner to the TL by utilising separate mappings $C_t \rightarrow C'_t$ and $C_{t+\Delta t^{(k-1)}} \rightarrow C'_{t+\Delta t^{(k-1)}}$ for the LHS and RHS of (2.33), respectively. The isoparametric mappings $C'_t \rightarrow C_r$ and $C'_{t+\Delta t^{(k-1)}} \rightarrow C_r$ are then utilised to express the LHS and RHS of the localised expression (2.33) in the 'parent' frame.

$$\int_{{}_rV} E\ \delta_{t'} e_{xx}\ \Delta\delta_{t'} e_{xx}^{(k)}\ J\ {}^rdV + \int_{{}_rV} \delta\Delta_{t'} \eta_{xx}^{(k)}\ {}^{t'}\tau_{xx}\ {}^{t'}J\ {}^rdV$$
$$= \int_{{}_r\Gamma_t} \delta_0\boldsymbol{u}^{\mathsf{T}} \cdot {}_0^{t+\Delta t}\boldsymbol{t}\ J_\Gamma\ {}^rd\Gamma_t - \int_{{}_rV} \delta_{t+\Delta t'} e_{xx}{}^{(k-1)}\ {}^{t+\Delta t'}\tau_{xx}^{(k-1)}\ {}^{t+\Delta t'}J^{(k-1)}\ {}^rdV. \tag{2.33}$$

The Jacobian transformation factors are defined as follows:

$$\begin{aligned} {}^{t'}J &\equiv \det\left(\left[{}_r^{t'}x_{i,j}\right]\right) = \frac{{}^tL}{2} \\ {}^{t+\Delta t'}J^{(k-1)} &\equiv \det\left(\left[{}_r^{t+\Delta t'}x_{i,j}^{(k-1)}\right]\right) = \frac{{}^{t+\Delta t}L^{(k-1)}}{2} \\ J_\Gamma &\equiv \left\| \left[{}_r^0x_{i,j}n_j\right] \right\|. \end{aligned}$$

The isoparametric mappings $C_r \rightarrow C'_t$ and $C_r \rightarrow C'_{t+\Delta t^{(k-1)}}$ are defined in the standard fashion:

- The incremental displacement in the *local* 'current' frame C'_t, ${}_0\boldsymbol{u}'$, is an interpolation based on the nodal incremental displacements ${}^t\boldsymbol{d}'$ in C'_t

$${}_t\boldsymbol{u}' = \boldsymbol{N}^{\mathsf{T}} \cdot {}^t\boldsymbol{d}'$$

with

$${}^t\boldsymbol{d}'^{\mathsf{T}} = \left[\ u'_1 \quad v'_1 \quad w'_1 \quad u'_2 \quad v'_2 \quad w'_2\ \right]_t.$$

The incremental displacements in C'_t are expressed in terms of the *global* nodal displacement vector ${}^t\boldsymbol{d}$ as

$${}_t\boldsymbol{u}' = \boldsymbol{N}^{\mathsf{T}} \cdot {}^t\boldsymbol{T} \cdot {}^t\boldsymbol{d}.$$

- In the RHS of (2.33) a similar procedure is utilised in order to define the interpolation function for the incremental displacements ${}_{t+\Delta t}\boldsymbol{u}^{(k-1)}$ in the $(k-1)^{th}$ iterative *local* 'current' frame $C'_{t+\Delta t^{(k-1)}}$

$$\begin{aligned} {}_{t+\Delta t}\boldsymbol{u}'^{(k-1)} &= \boldsymbol{N}^{\mathsf{T}} \cdot {}^{t+\Delta t}\boldsymbol{d}'^{(k-1)} \\ &= \boldsymbol{N}^{\mathsf{T}} \cdot {}^{t+\Delta t}\boldsymbol{T}^{(k-1)} \cdot {}^{t+\Delta t}\boldsymbol{d}^{(k-1)} \end{aligned}$$

with

$$ {}^{t+\Delta t}\boldsymbol{d}'^{(k-1)} = \left[\begin{array}{cccccc} u'_1 & v'_1 & w'_1 & u'_2 & v'_2 & w'_2 \end{array} \right]_{t+\Delta t^{(k-1)}}. $$

The definition of the transformation matrices proceed in a straightforward fashion from the preceding section:

Transforming from C'_t to C_t

$$ {}^{t}\boldsymbol{T} = \left[{}^{t}_{t'}x_{i,j} \right] = \left[\begin{array}{cc} {}^{t}\boldsymbol{\mathcal{T}} & \mathbf{0}_{3\times3} \\ \mathbf{0}_{3\times3} & {}^{t}\boldsymbol{\mathcal{T}} \end{array} \right] $$

with

$$ {}^{t}\boldsymbol{\mathcal{T}} = \left[\begin{array}{ccc} \cos{}^{t}\phi \cos{}^{t}\theta & -\sin{}^{t}\theta & -\sin{}^{t}\phi \cos{}^{t}\theta \\ \cos{}^{t}\phi \sin{}^{t}\theta & \cos{}^{t}\theta & -\sin{}^{t}\phi \sin{}^{t}\theta \\ \sin{}^{t}\phi & 0 & \cos{}^{t}\phi \end{array} \right] $$

and from $C'_{t+\Delta t}$ to $C_{t+\Delta t}$

$$ {}^{t+\Delta t}\boldsymbol{T}^{(k-1)} = \left[{}^{t+\Delta t}_{t+\Delta t'}x^{(k-1)}_{i,j} \right] = \left[\begin{array}{cc} {}^{t+\Delta t}\boldsymbol{\mathcal{T}} & \mathbf{0}_{3\times3} \\ \mathbf{0}_{3\times3} & {}^{t+\Delta t}\boldsymbol{\mathcal{T}} \end{array} \right] $$

with

$$ {}^{t+\Delta t}\boldsymbol{\mathcal{T}} = \left[\begin{array}{ccc} \cos\hat{\phi}\cos\hat{\theta} & -\sin\hat{\theta} & -\sin\hat{\phi}\cos\hat{\theta} \\ \cos\hat{\phi}\sin\hat{\theta} & \cos\hat{\theta} & -\sin\hat{\phi}\sin\hat{\theta} \\ \sin\hat{\phi} & 0 & \cos\hat{\phi} \end{array} \right] $$

where $\hat{\phi} \equiv {}^{t+\Delta t}\phi^{(k-1)}$, $\hat{\theta} \equiv {}^{t+\Delta t}\theta^{(k-1)}$.

The *locally* discretised form of (2.33) is

$$ \begin{aligned} & \delta_{t'}\boldsymbol{u}^{\mathsf{T}} \cdot \left(\left\{ {}^{t}A\, {}^{t}L\, E\, {}^{t}\boldsymbol{N}_{x,x} \otimes {}^{t}\boldsymbol{N}_{x,x}{}^{\mathsf{T}} \right\} + \left\{ {}^{t}A\, {}^{t}L\, {}^{t}\tau_{xx}\, {}^{t}\aleph \right\} \right) \cdot \Delta_{t'}\boldsymbol{u}^{(k)} \\ = \; & {}^{t+\Delta t}_{0}\boldsymbol{t} - \delta_{t+\Delta t'}\boldsymbol{u}^{\mathsf{T}(k-1)} \cdot \left\{ {}^{t+\Delta t}A^{(k-1)}\, {}^{t+\Delta t}L^{(k-1)} \right\} {}^{t+\Delta t}\boldsymbol{N}_{x,x}{}^{(k-1)}\, {}^{t+\Delta t}\tau_{xx}{}^{(k-1)}, \end{aligned} \tag{2.34} $$

where the symbols used in (2.34) are defined as

$$ \begin{aligned} {}^{t}\tau_{xx} &\equiv {}^{t'}\tau_{xx} \\ {}^{t}A &\equiv {}^{t'}A \\ {}^{t}L &\equiv {}^{t'}L = {}^{t'}x_2 - {}^{t'}x_1 \\ {}^{t+\Delta t}\tau_{xx}{}^{(k-1)} &\equiv {}^{t+\Delta t'}\tau_{xx}{}^{(k-1)} \\ {}^{t+\Delta t}A^{(k-1)} &\equiv {}^{t+\Delta t'}A^{(k-1)} \\ {}^{t+\Delta t}L^{(k-1)} &\equiv {}^{t+\Delta t'}L^{(k-1)} = {}^{t+\Delta t'}x_2{}^{(k-1)} - {}^{t+\Delta t'}x_1{}^{(k-1)} \\ E &\equiv \text{Young's modulus} \end{aligned} $$

$$
\begin{aligned}
{}^{t}N^{\top}{}_{x,x} &= \frac{1}{{}^{t}L}\begin{bmatrix} -1 & 0 & 0 & 1 & 0 & 0 \end{bmatrix} \\
{}^{t}N^{\top}{}_{y,x} &= \frac{1}{{}^{t}L}\begin{bmatrix} 0 & -1 & 0 & 0 & 1 & 0 \end{bmatrix} \\
{}^{t}N^{\top}{}_{z,x} &= \frac{1}{{}^{t}L}\begin{bmatrix} 0 & 0 & -1 & 0 & 0 & 1 \end{bmatrix} \\
{}^{t+\Delta t}N^{\top}{}_{x,x}{}^{(k-1)} &= \frac{1}{{}^{t+\Delta t}L^{(k-1)}}\begin{bmatrix} -1 & 0 & 0 & 1 & 0 & 0 \end{bmatrix} \\
{}^{t+\Delta t}_{0}t^{\top} &= \begin{bmatrix} t_{1x} & t_{1y} & t_{1z} & t_{2x} & t_{2y} & t_{2z} \end{bmatrix}
\end{aligned}
$$

$$
{}^{t}\aleph = {}^{t}N_{x,x} \otimes {}^{t}N^{\top}{}_{x,x} + {}^{t}N_{y,x} \otimes {}^{t}N^{\top}{}_{y,x} + {}^{t}N_{z,x} \otimes {}^{t}N^{\top}{}_{z,x}\,.
$$

Assuming material incompressibility

$$
\frac{{}^{t+\Delta t}\rho^{(k-1)}}{{}^{t}\rho} = \frac{{}^{t}V}{{}^{t+\Delta t}V^{(k-1)}} = \frac{{}^{t}A\,{}^{t}L}{{}^{t+\Delta t}A^{(k-1)}\,{}^{t+\Delta t}L^{(k-1)}} = 1\,,
$$

the expression for ${}^{t+\Delta t}\tau_{xx}{}^{(k-1)}$ in (2.34) simplifies as follows:

$$
\begin{aligned}
{}^{t+\Delta t}\tau_{xx}{}^{(k-1)} &= \det\left[{}^{t+\Delta t}_{t}x_{i,j}^{(k-1)}\right]\left({}^{t+\Delta t}_{t}x_{1,1}^{(k-1)}\right)\left({}^{t+\Delta t}_{t}S_{xx}{}^{(k-1)}\right)\left({}^{t+\Delta t}_{t}x_{1,1}^{(k-1)}\right) \\
&= \left(\frac{{}^{t+\Delta t}\rho^{(k-1)}}{{}^{t}\rho}\right)\left({}^{t+\Delta t}_{t}x_{1,1}^{(k-1)}\right)^{2}\left({}^{t+\Delta t}_{t}S_{xx}{}^{(k-1)}\right) \\
&= \left({}^{t+\Delta t}_{t}x_{1,1}^{(k-1)}\right)^{2}\left({}^{t+\Delta t}_{t}S_{xx}{}^{(k-1)}\right) \\
&= (\Phi)^{2}\left({}^{t+\Delta t}_{t}S_{xx}{}^{(k-1)}\right) \qquad (2.35)
\end{aligned}
$$

where

$$
\begin{aligned}
\Phi &\equiv \Phi\left({}^{t}\phi, {}^{t+\Delta t}\phi^{(k-1)}, {}^{t}\theta, {}^{t+\Delta t}\theta^{(k-1)}\right) \\
&= \left({}^{t+\Delta t}_{t}x_{1,1}^{(k-1)}\right) \\
&= \left[{}^{t+\Delta t}\boldsymbol{T}^{\top(k-1)} \cdot {}^{t}\boldsymbol{T}\right]_{(i,j=1)} \\
&= \cos\hat{\phi}\cos{}^{t}\phi\left(\cos\hat{\theta}\cos{}^{t}\theta + \sin\hat{\theta}\sin{}^{t}\theta\right)\,.
\end{aligned}
$$

The $(k-1)^{th}$ iterative stress estimate for the UL procedure takes on the form

$$
{}^{t+\Delta t}_{t}S_{xx}{}^{(k-1)} = {}^{t}\tau_{xx} + E\left({}^{t+\Delta t}\overline{\aleph}^{(k-1)}\right)\cdot {}^{t+\Delta t}\boldsymbol{u}'^{(k-1)}
$$

for

$$
{}^{t}\overline{\aleph} \equiv {}^{t}N^{\top}{}_{x,x} + \tfrac{1}{2}{}^{t}\boldsymbol{u}^{\top}\cdot{}^{t}\boldsymbol{T}^{\top}\cdot{}^{t}\aleph
$$

Globalising the discretised UL formulation, (2.34) becomes

$$
\underbrace{\left[{}^{t}\boldsymbol{T}^{\top}\cdot{}^{0}A\,{}^{0}L\left(\left\{E\,{}^{t}N_{x,x}\otimes{}^{t}N^{\top}{}_{x,x}\right\} + \left\{{}^{t}\tau_{xx}\,{}^{t}\aleph\right\}\right)\cdot{}^{t}\boldsymbol{T}\right]}_{{}^{t}\boldsymbol{K}}\cdot\Delta_{t}\boldsymbol{u}^{(k)}
$$

$$
= {}^{t+\Delta t}_{0}\boldsymbol{t} - \left[{}^{t+\Delta t}\boldsymbol{T}^{\top(k-1)}\cdot\boldsymbol{\mathcal{L}}^{(k-1)}\cdot{}^{t+\Delta t}\boldsymbol{T}^{(k-1)}\cdot{}_{t+\Delta t}\boldsymbol{u}^{(k-1)}\right] \qquad (2.36)
$$

where

$$\mathcal{L}^{(k-1)} = (\Phi)^2 \left\{ {}^0A\, {}^0L\, {}^{t+\Delta t}\boldsymbol{N}_{x,x}{}^{(k-1)} \right\} \left\{ {}^t\tau_{xx} + E\left({}^{t+\Delta t}\overline{\aleph}^{(k-1)} \right) \right\} .$$

A comparison between (2.28) and (2.36) emphasises the substantial differences which exist between the TL and UL methodologies.

From (2.36) the standard quasi Newton-Raphson iterative form for the UL is obtained:

$$\underbrace{{}^t\boldsymbol{K} \cdot \Delta_t\boldsymbol{u}^{(k)}}_{{}_t\boldsymbol{Q}^{(k)}} = {}^{t+\Delta t}_{0}\mathfrak{R} - {}^{t+\Delta t}_{0}\boldsymbol{Q}^{(k-1)} . \tag{2.37}$$

For the UL formulation the full Newton-Raphson iterative procedure could also have been employed, so that

$${}^{t+\Delta t}\boldsymbol{K}^{(k-1)} \cdot \Delta_t\boldsymbol{u}^{(k)} = {}^{t+\Delta t}_{0}\mathfrak{R} - {}^{t+\Delta t}_{0}\boldsymbol{Q}^{(k-1)} .$$

Chapter 3

Design Sensitivity Analysis

3.1 Variational Formulation

3.1.1 General Ideas on the formulation of Design Sensitivity Analysis

The object of DSA is to obtain a vector, $\nabla_{\boldsymbol{b}} \Psi \equiv \frac{d\Psi}{d\boldsymbol{b}}$, which expresses the sensitivity of an arbitrary functional $\Psi \equiv \Psi(\boldsymbol{b})$ subject to variation of the design parameters $\boldsymbol{b}$.

For realistic applications the sensitivity matrix $\nabla_{\boldsymbol{b}} \Psi$ is usually found for

$$\Psi \in \{\text{objective function, constraint functions}\} .$$

These sensitivities are crucial in implementing structural optimisation, for which DSA is commonly employed; that is, DSA has to solve for

$$\nabla_{\boldsymbol{b}} f, \ \nabla_{\boldsymbol{b}} g_i \qquad i \in I_\varepsilon, \ \varepsilon = \{\text{active constraints}\}$$

which represents the generalised cost functional $f(\boldsymbol{u}, \boldsymbol{b})$ and generalised constraints $g_i(\boldsymbol{u}, \boldsymbol{b})$, respectively.

More specifically, for the research presented here, the object of investigating DSA is to show that

i. Generalised DSA, specifically the direct differentiation method (DDM), can be reformulated and discretised in a manner *analogous* to the element formulations employed in Finite Element Analysis (FEA).

ii. The FE analogous, or 'pseudo-element', formulation can be implemented in the ABAQUS user element routine UEL in order to perform sensitivity analysis, thus enabling the implementation of structural optimisation using ABAQUS.

For problems in engineering mechanics the design parameters $\boldsymbol{b}$ fall broadly into four categories:[1] [27]

1. Parameters which influence the elasticity (or elastic-predictor) matrix. (ie. part of the material model)
2. Shape or configuration variables. (ie. the geometric design of a structure)
3. Support and loading conditions.
4. Topological support parameters, eg. number of joints, elements or connections.

The functional Ψ may be quite general, but for applications in mechanics is usually formulated in terms of position $\boldsymbol{x}$, response variables - such as displacement $\boldsymbol{u}$, strain $\boldsymbol{\varepsilon}$ or stress $\boldsymbol{\tau}$) - and design parameters $\boldsymbol{b}$, e.g. [35]

$$\begin{aligned}\Psi &= \int_{{}^{r}V} \mathcal{F}\left({}_{0}^{t+\Delta t}S_{ij},\ {}_{0}^{t+\Delta t}\varepsilon_{ij},\ {}_{0}^{t+\Delta t}u_i,\ b_i\right)\ J\ {}^{r}dV \\ &+ \int_{{}^{r}\Gamma_t} \mathcal{H}\left({}_{0}^{t+\Delta t}u_i,\ b_i\right)\ J_\Gamma\ {}^{r}d\Gamma_t \\ &+ \int_{{}^{r}\Gamma_u} \mathcal{G}\left({}_{0}^{t+\Delta t}t_i,\ b_i\right)\ J_\Gamma\ {}^{r}d\Gamma_u\end{aligned}$$

The complicating factor in obtaining sensitivity vectors for problems in mechanics is the *implicit* dependence of Ψ on the design parameters $\boldsymbol{b}$

$$\Psi \equiv \Psi\left({}_{0}^{t+\Delta t}\boldsymbol{u},\ \boldsymbol{b}\right) \equiv \Psi\left({}_{0}^{t+\Delta t}\boldsymbol{u}(\boldsymbol{b}),\ \boldsymbol{b}\right).$$

Further complexity arises from the dependence of Ψ on response variables other than displacement, e.g. ${}^{t+\Delta t}\boldsymbol{\tau}$ and ${}^{t+\Delta t}\boldsymbol{\varepsilon}$, especially where the response variables are implicitly formulated in terms of displacement, ${}_{0}^{t+\Delta t}\boldsymbol{u}$.

Using the chain rule, the sensitivity vector for the functional Ψ is simply obtained as

$$\left(\nabla_{\boldsymbol{b}}\Psi\right)_i = \frac{d\Psi}{db_i} = \frac{\partial\Psi}{\partial u_j}\frac{du_j}{db_i} + \frac{\partial\Psi}{\partial b_i} \tag{3.1}$$

[1] In this work only category **1** and **2** parameter sensitivities are investigated, generally referred to as *non-shape* and *shape* sensitivity, respectively.

where $\frac{\partial \Psi}{\partial u_j}$, as well as the *explicit* dependency of Ψ on $\boldsymbol{b}$, $\frac{\partial \Psi}{\partial b_i}$, can be derived analytically in a straightforward fashion.

The main pursuit of computational DSA then, is to find the *implicit* dependency of $\boldsymbol{u}$ on $\boldsymbol{b}$, i.e. $\frac{du_j}{db_i}$. As described in the introduction, several methods exist which, to varying degrees of success, enable the numerical solution of $\frac{du_j}{db_i}$ for various types of FEA problems. For the work presented here the Direct Differentiation Method (DDM) is preferred.

Three distinct DDM approaches are discussed, computationally implemented and analysed:

1. 'intuitive' non-shape DSA
2. 'rigorous' non-shape DSA
3. shape, or geometric, DSA

The DDM procedure starts by defining the state of equilibrium at time $t + \Delta t$, ${}^{t+\Delta t}F(\boldsymbol{u}, \boldsymbol{b})$, as:

$$ {}^{t+\Delta t}F(\boldsymbol{u}, \boldsymbol{b}) \equiv {}^{t+\Delta t}_{0}Q(\boldsymbol{u}, \boldsymbol{b}) - {}^{t+\Delta t}\Re = 0 \tag{3.2} $$

with

$$ \begin{aligned} {}^{t+\Delta t}_{0}Q &\equiv \int_{{}^{0}V} {}^{t+\Delta t}_{0}S_{ij}\, \delta {}^{t+\Delta t}_{0}\varepsilon_{ij}\, {}^{0}dV && \text{for TL}, \\ {}^{t+\Delta t}_{0}Q &\equiv \int_{{}^{t+\Delta t}V} {}^{t+\Delta t}\tau_{ij}\, \delta {}^{t+\Delta t}e_{ij}\, {}^{t+\Delta t}dV && \text{for UL}, \end{aligned} \tag{3.3} $$

so that for the I^{th} element of a generalised FE discretisation, (3.2) may be formulated as

$$ {}^{t+\Delta t}\boldsymbol{F}_I(\boldsymbol{u}, \boldsymbol{b}) \equiv {}^{t+\Delta t}_{0}\boldsymbol{Q}_I(\boldsymbol{u}, \boldsymbol{b}) - {}^{t+\Delta t}\Re_I = \boldsymbol{0} $$

Applying the design sensitivity operator $\overline{\delta} \equiv \nabla_{\boldsymbol{b}}$ (3.1), the differentiation operation on ${}^{t+\Delta t}F(\boldsymbol{u}, \boldsymbol{b})$ can be separated into distinct parts:

$$ \overline{\delta}\left({}^{t+\Delta t}F\right) = \left(\tilde{\delta} + \bar{\bar{\delta}}\right) {}^{t+\Delta t}F = 0 \tag{3.4} $$

where, from [35],

$$ \tilde{\delta} \equiv \frac{du_j}{db_i}\frac{\partial}{\partial u_j}, \quad \bar{\bar{\delta}} \equiv \frac{\partial}{\partial b_i}. $$

The variational expression (3.4) can thus be restated as

$$ \frac{\partial\, {}^{t+\Delta t}F}{\partial u_j}\frac{du_j}{db_i} = -\frac{\partial\, {}^{t+\Delta t}F}{\partial b_i} $$

or

$$\left(\frac{\partial\, {}^{t+\Delta t}\boldsymbol{F}}{\partial \boldsymbol{u}}_{I}\right)\cdot\left(\frac{d\boldsymbol{u}}{d\boldsymbol{b}_{I}}\right)=-\left(\frac{\partial\, {}^{t+\Delta t}\boldsymbol{F}}{\partial \boldsymbol{b}}\right)_{I} \tag{3.5}$$

for the I^{th} element of the FE discretisation.

Several assumptions are made which aim to simplify the DSA formulation while still reflecting the majority of actual DSA applications:

- Conservative, or 'non-follower', forces are assumed so that ${}^{t+\Delta t}\Re$ becomes deformation independent and

$$\left(\frac{\partial\, {}^{t+\Delta t}\boldsymbol{F}}{\partial \boldsymbol{u}}\right)_{I}=\left(\frac{\partial\, {}^{t+\Delta t}_{0}\boldsymbol{Q}}{\partial \boldsymbol{u}}\right)_{I}. \tag{3.6}$$

- In a similar vein, the concentrated nodal traction forces ${}^{t+\Delta t}_{0}\boldsymbol{t}$, included in ${}^{t+\Delta t}\Re$, have no *explicit* dependence on the *shape* design parameters $\boldsymbol{b} \equiv \boldsymbol{h}$ so that

$$\left(\frac{\partial^{t+\Delta t}\Re}{\partial \boldsymbol{b}_{t}}\right)_{I}=0.$$

- Furthermore, ${}^{t+\Delta t}\Re$ is assumed to have no *explicit* dependence on the *non-shape* design variables:

$$\left(\frac{\partial^{t+\Delta t}\Re}{\partial \boldsymbol{b}}\right)_{I}=0 \quad \forall \boldsymbol{b}.$$

  It follows that

$$\left(\frac{\partial\, {}^{t+\Delta t}\boldsymbol{F}}{\partial \boldsymbol{b}}\right)_{I}=\left(\frac{\partial\, {}^{t+\Delta t}_{0}\boldsymbol{Q}}{\partial \boldsymbol{b}}\right)_{I}. \tag{3.7}$$

Combining (3.6) and (3.7), equation (3.5) is reduced to

$$\left(\frac{\partial\, {}^{t+\Delta t}_{0}\boldsymbol{Q}}{\partial \boldsymbol{u}}\right)_{I}\cdot\left(\frac{d\boldsymbol{u}_{I}}{d\boldsymbol{b}}\right)_{I}=-\left(\frac{\partial\, {}^{t+\Delta t}_{0}\boldsymbol{Q}}{\partial \boldsymbol{b}}\right)_{I}.$$

The *non-shape* DDM design sensitivity approaches exhibit complementary characteristics:

- The 'intuitive' approach is approximate, but simpler to implement and computationally less expensive.

- The 'rigorous' approach is completely general and more accurate, but at the same time also more complex and computationally more expensive.

For the purposes of *shape* DSA, only the 'rigorous' approach is implemented due to its more accurate performance for a wider range of applications.

The section concludes by investigating the applications of DSA to displacement-based reponse variables, specifically stress $\boldsymbol{\tau}$.

3.1.2 'Intuitive' Approach

From (2.32) and (2.37) the quasi Newton-Raphson iterative solution scheme can be written generally, for TL and UL, as

$$\Delta \boldsymbol{Q}_I{}^{(k)} = {}^{t+\Delta t}\boldsymbol{\Re}_I - {}^{t+\Delta t}_{0}\boldsymbol{Q}_I{}^{(k-1)},$$

where $\Delta \boldsymbol{Q}_I{}^{(k)}$ is defined in terms of $\Delta \boldsymbol{u}_I$ by

$$\Delta \boldsymbol{Q}_I{}^{(k)} = \boldsymbol{K}_I \cdot \Delta \boldsymbol{u}_I . \tag{3.8}$$

Equation (3.8) suggests that the stiffness matrix $\boldsymbol{K} \equiv \boldsymbol{K}_I$ may be interpreted as an approximation to the expression in (3.6). Hence, the approximation

$$\boldsymbol{K} \equiv \frac{\partial\, {}^{t+\Delta t}_{0}\boldsymbol{Q}_I{}^{(k)}}{\partial \boldsymbol{u}_I} \approx \frac{\partial\, {}^{t+\Delta t}_{0}\boldsymbol{Q}_I}{\partial \boldsymbol{u}_I}$$

may be included in the DDM expression (3.8) so that

$$\boldsymbol{K} \cdot \frac{d\boldsymbol{u}_I}{d\boldsymbol{b}} = -\frac{\partial\, {}^{t+\Delta t}_{0}\boldsymbol{Q}_I}{\partial \boldsymbol{b}} . \tag{3.9}$$

The substitution of the stiffness matrix $\boldsymbol{K}$, obtained from the structural analysis phase, for $\frac{\partial\, {}^{t+\Delta t}_{0}\boldsymbol{Q}_I}{\partial \boldsymbol{u}_I}$ in the 'Intuitive' approach, characterises the central difference between the 'Rigorous' and 'Intuitive' methods of DSA; this substitution implicitly makes the 'Intuitive' method more approximate than the 'Rigorous' approach. The stiffness $\boldsymbol{K}$, stored after each structural analysis iteration, can be retrieved for the purpose of obtaining the matrix $\left(\frac{d\boldsymbol{u}}{d\boldsymbol{b}}\right)_I$. The RHS of (3.9) is analytically simplified, depending on whether shape or non-shape DSA is performed, and discretised.

The 'intuitive' method can be applied to *shape* and *non-shape* DSA problems alike. Since the method is by definition approximate, however, it is not applied to *shape* DSA, or structural optimisation for that matter, in the research presented here: *shape* DSA is dealt with exclusively in context of the 'rigorous' approach to DSA.

3.1.3 'Rigorous' Approach

For the sake of brevity, and particularly with a view towards introducing *shape* DSA, the TL formulation will be used exclusively in this section.

Employing the definitions in (3.2) and (3.3), and referring to Section 2.1.2, the expression (3.4) is restated for the TL formulation as

$$\begin{aligned} & \tilde{\delta}\left(\int_{{}_0V} {}_0^{t+\Delta t}S_{ij}\ \delta_0^{t+\Delta t}\varepsilon_{ij}\ {}^0dV - {}^{t+\Delta t}\Re\right) \\ + \quad & \bar{\bar{\delta}}\left(\int_{{}_0V} {}_0^{t+\Delta t}S_{ij}\ \delta_0^{t+\Delta t}\varepsilon_{ij}\ {}^0dV - {}^{t+\Delta t}\Re\right) = 0. \end{aligned} \tag{3.10}$$

In introducing the 'rigorous' approach, it is instructive to generalise the external load expression ${}^{t+\Delta t}\Re$ as

$${}^{t+\Delta t}\Re = \int_{{}_0V} {}_0^{t+\Delta t}\rho\ \delta_0^{t+\Delta t}\boldsymbol{u}^{\mathsf{T}} \cdot {}_0^{t+\Delta t}\boldsymbol{f}\ {}^0dV + \int_{{}_0\Gamma_t} \delta_0^{t+\Delta t}\boldsymbol{u}^{\mathsf{T}} \cdot {}_0^{t+\Delta t}\boldsymbol{t}\ {}^0d\Gamma_t,$$

by including body forces in the expression for the *externally* applied loadings, although these forces are neglected for the applications considered in this thesis.

Applying the combined localisation and isoparametric mapping $C_0 \rightarrow C'_0 \rightarrow C_r$, from the *global* 'initial' frame C_0 to the 'natural' frame C_r, to (3.10), $\bar{\delta}\left({}^{t+\Delta t}\boldsymbol{F}\right)$ in (3.4) is restated as

$$\begin{aligned} & \left\{\int_{{}_rV} \tilde{\delta}\left(\delta_0^{t+\Delta t}\boldsymbol{\varepsilon}^{\mathsf{T}} \cdot {}_0^{t+\Delta t}\boldsymbol{S}\ J\right)\ {}^rdV + \int_{{}_rV} \bar{\bar{\delta}}\left(\delta_0^{t+\Delta t}\boldsymbol{\varepsilon}^{\mathsf{T}} \cdot {}_0^{t+\Delta t}\boldsymbol{S}\ J\right)\ {}^rdV\right\} \\ - & \left\{\int_{{}_rV} \tilde{\delta}\left({}_0^{t+\Delta t}\rho\ \delta_0^{t+\Delta t}\boldsymbol{u}^{\mathsf{T}} \cdot {}_0^{t+\Delta t}\boldsymbol{f}\ J\right)\ {}^rdV + \int_{{}_rV} \bar{\bar{\delta}}\left({}_0^{t+\Delta t}\rho\ \delta_0^{t+\Delta t}\boldsymbol{u}^{\mathsf{T}} \cdot {}_0^{t+\Delta t}\boldsymbol{f}\ J\right)\ {}^rdV\right\} \\ - & \left\{\int_{{}_r\Gamma_t} \tilde{\delta}\left(\delta_0^{t+\Delta t}\boldsymbol{u}^{\mathsf{T}} \cdot {}_0^{t+\Delta t}\boldsymbol{t}\ J_\Gamma\right)\ {}^rd\Gamma_t + \int_{{}_r\Gamma_t} \bar{\bar{\delta}}\left(\delta_0^{t+\Delta t}\boldsymbol{u}^{\mathsf{T}} \cdot {}_0^{t+\Delta t}\boldsymbol{t}\ J_\Gamma\right)\ {}^rd\Gamma_t\right\} = 0. \end{aligned}$$

The expression in (3.10) simplifies the DSA procedure subject to several assumptions and conditions, pertaining primarily to the loading conditions. The assumptions introduced are standard in much of the literature on DSA; the slight reduction in generality of the DSA formulation is more than offset by the considerable simplification of (3.10):

- Assuming material incompressibility implies

  $${}^0\rho = {}_0^t\rho = {}_0^{t+\Delta t}\rho$$

  so that effectively

  $$\tilde{\delta}\left({}_0^{t+\Delta t}\rho\right) = 0.$$

- The variation of deformation $\delta_0^{t+\Delta t}\boldsymbol{u}$ is arbitrary and, therefore, design parameter independent:

$$\overline{\delta}\left(\delta_0^{t+\Delta t}\boldsymbol{u}\right) = \tilde{\delta}\left(\delta_0^{t+\Delta t}\boldsymbol{u}\right) + \overline{\overline{\delta}}\left(\delta_0^{t+\Delta t}\boldsymbol{u}\right) = 0.$$

- Assuming 'non-follower' forces, ie. the traction ${}_0^{t+\Delta t}\boldsymbol{t}$ and body force ${}_0^{t+\Delta t}\boldsymbol{f}$ are not deformation, ${}_0^{t+\Delta t}\boldsymbol{u}$, dependent:

$$\tilde{\delta}\left({}_0^{t+\Delta t}\boldsymbol{t}\right) = 0, \quad \tilde{\delta}\left({}_0^{t+\Delta t}\boldsymbol{f}\right) = 0.$$

Imposing the conditions above, equation (3.10) reduces to

$$\begin{aligned}
&\left\{\int_{{}^rV} \tilde{\delta}\left(\delta_0^{t+\Delta t}\boldsymbol{\varepsilon}^{\mathsf{T}} \cdot {}_0^{t+\Delta t}\boldsymbol{S}\right)\, J\, {}^rdV + \int_{{}^rV} \overline{\overline{\delta}}\left(\delta_0^{t+\Delta t}\boldsymbol{\varepsilon}^{\mathsf{T}} \cdot {}_0^{t+\Delta t}\boldsymbol{S}\, J\right)\, {}^rdV\right\} \\
&- \int_{{}^rV} \overline{\overline{\delta}}\left({}_0^{t+\Delta t}\rho\, \delta_0^{t+\Delta t}\boldsymbol{u}^{\mathsf{T}} \cdot {}_0^{t+\Delta t}\boldsymbol{f}\, J\right)\, {}^rdV - \int_{{}^r\Gamma_t} \overline{\overline{\delta}}\left(\delta_0^{t+\Delta t}\boldsymbol{u}^{\mathsf{T}} \cdot {}_0^{t+\Delta t}\boldsymbol{t}\, J_\Gamma\right)\, {}^rd\Gamma_t \\
&= 0
\end{aligned} \tag{3.10}$$

The following specific assumptions are introduced in order to simplify (3.10) for the particular applications considered here:

- Body force is negligible compared to traction, thus

$${}_0^{t+\Delta t}\boldsymbol{f} \to 0.$$

- Traction force ${}_0^{t+\Delta t}\boldsymbol{t}$ has no *shape* or *non-shape* design parameter dependence

$$\overline{\overline{\delta}}\left({}_0^{t+\Delta t}\boldsymbol{t}\right) = 0.$$

- Traction ${}_0^{t+\Delta t}\boldsymbol{t}$ is a concentrated nodal force, so that

$$\begin{aligned}
&\int_{{}^r\Gamma_t} \overline{\overline{\delta}}\left(\delta_0^{t+\Delta t}\boldsymbol{u}^{\mathsf{T}} \cdot {}_0^{t+\Delta t}\boldsymbol{t}\, J_\Gamma\right)\, {}^rd\Gamma_t \\
&= \left[\overline{\overline{\delta}}\left(\delta_0^{t+\Delta t}\boldsymbol{u}^{\mathsf{T}} \cdot {}_0^{t+\Delta t}\boldsymbol{t}\right)\right]_{node=1} + \left[\overline{\overline{\delta}}\left(\delta_0^{t+\Delta t}\boldsymbol{u}^{\mathsf{T}} \cdot {}_0^{t+\Delta t}\boldsymbol{t}\right)\right]_{node=2} \\
&= 0.
\end{aligned}$$

Introducing these further assumptions into (3.10), the variational form of the 'rigorous' DSA formulation may then simply be stated as

$$\int_{{}^rV} \tilde{\delta}\left(\delta_0^{t+\Delta t}\boldsymbol{\varepsilon}^{\mathsf{T}} \cdot {}_0^{t+\Delta t}\boldsymbol{S}\right)\, J\, {}^rdV + \int_{{}^rV} \overline{\overline{\delta}}\left(\delta_0^{t+\Delta t}\boldsymbol{\varepsilon}^{\mathsf{T}} \cdot {}_0^{t+\Delta t}\boldsymbol{S}\, J\right)\, {}^rdV = 0 \tag{3.11}$$

which applies generally to problems involving *shape* or *non-shape* design parameters, subject to the constraints and assumptions imposed above.

The next two sections discuss further simplifications that may be introduced, depending on whether *shape* or *non-shape* design parameters $\boldsymbol{b}$ are utilised.

Shape DSA

In general many real-world structural optimisation applications investigated focus on finding an optimal geometric structural design and, consequently *shape* DSA plays an important role in computational sensitivity analysis.

Several unified formulations which accommodate both *shape* and *non-shape* DSA have been introduced in recent years. The *shape* DSA procedure employed here is based on a Euler-Lagrange kinematic description first proposed by Haber[16].

Conceptually, *shape* design sensitivity analysis is implemented by introducing a *perturbation* mapping, $C_0^\star \rightarrow C_0$, into Fig.[3.1].

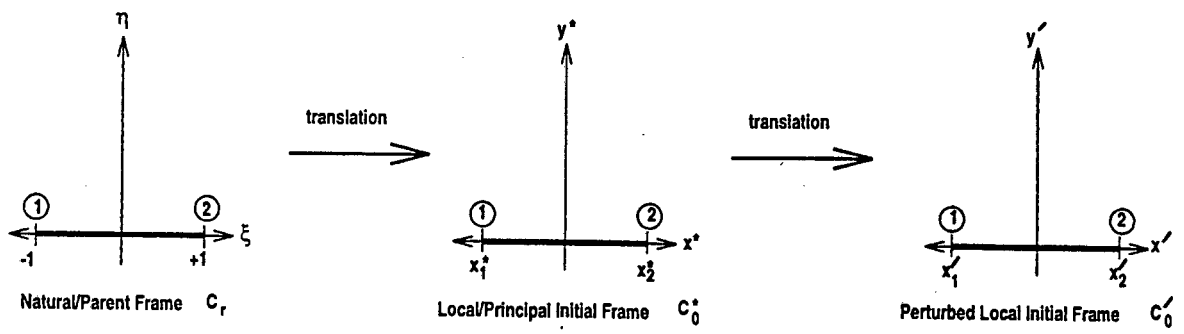

Figure 3.1: *Shape* design parameters.

The perturbation mapping from the original, or 'template', *local* 'initial' frame $C_0^\star$ [2] to the *perturbed global* 'initial' frame C_0 is defined in terms of *shape* design variables $\boldsymbol{b} = \boldsymbol{b}_t$.

For each truss element the perturbation may be as simple as

$$x_1 = x_1^\star + \Delta h_1\,,$$
$$x_2 = x_2^\star + \Delta h_2\,,$$

for positive or negative structural design perturbations $\Delta \boldsymbol{h}$.

Recalling (2.24) there now exists a clear *shape* design variable dependence in the transformation matrix[3] ${}^0\hat{T}_{ij} \equiv {}^0T_{ij}(\boldsymbol{h})_{,j} \equiv {}^{0'}_{0}x_{i,j}$, and hence, a *shape* design dependence for both the Jacobian integration factors J and J_Γ. As a consequence of this dependence, (3.11) cannot be further simplified in its variational form for *shape* DSA.

[2] Refer to Fig.[3.1]

[3] The transformation matrix ${}^0\widehat{\boldsymbol{T}}^{\mathsf{T}}$ now *implicitly* represents the perturbation mapping $C_0^\star \rightarrow C_0 \rightarrow C'_0$.

Non-shape DSA

A significant portion of the physical problems to which DSA is applied, utilise only *non-shape* design parameters and thereby avoid the various attendant complications of 'shape' DSA.

Young's modulus and the truss cross-sectional area[4] are frequently employed as (*non-shape*) design parameters for the specific case of the truss/bar element implementation. For the research conducted and results presented here the truss cross-section ${}^0A$ was consistently chosen as a representative *non-shape* design parameter.

Selecting ${}^0A$ as a single *non-shape* design parameter, the DSA variational formulation in (3.11) simplifies to

$$\int_{{}^rV} \tilde{\delta}\left(\delta_0^{t+\Delta t}\boldsymbol{\varepsilon}^{\mathsf{T}} \cdot {}_0^{t+\Delta t}\boldsymbol{S}\right) J\, {}^rdV + \bar{\bar{\delta}}\left({}^0A\right) \int_{{}^rL} \delta_0^{t+\Delta t}\boldsymbol{\varepsilon}^{\mathsf{T}} \cdot {}_0^{t+\Delta t}\boldsymbol{S}\, J\, {}^rdL = 0\,.$$

3.1.4 Stress Sensitivity Analysis

For displacement based *one-field* variational formulations, eg. TL or UL, displacement is the primary solution variable from which the other reponse variables, for instance strain, are derived. Recalling the form of the sensitivity operators (cf. (3.1) and (3.4)) introduced in Section (3.1.1), the design sensitivity procedures investigated thus far can justifiably be referred to as *displacement* DSA. In the majority of physical applications, however, objective and constraint functions are commonly defined in terms of a combination of reponse variables (displacement, strain, stress). Investigating a generalised stress constraint of the form $\Psi \equiv \Psi(\boldsymbol{\tau})$, the definition of the sensitivity operator in (3.1) is altered as follows:

$$\begin{aligned} \nabla_{\boldsymbol{b}} \Psi \equiv \frac{d\Psi}{d\boldsymbol{b}} &= \frac{\partial \Psi}{\partial \boldsymbol{\tau}} \cdot \nabla_{\boldsymbol{b}} \boldsymbol{\tau} + \frac{\partial \Psi}{\partial \boldsymbol{b}} \\ &= \frac{\partial \Psi}{\partial \boldsymbol{\tau}} \left(\frac{\partial \boldsymbol{\tau}}{\partial \boldsymbol{u}} \cdot \nabla_{\boldsymbol{b}} \boldsymbol{u} + \frac{\partial \boldsymbol{\tau}}{\partial \boldsymbol{b}} \right) + \frac{\partial \Psi}{\partial \boldsymbol{b}}\,. \end{aligned} \tag{3.13}$$

Even for the relatively simple formulation of a truss structure subject to a stress constraint $\Psi(\boldsymbol{\tau})$, analytically deriving the constraint sensitivity expression, as formulated in (3.12), is a non-trivial exercise, as is demonstrated in the next section.

[4] Variations in the *initial* truss cross-section ${}^0A$ do not influence the *initial* structural configuration.

3.2 Discretisation

3.2.1 'Intuitive' Non-shape DSA

Although the theoretical formulations and concepts introduced for the various DSA procedures in the previous section are relatively straightforward, performing the discretisation of these formulations is somewhat more complex. The discretisations for the 'intuitive' non-shape, 'rigorous' non-shape and shape DSA implementations are entirely original and are generally formulated to enable integration within the user element routines of most FEA codes as 'pseudo'-elements, in particular the UEL module in ABAQUS.

The 'intuitive' approach to DSA is inherently approximate, as mentioned in Section 3.1.2, and is employed exclusively in applications involving *non-shape* design parameters for the purposes of the research presented here. In addition, since the 'intuitive' approach is based on the UL formulation, the procedure is usually limited to small strain behaviour, whereas the TL-based 'rigorous' approach is more commonly used for *large* deformation accompanied by a *large* strain response.

For the applications considered here, the truss element cross-sectional area A, as a representative *non-shape* design parameter, was used consistently in generating results for *non-shape* DSA.

The discretised form of the 'intuitive' approach, for the design parameter A, follows from (2.28), (2.36) and (3.9):

$$\boldsymbol{K} \cdot \frac{d\boldsymbol{u}_I}{d\boldsymbol{b}} \equiv \boldsymbol{K} \cdot \nabla_{\boldsymbol{b}} \boldsymbol{u}_I = -\frac{\partial \left({}^{t+\Delta t}_{0}\boldsymbol{Q}_I \right)}{\partial \boldsymbol{b}}$$

which, for the UL, becomes

$$\begin{aligned} & \left[{}^{t}\boldsymbol{T}^{\mathsf{T}} \cdot {}^{0}A\, {}^{0}L \left(\left\{ E\, {}^{t}\boldsymbol{N}_{x,x} \otimes {}^{t}\boldsymbol{N}^{\mathsf{T}}{}_{x,x} \right\} + \left\{ {}^{t}\tau_{xx}\, {}^{t}\aleph \right\} \right) \cdot {}^{t}\boldsymbol{T} \right] \cdot \left(\nabla_{{}^{0}_{A}} {}^{t+\Delta t}\boldsymbol{u} \right) \\ = \; & - \left[{}^{t+\Delta t}\boldsymbol{T}^{\mathsf{T}} \cdot \overline{\mathcal{L}} \cdot {}^{t+\Delta t}\boldsymbol{T} \cdot {}_{t+\Delta t}\boldsymbol{u} \right] , \end{aligned}$$

where

$$\overline{\mathcal{L}} = \nabla_{{}^{0}_{A}} \mathcal{L} = (\Phi)^2 \left\{ {}^{0}L\, {}^{t+\Delta t}\boldsymbol{N}_{x,x} \right\} \left\{ {}^{t}\tau_{xx} + E \left({}^{t+\Delta t}\hat{\aleph} \right) \right\} ,$$

and for the TL takes on the form

$$\begin{aligned} & \left[{}^{0}\boldsymbol{T}^{\mathsf{T}} \cdot {}^{0}A\, {}^{0}L \left(\left\{ E\, {}^{0}\boldsymbol{N}_{x,x} \otimes {}^{0}\boldsymbol{N}^{\mathsf{T}}{}_{x,x} \right\} + \left\{ {}^{t}_{0}S_{xx}\, {}^{0}\aleph \right\} \right) \cdot {}^{0}\boldsymbol{T} \right] \cdot \left(\nabla_{{}^{0}_{A}} {}^{t+\Delta t}_{0}\boldsymbol{u} \right) \\ = \; & - \left[{}^{0}\boldsymbol{T}^{\mathsf{T}} \cdot \overline{\mathcal{K}} \cdot {}^{0}\boldsymbol{T} \cdot {}^{t+\Delta t}_{0}\boldsymbol{u} \right] , \end{aligned} \tag{3.14}$$

with

$$\overline{\mathcal{K}} = \nabla_{{}^{0}_{A}} \mathcal{K} = \left({}^{0}L\, E \right) {}^{0}\tilde{\aleph} \cdot {}^{0}\tilde{\hat{\aleph}}^{\mathsf{T}} .$$

3.2.2 'Rigorous' Non-shape DSA

Recalling the (TL) formulation for $\tilde{\delta}\left({}^{t+\Delta t}\boldsymbol{F}_I\right)$

$$\int_{{}^rV} \tilde{\delta}\left(\delta_0^{t+\Delta t}\boldsymbol{\varepsilon}^{\mathsf{T}} \cdot {}_0^{t+\Delta t}\boldsymbol{S}\right) J\, {}^rdV + \int_{{}^rV} \overline{\overline{\delta}}\left(\delta_0^{t+\Delta t}\boldsymbol{\varepsilon}^{\mathsf{T}} \cdot {}_0^{t+\Delta t}\boldsymbol{S}\, J\right) {}^rdV = 0 \tag{3.14}$$

from (3.11), and discretising (3.14) in the standard fashion by utilising the isoparametric mapping so that, recalling (2.28), the following expression is obtained:

$$\int_{{}^rV} \delta_0^{t+\Delta t}\boldsymbol{\varepsilon}^{\mathsf{T}} \cdot {}_0^{t+\Delta t}\boldsymbol{S}\, J\, {}^rdV = \delta\boldsymbol{u}^{\mathsf{T}} \cdot {}^0\boldsymbol{T}^{\mathsf{T}} \cdot \boldsymbol{\mathcal{K}} \cdot {}^0\boldsymbol{T} \cdot {}_0^{t+\Delta t}\boldsymbol{u}. \tag{3.15}$$

Substituting the discretised expression (3.15) into (3.14):

$$\tilde{\delta}\left({}^0\boldsymbol{T}^{\mathsf{T}} \cdot \boldsymbol{\mathcal{K}} \cdot {}^0\boldsymbol{T} \cdot {}_0^{t+\Delta t}\boldsymbol{u}\right) = -\,\overline{\overline{\delta}}\left({}^0\boldsymbol{T}^{\mathsf{T}} \cdot \boldsymbol{\mathcal{K}} \cdot {}^0\boldsymbol{T} \cdot {}_0^{t+\Delta t}\boldsymbol{u}\right). \tag{3.16}$$

For *non-shape* DSA, using the truss cross-sectional area ${}^0A$ as a representative design parameter, and referring to the RHS of (3.13) for the result of

$$\overline{\overline{\delta}}\left({}^0\boldsymbol{T}^{\mathsf{T}} \cdot \boldsymbol{\mathcal{K}} \cdot {}^0\boldsymbol{T} \cdot {}_0^{t+\Delta t}\boldsymbol{u}\right) \tag{3.17}$$

(3.16) becomes

$${}^0\boldsymbol{T}^{\mathsf{T}} \cdot \left[\left(\tilde{\delta}\boldsymbol{\mathcal{K}}\right) \cdot {}^0\boldsymbol{T} \cdot {}_0^{t+\Delta t}\boldsymbol{u} + \boldsymbol{\mathcal{K}} \cdot {}^0\boldsymbol{T} \cdot \tilde{\delta}\left({}_0^{t+\Delta t}\boldsymbol{u}\right)\right] = -\left[{}^0\boldsymbol{T}^{\mathsf{T}} \cdot \overline{\boldsymbol{\mathcal{K}}} \cdot {}^0\boldsymbol{T} \cdot {}_0^{t+\Delta t}\boldsymbol{u}\right]$$

which, after a not inconsiderable amount of analytical manipulation, adopts a 'pseudo'-element discretisation

$$\boldsymbol{K}' \cdot \nabla_{{}^0A}\, {}_0^{t+\Delta t}\boldsymbol{u} = \boldsymbol{R}', \tag{3.18}$$

where the 'pseudo' stiffness matrix $\boldsymbol{K}'$ is defined as

$$\boldsymbol{K}' = {}^0\boldsymbol{T}^{\mathsf{T}} \cdot \boldsymbol{M} \cdot {}^0\boldsymbol{T}$$

for

$$\boldsymbol{M} = \left(E\, {}^0L\, {}^0A\right)\left[{}^0\tilde{\boldsymbol{\aleph}}^{\mathsf{T}} \cdot {}^0\boldsymbol{T} \cdot {}_0^{t+\Delta t}\boldsymbol{u} \cdot {}^0\boldsymbol{\aleph} + {}^0\tilde{\boldsymbol{\aleph}} \cdot {}_0^{t+\Delta t}\boldsymbol{u}^{\mathsf{T}} \cdot {}^0\boldsymbol{T}^{\mathsf{T}} \cdot \left(\tfrac{1}{2}\right) {}^0\boldsymbol{\aleph} + {}^0\tilde{\boldsymbol{\aleph}} \cdot {}^0\tilde{\boldsymbol{\aleph}}^{\mathsf{T}}\right],$$

and the 'pseudo' external loading $\boldsymbol{R}'$ may be expressed as

$$\boldsymbol{R}' = -\left[{}^0\boldsymbol{T}^{\mathsf{T}} \cdot \overline{\boldsymbol{\mathcal{K}}} \cdot {}^0\boldsymbol{T} \cdot {}_0^{t+\Delta t}\boldsymbol{u}\right].$$

The ability to formulate the discretised DSA equations in a 'pseudo'-element format is crucially important in enabling implementation of DSA into large FE codes, for example ABAQUS.

3.2.3 'Rigorous' Shape DSA

Referring to the analytical formulation of *shape* DSA in Section 3.1.3, the discretised DSA formulation in (3.16) is rewritten for *shape* DSA, in a form similar to (3.16), as

$$\tilde{\delta}\left({}^{0}\hat{\boldsymbol{T}}^{\mathsf{T}} \cdot \hat{\boldsymbol{\mathcal{K}}} \cdot {}^{0}\hat{\boldsymbol{T}} \cdot {}^{t+\Delta t}_{0}\boldsymbol{u} \right) = - \bar{\bar{\delta}}\left({}^{0}\hat{\boldsymbol{T}}^{\mathsf{T}} \cdot \hat{\boldsymbol{\mathcal{K}}} \cdot {}^{0}\hat{\boldsymbol{T}} \cdot {}^{t+\Delta t}_{0}\boldsymbol{u} \right) , \tag{3.19}$$

where $\boldsymbol{T} \equiv \hat{\boldsymbol{T}}$ and $\boldsymbol{\mathcal{K}} \equiv \hat{\boldsymbol{\mathcal{K}}}$ are sensitive[5] to perturbations in the *shape* design parameters $\boldsymbol{b} \equiv \boldsymbol{h}$, ie. $\hat{\boldsymbol{T}}$ and $\hat{\boldsymbol{\mathcal{K}}}$ are *explicitly* dependent on variations of the shape or structural configuration in the mapping $C_0^{\star} \rightarrow C'_0$. The difference between (3.16) and (3.19) arising from the substantially greater complexity involved in implementing the operator $\bar{\bar{\delta}}(\ldots)$ for *shape* DSA.

The LHS of (3.19) is not affected by the introduction of *shape* design parameters and, referring to (3.18), (3.19) is therefore simply restated as

$$\boldsymbol{K}' \cdot \nabla_{{}^{0}_{A}0} {}^{t+\Delta t}_{0}\boldsymbol{u} = - \bar{\bar{\delta}}\left({}^{0}\hat{\boldsymbol{T}}^{\mathsf{T}} \cdot \hat{\boldsymbol{\mathcal{K}}} \cdot {}^{0}\hat{\boldsymbol{T}} \cdot {}^{t+\Delta t}_{0}\boldsymbol{u} \right) . \tag{3.20}$$

The RHS of (3.20), after some manipulation, takes on the form

$$- \left[\bar{\bar{\delta}}\left({}^{0}\hat{\boldsymbol{T}}^{\mathsf{T}} \right) \cdot \hat{\boldsymbol{\mathcal{K}}} \cdot {}^{0}\hat{\boldsymbol{T}} + {}^{0}\hat{\boldsymbol{T}}^{\mathsf{T}} \cdot \bar{\bar{\delta}}\left(\hat{\boldsymbol{\mathcal{K}}} \right) \cdot {}^{0}\hat{\boldsymbol{T}} + {}^{0}\hat{\boldsymbol{T}}^{\mathsf{T}} \cdot \hat{\boldsymbol{\mathcal{K}}} \cdot \bar{\bar{\delta}}\left({}^{0}\hat{\boldsymbol{T}} \right) \right] \cdot {}^{t+\Delta t}_{0}\boldsymbol{u} , \tag{3.21}$$

where, referring to the TL variational formulation, particularly relations (2.27), (2.29) and (2.30), the *shape* parameter, $\boldsymbol{h}$, dependent factors in (2.23) are recounted as:

$$\hat{\boldsymbol{\mathcal{K}}} \equiv \left({}^{0}A \, {}^{0}\hat{L} \, E \right) {}^{0}\hat{\hat{\boldsymbol{\aleph}}} \cdot {}^{0}\hat{\hat{\boldsymbol{\aleph}}}^{\mathsf{T}}$$

with

$$\begin{aligned} {}^{0}\hat{\hat{\boldsymbol{\aleph}}} &= {}^{0}\hat{\boldsymbol{N}}_{x,x} + {}^{0}\hat{\boldsymbol{\aleph}} \cdot {}^{0}\hat{\boldsymbol{T}} \cdot {}^{t+\Delta t}_{0}\boldsymbol{u} , \\ {}^{0}\hat{\hat{\boldsymbol{\aleph}}}^{\mathsf{T}} &= {}^{0}\hat{\boldsymbol{N}}^{\mathsf{T}}_{x,x} + \left(\tfrac{1}{2} \right) {}^{t+\Delta t}_{0}\boldsymbol{u}^{\mathsf{T}} \cdot {}^{0}\hat{\boldsymbol{T}}^{\mathsf{T}} \cdot {}^{0}\hat{\boldsymbol{\aleph}} . \end{aligned}$$

Evaluating $\bar{\bar{\delta}}\left(\hat{\boldsymbol{\mathcal{K}}} \right)$ in (3.21) produces

$$\begin{aligned} \bar{\bar{\delta}}\left(\hat{\boldsymbol{\mathcal{K}}} \right) = {} & \bar{\bar{\delta}}\left({}^{0}\hat{\hat{\boldsymbol{\aleph}}} \right) \cdot \left({}^{0}A \, {}^{0}\hat{L} \, E \right) {}^{0}\hat{\hat{\boldsymbol{\aleph}}}^{\mathsf{T}} + {}^{0}\hat{\hat{\boldsymbol{\aleph}}} \cdot \left({}^{0}A \, \bar{\bar{\delta}}\left({}^{0}\hat{L} \right) E \right) {}^{0}\hat{\hat{\boldsymbol{\aleph}}}^{\mathsf{T}} \\ & + {}^{0}\hat{\hat{\boldsymbol{\aleph}}} \cdot \left({}^{0}A \, {}^{0}\hat{L} \, E \right) \bar{\bar{\delta}}\left({}^{0}\hat{\hat{\boldsymbol{\aleph}}}^{\mathsf{T}} \right) \end{aligned}$$

[5] $\hat{\boldsymbol{\mathcal{K}}}$ includes the Jacobian integration factors J and J_{Γ}, both of which have an *explicit* dependency on the it shape design parameters.

with

$$\bar{\bar{\delta}}\left({}^{0}\hat{\aleph}\right) = \left(-\frac{1}{{}^{0}\hat{L}}\right){}^{0}\hat{N}_{x,x}\cdot\nabla_{\boldsymbol{b}}{}^{0}\hat{L} - \left(\frac{2}{{}^{0}\hat{L}}\right){}^{0}\hat{\aleph}\cdot\nabla_{\boldsymbol{b}}{}^{0}\hat{L}\cdot{}^{0}\hat{\boldsymbol{T}}\cdot{}^{t+\Delta t}_{0}\boldsymbol{u} + {}^{0}\hat{\aleph}\cdot\bar{\bar{\delta}}\left({}^{0}\hat{\boldsymbol{T}}\right)\cdot{}^{t+\Delta t}_{0}\boldsymbol{u}$$

and

$$\bar{\bar{\delta}}\left({}^{0}\hat{\tilde{\aleph}}^{\mathsf{T}}\right) = \left(-\frac{1}{{}^{0}\hat{L}}\right){}^{0}\hat{N}^{\mathsf{T}}_{x,x}\cdot\nabla_{\boldsymbol{b}}{}^{0}\hat{L} + \left(\tfrac{1}{2}\right){}^{t+\Delta t}_{0}\boldsymbol{u}^{\mathsf{T}}\cdot\bar{\bar{\delta}}\left({}^{0}\hat{\boldsymbol{T}}^{\mathsf{T}}\right)\cdot{}^{0}\hat{\aleph} - \frac{1}{{}^{0}\hat{L}}{}^{t+\Delta t}_{0}\boldsymbol{u}^{\mathsf{T}}\cdot{}^{0}\hat{\boldsymbol{T}}^{\mathsf{T}}\cdot{}^{0}\hat{\aleph}\cdot\nabla_{\boldsymbol{b}}{}^{0}\hat{L}.$$

Now, applying the *explicit* sensitivity operator $\bar{\bar{\delta}}(\ldots)$ to the shape parameter dependent TL transformation matrix[6] ${}^{0}\hat{\boldsymbol{T}} \equiv {}^{0}\boldsymbol{T}(\boldsymbol{h})$ in (2.25) results in

$$\bar{\bar{\delta}}\left({}^{0}\hat{\boldsymbol{T}}\right) \equiv \nabla_{\boldsymbol{b}}{}^{0}\hat{\boldsymbol{T}} \equiv \nabla_{\boldsymbol{b}}\left[{}^{0^{\star}}_{0}x_{i,j}\right] \equiv \begin{bmatrix} \boldsymbol{\mathcal{T}} & \mathbf{0}_{3\times3} \\ \mathbf{0}_{3\times3} & \boldsymbol{\mathcal{T}} \end{bmatrix},$$

where

$$\boldsymbol{\mathcal{T}} = \begin{bmatrix} \{\alpha_c\cos\theta + \cos\phi\beta_c\} & -\{\beta_s\} & -\{\alpha_s\cos\theta + \sin\phi\beta_c\} \\ \{\alpha_c\sin\theta + \cos\phi\beta_s\} & \{\beta_c\} & -\{\alpha_s\sin\theta + \sin\phi\beta_s\} \\ \{\alpha_s\} & 0 & \{\alpha_c\} \end{bmatrix}$$

for

$$\alpha_c = \bar{\bar{\delta}}(\cos\phi)\ ,\ \alpha_s = \bar{\bar{\delta}}(\sin\phi)\ ,\ \beta_c = \bar{\bar{\delta}}(\cos\theta)\ ,\ \beta_s = \bar{\bar{\delta}}(\sin\theta)\ .$$

It remains to derive and calculate the specific form of the expressions

$$\begin{aligned} \bar{\bar{\delta}}(\sin\theta) &= \frac{d\sin\theta}{dh} \quad , \quad \bar{\bar{\delta}}(\cos\theta) = \frac{d\cos\theta}{dh}, \\ \bar{\bar{\delta}}(\sin\phi) &= \frac{d\sin\phi}{dh} \quad , \quad \bar{\bar{\delta}}(\cos\phi) = \frac{d\cos\phi}{dh}, \end{aligned} \tag{3.22}$$

as well as $\bar{\bar{\delta}}({}^{0}L)$, for each element I of the FE discretisation, in order to obtain the RHS of (3.20). The expressions in (3.22), and $\bar{\bar{\delta}}({}^{0}L)$, are application dependent and can consequently not be formulated generally.

Referring to the pylon truss structure[7] in Section 6.4, where the positions of nodes 7-10, and thus the formulation of various elements, are dependent on a *single* shape design parameter h, these expressions take on the form summarised in Table[3.1][8].

[6] Refer to Section 3.1.3.
[7] Refer to Fig.[6.4.3].
[8] Refer to Fig.[2.4]

3.2.4 Stress DSA

As stated in Section 3.1.4, many generalised functions, specifically the objective and constraint functionals used in structural optimisation, have a dependence on response variables other than displacement.

The method of derivation of the sensitivity vector for a generalised constraint $\nabla_{\boldsymbol{b}} \Psi$ where, for example, Ψ has a stress dependency $\Psi \equiv \Psi(\boldsymbol{\tau})$, reduces to the problem of obtaining an expression $\frac{\partial \boldsymbol{\tau}}{\partial \boldsymbol{u}}$, where $\nabla_{\boldsymbol{b}} \boldsymbol{u}$ has already been solved for, and having analytically derived $\frac{\partial \Psi}{\partial \boldsymbol{\tau}}$, $\frac{\partial \boldsymbol{\tau}}{\partial \boldsymbol{b}}$ and $\frac{\partial \Psi}{\partial \boldsymbol{b}}$ in equation (3.12):

$$\nabla_{\boldsymbol{b}} \Psi = \frac{\partial \Psi}{\partial \boldsymbol{\tau}} \left(\frac{\partial \boldsymbol{\tau}}{\partial \boldsymbol{u}} \cdot \nabla_{\boldsymbol{b}} \boldsymbol{u} + \frac{\partial \boldsymbol{\tau}}{\partial \boldsymbol{b}} \right) + \frac{\partial \Psi}{\partial \boldsymbol{b}} . \tag{3.23}$$

The expression in (3.23) reflects the fact that the majority of stress-based constraints g_i prefer to employ the physically measurable Cauchy stress $\boldsymbol{\tau}$, instead of the 2^{nd} Piola-Kirchhoff stress $\boldsymbol{S}$. Utilising $\boldsymbol{\tau}$ does, however, significantly complicate the derivation of $\frac{\partial \boldsymbol{\tau}}{\partial \boldsymbol{u}}$.

Employing the TL formulation, $\boldsymbol{\tau} \equiv {}^{t+\Delta t}\boldsymbol{\tau}$, is found from the frame transformation operation:

$$\begin{aligned} {}^{t+\Delta t}\boldsymbol{\tau} &= \left(\frac{{}^{t+\Delta t}\rho}{{}^{0}\rho} \right) {}^{0}_{t+\Delta t}\boldsymbol{\mathcal{X}}^{\mathsf{T}} \cdot {}^{t+\Delta t}_{0}\boldsymbol{S} \cdot {}^{0}_{t+\Delta t}\boldsymbol{\mathcal{X}} \\ &= {}^{0}_{t+\Delta t}\boldsymbol{\mathcal{X}}^{\mathsf{T}} \cdot {}^{t+\Delta t}_{0}\boldsymbol{S} \cdot {}^{0}_{t+\Delta t}\boldsymbol{\mathcal{X}} \end{aligned}$$

by assuming material incompressibility, and

$${}^{0}_{t+\Delta t}\boldsymbol{\mathcal{X}} = {}^{0}\boldsymbol{T}^{\mathsf{T}} \cdot {}^{t+\Delta t}\boldsymbol{T}$$

for

$$\begin{aligned} {}^{0}\boldsymbol{T}^{\mathsf{T}} \quad &\text{mapping} \quad C'_0 \rightarrow C_0 , \\ {}^{t+\Delta t}\boldsymbol{T} \quad &\text{mapping} \quad C_{t+\Delta t} \rightarrow C'_0 , \end{aligned}$$

so that ${}^{t+\Delta t}\boldsymbol{T}$ is dependent on the material deformation ${}^{t+\Delta t}_{0}\boldsymbol{u}$.

Referring to (2.31), the 2^{nd} P-K stress for a truss element implementation takes on the form

$${}^{t+\Delta t}_{0}S_{xx} \equiv E, {}^{0}\tilde{\tilde{\boldsymbol{\aleph}}}^{\mathsf{T}} \cdot {}^{0}\boldsymbol{T} \cdot {}^{t+\Delta t}_{0}\boldsymbol{u}$$

and in a similar vein to the process in (2.35)

$$\begin{aligned} {}^{t+\Delta t}\tau_{xx} &= \left[{}^{0}_{t+\Delta t}\boldsymbol{\mathcal{X}} \right]^{2}_{i,j=1} {}^{t+\Delta t}_{0}S_{xx} \\ &= \Phi^2 E \, {}^{0}\tilde{\tilde{\boldsymbol{\aleph}}}^{\mathsf{T}} \cdot {}^{0}\boldsymbol{T} \cdot {}^{t+\Delta t}_{0}\boldsymbol{u} , \end{aligned}$$

node: **7** Elements affected: **15, 18, 23**
$\frac{dL}{dh} = \frac{x-y}{L}$ $\frac{d\sin\theta}{dh} = \frac{-1}{PL} - \left(\frac{y}{PL^2}\right)\left(\frac{x-y}{PL}\right)$ $\quad$ $\frac{d\cos\theta}{dh} = \frac{1}{PL} - \left(\frac{x}{PL^2}\right)\left(\frac{x-y}{PL}\right)$ $\frac{d\sin\phi}{dh} = -\left(\frac{z}{L^2}\right)\left(\frac{x-y}{L}\right)$ $\quad$ $\frac{d\cos\phi}{dh} = \left(\frac{x-y}{PL}\right)\left(\frac{1}{L}\right) - \left(\frac{PL}{L^2}\right)\left(\frac{x-y}{L}\right)$
node: **8** Elements affected: **17, 19, 25**
$\frac{dL}{dh} = \frac{-(x+y)}{L}$ $\frac{d\sin\theta}{dh} = \frac{-1}{PL} - \left(\frac{y}{PL^2}\right)\left(\frac{-(x+y)}{PL}\right)$ $\quad$ $\frac{d\cos\theta}{dh} = \frac{-1}{PL} - \left(\frac{x}{PL^2}\right)\left(\frac{-(x+y)}{PL}\right)$ $\frac{d\sin\phi}{dh} = -\left(\frac{z}{L^2}\right)\left(\frac{-(x+y)}{L}\right)$ $\quad$ $\frac{d\cos\phi}{dh} = \left(\frac{-(x+y)}{PL}\right)\left(\frac{1}{L}\right) - \left(\frac{PL}{L^2}\right)\left(\frac{-(x+y)}{L}\right)$
node: **9** Elements affected: **16, 21, 24**
$\frac{dL}{dh} = \frac{y-x}{L}$ $\frac{d\sin\theta}{dh} = \frac{1}{PL} - \left(\frac{y}{PL^2}\right)\left(\frac{y-x}{PL}\right)$ $\quad$ $\frac{d\cos\theta}{dh} = \frac{-1}{PL} - \left(\frac{x}{PL^2}\right)\left(\frac{y-x}{PL}\right)$ $\frac{d\sin\phi}{dh} = -\left(\frac{z}{L^2}\right)\left(\frac{y-x}{L}\right)$ $\quad$ $\frac{d\cos\phi}{dh} = \left(\frac{y-x}{PL}\right)\left(\frac{1}{L}\right) - \left(\frac{PL}{L^2}\right)\left(\frac{y-x}{L}\right)$
node: **10** Elements affected: **14, 20, 22**
$\frac{dL}{dh} = \frac{x+y}{L}$ $\frac{d\sin\theta}{dh} = \frac{1}{PL} - \left(\frac{y}{PL^2}\right)\left(\frac{x+y}{PL}\right)$ $\quad$ $\frac{d\cos\theta}{dh} = \frac{1}{PL} - \left(\frac{x}{PL^2}\right)\left(\frac{x+y}{PL}\right)$ $\frac{d\sin\phi}{dh} = -\left(\frac{z}{L^2}\right)\left(\frac{x+y}{L}\right)$ $\quad$ $\frac{d\cos\phi}{dh} = \left(\frac{x+y}{PL}\right)\left(\frac{1}{L}\right) - \left(\frac{PL}{L^2}\right)\left(\frac{x+y}{L}\right)$
The symbols x, y and z all pertain to node **1** in the parent frame, ie. $x \equiv x_{(1)}$, $y \equiv y_{(1)}$ and $z \equiv z_{(1)}$. $PL = \sqrt{x^2 + y^2}$ $L = \sqrt{x^2 + y^2 + z^2}$

Table 3.1: Shape sensitivity factors for the pylon truss structure

where

$$\begin{aligned}\Phi &= \Phi\left({}^{0}\phi,\ {}^{t+\Delta t}\phi,\ {}^{0}\theta,\ {}^{t+\Delta t}\theta\right)\\ &= \cos{}^{t+\Delta t}\phi\cos{}^{0}\phi\left(\cos{}^{t+\Delta t}\theta\cos{}^{0}\phi+\sin{}^{t+\Delta t}\theta\sin{}^{0}\theta\right),\end{aligned}$$

so that $\left(\frac{\partial \boldsymbol{T}}{\partial \boldsymbol{u}}\right)\cdot\nabla_{\boldsymbol{b}}\boldsymbol{u}$ in the generalised constraint sensitivity equation (3.23) for the TL truss element formulation, becomes

$$\begin{aligned}&\left(\frac{\partial^{t+\Delta t}T_{xx}}{\partial \boldsymbol{u}}\right)\cdot\nabla_{\boldsymbol{b}}\boldsymbol{u}\\ =\ &\left(\frac{\partial(\Phi^2)}{\partial \boldsymbol{u}}\cdot\nabla_{\boldsymbol{b}}\boldsymbol{u}\right)\cdot{}^{0}\tilde{\tilde{\boldsymbol{\aleph}}}^{\mathsf{T}}\cdot{}^{0}\boldsymbol{T}\cdot{}^{t+\Delta t}_{0}\boldsymbol{u}+\Phi^2\left(\frac{\partial\,{}^{0}\tilde{\tilde{\boldsymbol{\aleph}}}^{\mathsf{T}}}{\partial \boldsymbol{u}}\cdot\nabla_{\boldsymbol{b}}\boldsymbol{u}\right)\cdot{}^{0}\boldsymbol{T}\cdot{}^{t+\Delta t}_{0}\boldsymbol{u}\\ &+\Phi^2\,{}^{0}\tilde{\tilde{\boldsymbol{\aleph}}}^{\mathsf{T}}\cdot{}^{0}\boldsymbol{T}\cdot\left(\frac{\partial\,{}^{t+\Delta t}_{0}\boldsymbol{u}}{\partial \boldsymbol{u}}\cdot\nabla_{\boldsymbol{b}}\boldsymbol{u}\right)\\ =\ &\left(2\Phi\frac{\partial\Phi}{\partial \boldsymbol{u}}\cdot\nabla_{\boldsymbol{b}}\boldsymbol{u}\right)\cdot{}^{0}\tilde{\tilde{\boldsymbol{\aleph}}}^{\mathsf{T}}\cdot{}^{0}\boldsymbol{T}\cdot{}^{t+\Delta t}_{0}\boldsymbol{u}+\left(\tfrac{1}{2}\right)\Phi^2\left(\nabla_{\boldsymbol{b}}\boldsymbol{u}\right)^{\mathsf{T}}\cdot{}^{0}\boldsymbol{T}^{\mathsf{T}}\cdot{}^{0}\boldsymbol{\aleph}\cdot{}^{0}\boldsymbol{T}\cdot{}^{t+\Delta t}_{0}\boldsymbol{u}\\ &+\Phi^2\,{}^{0}\tilde{\tilde{\boldsymbol{\aleph}}}^{\mathsf{T}}\cdot{}^{0}\boldsymbol{T}\cdot\nabla_{\boldsymbol{b}}\boldsymbol{u}.\end{aligned}$$

The form of $\frac{\partial\Phi}{\partial \boldsymbol{u}}$ is easily obtained, having first derived expressions for $\frac{\partial\cos{}^{t+\Delta t}\phi}{\partial \boldsymbol{u}}$, $\frac{\partial\cos{}^{t+\Delta t}\theta}{\partial \boldsymbol{u}}$ and $\frac{\partial\sin{}^{t+\Delta t}\theta}{\partial \boldsymbol{u}}$, and retrieving the values for similar expressions in terms of ${}^{0}\theta$ and ${}^{0}\phi$ from storage. Here again, as was the case at the end of Section 3.2.3, the formulation of these expressions is specific to the particular application and can, therefore, not be generalised.

Referring to the 200-bar truss structure investigated in Section 6.3, the expressions listed in the previous paragraph take on the form summarised in Table[3.2].

$\frac{\partial}{\partial u_{1x}}$, $\frac{\partial}{\partial u_{2x}}$ are the x-direction nodal displacement sensitivities for, respectively, node **1** and **2**.
$\frac{\partial \cos^{t+\Delta t}\theta}{\partial u_{1x}} = \frac{1}{\gamma}\left(\frac{\alpha^2}{\gamma^2} - 1\right)$ $\quad$ $\frac{\partial \sin^{t+\Delta t}\theta}{\partial u_{1x}} = -\frac{\alpha\beta}{\gamma^3}$ $\frac{\partial \cos^{t+\Delta t}\theta}{\partial u_{2x}} = -\frac{1}{\gamma}\left(\frac{\alpha^2}{\gamma^2} - 1\right)$ $\quad$ $\frac{\partial \sin^{t+\Delta t}\theta}{\partial u_{2x}} = \frac{\alpha\beta}{\gamma^3}$
$\frac{\partial}{\partial u_{1y}}$, $\frac{\partial}{\partial u_{2y}}$ are the y-direction nodal displacement sensitivities for, respectively, node **1** and **2**.
$\frac{\partial \cos^{t+\Delta t}\theta}{\partial u_{1y}} = -\frac{\alpha\beta}{\gamma^3}$ $\quad$ $\frac{\partial \sin^{t+\Delta t}\theta}{\partial u_{1y}} = \frac{1}{\gamma}\left(\frac{\beta^2}{\gamma^2} - 1\right)$ $\frac{\partial \cos^{t+\Delta t}\theta}{\partial u_{2y}} = \frac{\alpha\beta}{\gamma^3}$ $\quad$ $\frac{\partial \sin^{t+\Delta t}\theta}{\partial u_{2y}} = -\frac{1}{\gamma}\left(\frac{\beta^2}{\gamma^2} - 1\right)$
$\alpha = ({}^t x_1 - {}^t x_2) + ({}^t u_{1x} - {}^t u_{2x})$ $\beta = ({}^t y_1 - {}^t y_2) + ({}^t u_{1y} - {}^t u_{2y})$ $\gamma = \sqrt{\alpha^2 + \beta^2}$ where $({}^t x_1, {}^t y_1, {}^t z_1)$ and $({}^t x_2, {}^t y_2, {}^t z_2)$ are the *global* coordinates for nodes **1** and **2**, respectively.

Table 3.2: Stress sensitivity factors for the 200-bar truss structure

Chapter 4

Structural Optimisation

4.1 Structural Optimisation, Design Sensitivity and Finite Element Analysis

As an extension of the work in Chapter 3 on the formulation and discretisation of various DSA procedures and their implementation into ABAQUS, this chapter goes further by developing a comprehensive optimisation model to be used in conjunction with ABAQUS. This brings to completion two of the primary objectives of this research, namely, the implemention of DSA and structural optimisation into an established FEA code, viz. ABAQUS.

For computational optimisation, particularly in the field of mechanics, the primary focus usually rests on the sensitivity analysis procedure; i.e. the process utilised in obtaining a **reliable** sensitivity vector $\nabla_{\boldsymbol{b}} \Psi$ is crucial. In the work presented here this particular sentiment is supported by employing one particular optimisation model, the Pshenichny-Lim-Belegundu-Arora recursive quadratic programming (PLBA RQP) method, throughout. Although computational optimisation theory is an entirely self-contained field of research worthy of investigation, a full analysis and discussion of the PLBA RQP is beyond the scope of this work; the optimisation method purely serves as a vehicle for the **practical** implementation of various DSA procedures into ABAQUS.

The purpose of structural optimisation is to minimise a generalised cost functional

$$f \equiv f(\boldsymbol{u}, \boldsymbol{b}) \equiv f(\boldsymbol{u}(\boldsymbol{b}), \boldsymbol{b})$$

for *shape* or *non-shape* design parameters $\boldsymbol{b}$, subject to a set of generalised equality and inequality constraints

$$g_i \equiv g_i(\boldsymbol{u}, \boldsymbol{b}) \equiv g_i(\boldsymbol{u}(\boldsymbol{b}), \boldsymbol{b})$$

Commonly f represents the volume of material employed in a structure, or the financial cost as a proportion of the volume of material, whereas the constraints g_i generally reflect displacement, strain or stress limits imposed on the structural behaviour.

The approach adopted in the optimisation model employed here is an enhancement of the standard Lagrange multiplier method. A Lagrangian function $P(\boldsymbol{b}, \boldsymbol{\mu})$ is defined in terms of the addition of the cost functional and scalar multiples of the *active* constraints[1] ; $\boldsymbol{b}$ and $\boldsymbol{\mu}$, respectively, represent the design parameters and Lagrange multipliers. The optimisation problem now reduces to a process of minimising the unconstrained Lagrangian function

$$P(\boldsymbol{b}, \boldsymbol{\mu}) \equiv L(\boldsymbol{b}, \boldsymbol{\mu}) = f(\boldsymbol{u}, \boldsymbol{b}) + \sum_i \mu_i g_i(\boldsymbol{u}, \boldsymbol{b}) \, .$$

In order to generate a series of iteratively improved approximations to the optimal set of design parameters, $\overline{\boldsymbol{b}}$, the optimisation routine requires values for the first derivatives of the cost and constraint functionals,

$$\nabla_{\boldsymbol{b}} f \equiv \nabla_{\boldsymbol{b}} f(\boldsymbol{u}, \boldsymbol{b}) \, , \; \nabla_{\boldsymbol{b}} g_i \equiv \nabla_{\boldsymbol{b}} g_i(\boldsymbol{u}, \boldsymbol{b})$$

for each iterative set of design parameters $\boldsymbol{b}^{(k)}$.

For the computational implementation of structural optimisation, the finite element analysis procedure solves for values of the material displacement $\boldsymbol{u} \equiv \boldsymbol{u}(\boldsymbol{b}^{(k)})$ for a given set of design parameters $\boldsymbol{b}^{(k)}$. The design sensitivity analysis routine generates the cost and constraint function sensitivity vectors, $\nabla_{\boldsymbol{b}} f$ and $\nabla_{\boldsymbol{b}} g_i$, respectively.

The optimisation algorithm implemented here is designed to interface with finite element and design sensitivity analysis algorithms in exactly the fashion described above. As mentioned above, the specific optimisation model employed is based on the extension of Pshenichny's RQP[2] linearisation method for constrained optimisation, referred to as the PLBA RQP method, as presented by Lim & Arora [26]; the procedure is described in the following section.

4.1.1 Structural Optimisation with the PLBA RQP

The PLBA optimisation routine is structured into three conceptually separate parts:

- Part I solves for the direction of optimal change $\boldsymbol{p}$.

[1] Constraints which are violated for a particular set of design parameters $\boldsymbol{b}$ become 'active'. Only *active* constraints are considered in the optimisation procedure.

[2] Recursive Quadratic Programming.

- Part **II** solves for the stepsize α in the direction $\boldsymbol{p}$, thereby establishing the **magnitude** of the design parameter change.
- Part **III** employs a variation of the BFGS method to update $\boldsymbol{W}$, thereby serving to accelerate the optimisation procedure.

Parts **I-III** are repeated until the variation in the design magnitude $\alpha^{(k)}\|\boldsymbol{p}^{(k)}\|$ is less than a set tolerance value.

I - Solving for the vector direction of optimal change $\boldsymbol{p}$

The family of quadratic programming (QP) optimisation methods proceed by approximating the *nonlinear* cost and constraint functionals by quadratic functions. That is, the *nonlinear* optimisation problem

$$\begin{aligned} &\textit{minimize} && f(\boldsymbol{u},\boldsymbol{b}) \\ &\textit{subject to} && g_i(\boldsymbol{u},\boldsymbol{b}) = 0\ ,\ i \in I_1 \\ &&& g_i(\boldsymbol{u},\boldsymbol{b}) \leq 0\ ,\ i \in I_2 \end{aligned}$$

where

$$\begin{aligned} I_1 &= \text{active equality constraints} \\ I_2 &= \text{active inequality constraints} \end{aligned}$$

reduces to the quadratic programming problem (QPP)

$$\begin{aligned} &\textit{minimize} && \tfrac{1}{2}\boldsymbol{p}^{\mathsf{T}} \cdot \boldsymbol{W} \cdot \boldsymbol{p} + \boldsymbol{G}^{0^{\mathsf{T}}} \cdot \boldsymbol{p} \\ &\textit{subject to} && \boldsymbol{G}^{i^{\mathsf{T}}} \cdot \boldsymbol{p} + g_i = 0\ ,\ i \in I_1 \\ &&& \boldsymbol{G}^{i^{\mathsf{T}}} \cdot \boldsymbol{p} + g_i \leq 0\ ,\ i \in I_2 \end{aligned}$$

with

- $\boldsymbol{p} \equiv$ vector direction of change in design variables that has to be solved for.
- $\boldsymbol{W} \equiv$ symmetric positive-definite *approximation* to the Hessian of the Lagrangian function

$$L(\boldsymbol{b},\boldsymbol{\mu}) = f(\boldsymbol{u},\boldsymbol{b}) + \sum_i \mu_i g_i(\boldsymbol{u},\boldsymbol{b})\ ,\quad i \in I_\varepsilon,\ I_\varepsilon = I_1 \cup I_2\ .$$

$\boldsymbol{W}$ is iteratively improved with every optimisation step, starting with an initial value of $\boldsymbol{W}^{(0)} = \boldsymbol{I}$. Since $\boldsymbol{W}$ is symmetric positive-definite, Cholesky decomposition can be utilised to formulate $\boldsymbol{W}$ in terms of two upper triangular matrices $\boldsymbol{U}$

- G^0 and G^i are, respectively, the sensitivity vectors for the cost and constraint functions, i.e.

$$G^0 \equiv \nabla_{\boldsymbol{b}} f(\boldsymbol{u}, \boldsymbol{b}) ,$$
$$G^i \equiv \nabla_{\boldsymbol{b}} g_i(\boldsymbol{u}, \boldsymbol{b}) ,$$

  obtained directly from the computational DSA procedures.

Since the objective of the QPP is to solve **only** for the vector **direction**, and not magnitude, of optimal change in the design parameters, the usual QPP normalisation is introduced:

$$\textit{minimize} \quad \tfrac{1}{2}\overline{\boldsymbol{s}}^{\mathsf{T}} \cdot \overline{\boldsymbol{s}} + \overline{G}^{0^{\mathsf{T}}} \cdot \overline{\boldsymbol{s}}$$

$$\textit{subject to} \quad \overline{G}^{i^{\mathsf{T}}} \cdot \overline{\boldsymbol{s}} + \overline{g}_i = 0 \ , \ i \in I_1$$
$$\overline{G}^{i^{\mathsf{T}}} \cdot \overline{\boldsymbol{s}} + \overline{g}_i \leq 0 \ , \ i \in I_2$$

where

$$\overline{\boldsymbol{s}} = \frac{\boldsymbol{s}}{c_0} , \qquad \overline{G}^0 = \frac{\left(\boldsymbol{U}^{-1}\right)^{\mathsf{T}} \cdot \boldsymbol{G}^0}{c_0} ,$$

$$\overline{g}_i = \frac{g_i}{c_0 c_i} , \qquad \overline{G}^i = \frac{\left(\boldsymbol{U}^{-1}\right)^{\mathsf{T}} \cdot \boldsymbol{G}^i}{c_i} ,$$

$$c_0 = \left\| \left(\boldsymbol{U}^{-1}\right)^{\mathsf{T}} \cdot \boldsymbol{G}^0 \right\| , \quad c_i = \left\| \left(\boldsymbol{U}^{-1}\right)^{\mathsf{T}} \cdot \boldsymbol{G}^i \right\| ,$$

$$\boldsymbol{s} = \boldsymbol{U} \cdot \boldsymbol{p} \quad ,$$

$$\boldsymbol{W} = \boldsymbol{U}^{\mathsf{T}} \cdot \boldsymbol{U} \qquad \text{by Cholesky decomposition.}$$

The *normalised* QPP is solved for $\overline{\boldsymbol{s}}$ in a straightforward manner by first linearising the problem, using the Kuhn-Tucker conditions, before implementing a variation of the SIMPLEX method to solve the resulting linear optimisation problem.

- For the purpose of implementing structural optimisation only *inequality* constraints are considered. Consequently the normalised QPP may be symbolically reformulated, in preparation for the SIMPLEX method, as:

$$\textit{maximise} \quad \mathsf{f}(\mathsf{X}) = \mathsf{C}^{\mathsf{T}} \cdot \mathsf{X} + \mathsf{X}^{\mathsf{T}} \cdot \mathsf{D}^{\mathsf{T}} \cdot \mathsf{X}$$

$$\textit{subject to} \quad \mathsf{A} \cdot \mathsf{X} - \mathsf{B} \leq 0$$
$$-\mathsf{X} \leq 0$$

where[3]

$$\mathsf{X} \equiv \overline{s}, \quad \mathsf{D} \equiv -\tfrac{1}{2}I, \quad \mathsf{C} \equiv -\overline{G}^0, \quad \mathsf{A} \equiv \left[\overline{G}^i\right]^\mathsf{T}, \quad \mathsf{B} \equiv -\left[\overline{g}_i\right].$$

- Applying the Kuhn-Tucker conditions the quadratic equations are linearised and the SIMPLEX method seeks to construct a suitable basis of non-zero design variables X and multipliers, λ and δ, simultaneously satisfying the equations

$$\begin{aligned} -2\mathsf{D}^\mathsf{T} \cdot \mathsf{X} + \mathsf{A}^\mathsf{T} \cdot \lambda - \delta + \mathsf{S}^\star &= \mathsf{C} \\ \mathsf{A} \cdot \mathsf{X} + \mathsf{S} &= \mathsf{B} \\ \delta^\mathsf{T} \cdot \mathsf{X} &= 0 \\ \lambda^\mathsf{T} \cdot \mathsf{S} &= 0 \end{aligned}$$

with[4]

$$\mathsf{X} \geq 0, \quad \lambda \geq 0, \quad \delta \geq 0, \quad \mathsf{S} \geq 0, \quad \mathsf{S}^\star \geq 0$$

and a 'pseudo' objective function

$$\mathsf{S}^\star{}_0 = \sum_i \mathsf{S}^\star{}_i = 0.$$

Having obtained a solution to the normalised QPP in terms of $\mathsf{X} \equiv \overline{s}$ and $\lambda \equiv \overline{\mu}$, the optimal direction of change $\boldsymbol{p}$ and Lagrange multipliers $\boldsymbol{\mu}$ are found to be

$$\boldsymbol{p} = c_0 \left(U^{-1}\right) \cdot \overline{s}, \quad \mu_i = \left(\frac{c_0}{c_i}\right) \overline{\mu}_i.$$

II - Calculating stepsize α in the direction $\boldsymbol{p}$

The vector direction of optimal change of design, $\boldsymbol{p} \equiv \boldsymbol{p}^{(k)}$, is adjusted by a stepsize parameter $\alpha \equiv \alpha^{(k)}$, so that the next iterative approximation $\boldsymbol{b}^{(k+1)}$ to the set of optimal design parameters is estimated as

$$\overline{\boldsymbol{b}} \equiv \boldsymbol{b}^{(k+1)} = \boldsymbol{b}^{(k)} + \alpha^{(k)} \boldsymbol{p}^{(k)},$$

with

$$\alpha^{(k)} = \left(\tfrac{1}{2}\right)^{J^k},$$

where J^k is the smallest integer q that satisfies the inequality

$$\Phi\left(\boldsymbol{b}^{(k)} + 0.5^q \boldsymbol{p}^{(k)}\right) \leq \Phi\left(\boldsymbol{b}^{(k)}\right) - 0.5^q \beta \|\boldsymbol{p}^{(k)}\|^2.$$

---

[3] '[]' indicates a matrix, or vector, constituted over all $i \in I_e \equiv I_2$.

[4] S and S* are *slack* variables.

J^k is obtained by employing a simple Newton-Raphson line search procedure:

- The estimate $0 < \beta < 1$ functions as a 'calibrating' parameter proportional to the relative 'flatness' of the functional Φ; i.e. $\beta \approx 0$ for $\nabla_{\boldsymbol{b}} \Phi \approx 0$ over some closed domain $\Re^n$ with $n \equiv$ number of design parameters.
- The 'pseudo' Lagrangian function $\Phi(\boldsymbol{b})$ used to determine the stepsize α is defined as

$$\Phi\left(\boldsymbol{b}^{(k)}\right) \equiv f\left(\boldsymbol{u}^{(k)}, \boldsymbol{b}^{(k)}\right) + R F_\varepsilon\left(\boldsymbol{u}^{(k)}, \boldsymbol{b}^{(k)}\right),$$

where

$$\begin{aligned} f\left(\boldsymbol{u}^{(k)}, \boldsymbol{b}^{(k)}\right) &\equiv \text{cost functional}, \\ F_\varepsilon\left(\boldsymbol{u}^{(k)}, \boldsymbol{b}^{(k)}\right) &\equiv \max\left\{0,\ g_i\left(\boldsymbol{u}^{(k)}, \boldsymbol{b}^{(k)}\right) : i \in I_\varepsilon \equiv I_2\right\}, \\ R &\equiv \text{estimate such that } R \geq r \geq 0, \\ r &= \sum_i |\mu_i|\ ,\ i \in I_\varepsilon, \end{aligned}$$

for

$$\begin{aligned} I_2 &= \left\{i : g_i\left(\boldsymbol{u}^{(k)}, \boldsymbol{b}^{(k)}\right) + \epsilon\left(\boldsymbol{u}^{(k)}, \boldsymbol{b}^{(k)}\right)\right\}, \\ \epsilon\left(\boldsymbol{u}^{(k)}, \boldsymbol{b}^{(k)}\right) &= \delta^{(k)} - F\left(\boldsymbol{u}^{(k)}, \boldsymbol{b}^{(k)}\right), \\ F\left(\boldsymbol{u}^{(k)}, \boldsymbol{b}^{(k)}\right) &\equiv \max\left\{0,\ g_i\left(\boldsymbol{u}^{(k)}, \boldsymbol{b}^{(k)}\right)\right\}, \\ & \quad i \in \{\text{all inequality constraints}\} \end{aligned}$$

and $\delta^{(k)}$ is a user-defined constraint violation tolerance parameter, e.g. $\delta = F$ defines a violation non-tolerance scenario.

III - Improving the Hessian estimate $\boldsymbol{W}$

In order to achieve superlinear convergence, the Hessian $\boldsymbol{W}$, chosen such that $\boldsymbol{W} = \boldsymbol{I}$ for the first iteration $k = 0$, is revised using the BFGS update formula, as introduced by Lim & Arora [26].

The Hessian approximation $\boldsymbol{W}$ to the Lagrange function $L(\boldsymbol{b}, \boldsymbol{\mu})$ is obtained from the following procedure, summarised in a stepwise fashion:

- Calculate the vector

$$\boldsymbol{q} = \nabla_{\boldsymbol{b}} L\left(\overline{\boldsymbol{b}}, \boldsymbol{\mu}\right) - \nabla_{\boldsymbol{b}} L\left(\boldsymbol{b}, \boldsymbol{\mu}\right),$$

where $\boldsymbol{\mu}$ is obtained from the solution of the QPP in part (**I**).

- The design vector increment is

$$\boldsymbol{t} \equiv \overline{\boldsymbol{b}} - \boldsymbol{b} = \alpha \boldsymbol{p}.$$

- In order to ensure the positive-definiteness of $\boldsymbol{W}$, the convexity condition $\boldsymbol{t}^{\mathsf{T}} \cdot \boldsymbol{q} \geq 0$ has to be maintained. Hence a convex linear combination of $\boldsymbol{q}$ and $\boldsymbol{W} \cdot \boldsymbol{t}$ is defined

$$\boldsymbol{q}' = \Theta \boldsymbol{q} + (1 - \Theta)\, \boldsymbol{W} \cdot \boldsymbol{t},$$

where

$$\Theta = \left\{ \begin{array}{ll} 1\,, & \xi \geq (0.2)\gamma \\ \dfrac{(0.8)\gamma}{\gamma - \xi}\,, & \xi < (0.2)\gamma \end{array} \right\}$$

with

$$\xi = \boldsymbol{t}^{\mathsf{T}} \cdot \boldsymbol{q}\,, \quad \gamma = \boldsymbol{t}^{\mathsf{T}} \cdot \boldsymbol{W} \cdot \boldsymbol{t}.$$

- The Hessian $\boldsymbol{W}$ is updated to $\overline{\boldsymbol{W}} \equiv \boldsymbol{W}^{(k+1)}$

$$\overline{\boldsymbol{W}} = \boldsymbol{W} + \boldsymbol{a} \otimes \boldsymbol{a}^{\mathsf{T}} - \boldsymbol{e} \otimes \boldsymbol{e}^{\mathsf{T}}$$

with

$$\boldsymbol{a} = \frac{\boldsymbol{q}'}{\sqrt{\xi}}\,, \quad \boldsymbol{e} = \sqrt{\gamma}\, \boldsymbol{W} \cdot \boldsymbol{t}.$$

This updating procedure is guaranteed to produce a positive-definite matrix $\overline{\boldsymbol{W}}$ when the original Hessian $\boldsymbol{W}$ is positive-definite, e.g. $\boldsymbol{W} = \boldsymbol{I}$. The procedure similarly produces a symmetric matrix $\overline{\boldsymbol{W}}$ when initialised with a symmetric matrix $\boldsymbol{W}$.

4.1.2 The PLBA RQP method algorithm

The PLBA recursive quadratic programming algorithm is briefly summarised in following stepwise list:

1. Initial state
   - Estimate: $\boldsymbol{b}^{(0)} \in \Re^n$, $R^{(0)} > 0$, $\delta^{(0)} > 0$, $0 < \beta < 1$,
   - Set: $\boldsymbol{W}^{(0)} \equiv \boldsymbol{I}$
2. Search direction
   - Determine: $F\left(\boldsymbol{u}^{(k)}, \boldsymbol{b}^{(k)}\right) \Rightarrow I_\varepsilon{}^{(k)} \equiv I_2{}^{(k)}$
   - Set: $\boldsymbol{G}^{0(k)} \equiv \nabla_{\boldsymbol{b}} f\left(\boldsymbol{u}^{(k)}, \boldsymbol{b}^{(k)}\right)$, $\boldsymbol{G}^{i(k)} \equiv \nabla_{\boldsymbol{b}} g_i\left(\boldsymbol{u}^{(k)}, \boldsymbol{b}^{(k)}\right)$
   - Solve: QPP for $\boldsymbol{p}^{(k)}$, $\mu_i{}^{(k)}$, $i \in I_\varepsilon{}^{(k)}$
   - Check: QP subproblem constraint incompatability $\Rightarrow$ expand feasibility region by setting $\delta^{(k+1)} = \left(\frac{1}{2}\right)\delta^{(k)}$
3. Convergence criteria
   - Check: $F\left(\boldsymbol{u}^{(k)}, \boldsymbol{b}^{(k)}\right)$, $\alpha^{(k)}\|\boldsymbol{p}^{(k)}\| <$ convergence accuracy then EXIT the optimisation routine.
4. Penalty parameter
   - Calculate: $r^{(k)} = \sum |\mu_i^{(k)}|$, $i \in I_\varepsilon{}^{(k)}$
   - Check:

if	$R^{(k)} \geq r^{(k)}$ + feasible design	then	$R^{(k+1)} = \left(\frac{1}{2}\right)\left(R^{(k)} + r\right)$
else if	$R^{(k)} \geq r^{(k)}$ + NON feasible design	then	$R^{(k+1)} = R^{(k)}$
else if	$R^{(k)} < r^{(k)}$	then	$R^{(k+1)} = 2r$

5. Step size
   - Calculate: $\alpha^{(k)} \Rightarrow \boldsymbol{b}^{(k+1)}$
6. Hessian update
   - Calculate: $\boldsymbol{q}^{(k)}$, Θ, $\boldsymbol{t}^{(k)} \Rightarrow \boldsymbol{q}'^{(k)}$
   - Calculate: $\boldsymbol{a}$, $\boldsymbol{e} \Rightarrow \overline{\boldsymbol{W}}$
7. New iteration
   - Set: $k = k + 1$
   - Recurse: Go to step 2

Chapter 5

Implementing DSA and Optimisation into ABAQUS

The formulation of design sensitivity analysis (DSA) in order to facilitate the incorporation of structural optimisation into an established finite element analysis code was one of the primary objectives of the research undertaken for the purposes of this thesis. This chapter aims to present a systematic description of the manner in which DSA and structural optimisation were implemented in conjunction with the FEA code ABAQUS 5.4.

Including structural optimisation with an established FEA code provides the DSA and optimisation procedures with access to a host of features and facilities in the FEA package, thereby enabling the application of structural optimisation to a much wider range of problems than would be possible with a small purpose-built analysis and optimisation package.

The various sections of this chapter focus on, respectively,

1. the standard analysis facilities available in ABAQUS and employed in this work,
2. the implementation of DSA into ABAQUS, and
3. the structural optimisation procedure used in conjunction with ABAQUS.

Structural Analysis

ABAQUS is a *general* finite element analysis program and includes kinematic and material formulations for a wide range of possible applications, including topics as diverse as thermo-mechanics, rock mechanics and electro-magnetism.

displacement files becomes essential. The property files are used to separately store

Chapter 5

Implementing DSA and Optimisation into ABAQUS

The formulation of design sensitivity analysis (DSA) in order to facilitate the incorporation of structural optimisation into an established finite element analysis code was one of the primary objectives of the research undertaken for the purposes of this thesis. This chapter aims to present a systematic description of the manner in which DSA and structural optimisation were implemented in conjunction with the FEA code ABAQUS 5.4.

Including structural optimisation with an established FEA code provides the DSA and optimisation procedures with access to a host of features and facilities in the FEA package, thereby enabling the application of structural optimisation to a much wider range of problems than would be possible with a small purpose-built analysis and optimisation package.

The various sections of this chapter focus on, respectively,

1. the standard analysis facilities available in ABAQUS and employed in this work,
2. the implementation of DSA into ABAQUS, and
3. the structural optimisation procedure used in conjunction with ABAQUS.

Structural Analysis

ABAQUS is a *general* finite element analysis program and includes kinematic and material formulations for a wide range of possible applications, including topics as diverse as thermo-mechanics, rock mechanics and electro-magnetism.

Each simulation is prepared with an input deck which provides a description of the structure to be analysed and the FE facilities to be utilised; the input deck contains information on

- the structure design, location and orientation,
- the loads and boundary conditions imposed,
- the type of element and material model to be used, and
- the step-wise routine outlining the progression of the simulation.

Details of the mesh nodes and element composition are defined in external input files.

ABAQUS makes provision for the implementation of user-defined kinematic models, in conjunction with user-defined material models, via the user-element routine UEL.

During each analysis iteration ABAQUS constructs and solves the global element matrices using a Newton-Raphson procedure employing an optimal wavefront solution algorithm.

The UEL routine

- receives information from the solver for each individual element in the mesh. This information includes the node coordinates, total and incremental displacement, the element type, step number, increment number and iteration number;
- constructs the stiffness matrix AMATRX and the internal load vector RHS;
- returns AMATRX and RHS to ABAQUS for assembly into the global stiffness matrix and internal load vector, respectively.

The Total Lagrange (TL) formulation is implemented into ABAQUS in a straightforward fashion. Implementing the Update Lagrange (UL) formulation, however, requires the UEL routine to access external property and displacement definition files. In order to standardise the TL and UL UEL implementations, the practice of employing external property and displacement files with the UEL routine was later introduced for the TL formulation; this approach forms the basis for the inclusion of DSA into ABAQUS.

The analysis procedure may be summarised in algorithmic form as illustrated in Fig.[5.1].

```
Start: Initiate the simulation
        For: Each step:
        {
                Define: Boundary conditions and loads

                For: Each load increment
                {
                        Check: Displacement and Internal Loads convergence

                        If: No convergence
                        {
                                For: Each element
                                {
                                        Call: UEL

                                           UEL - Import:   Element information from ABAQUS
                                           UEL - Set:      Construct AMATRX and RHS
                                           UEL - Return:   AMATRX and RHS

                                        Assemble:  Global stiffness matrix and force vector

                                        Determine: Solve for displacement increments
                                }
                        }
                }
        }
End: Terminate the simulation
```

Figure 5.1: The ABAQUS analysis procedure.

Design Sensitivity Analysis

In order to implement DSA into ABAQUS, the user element routine UEL had to be suitably altered. A significant component of the research effort contributing to this thesis was focused on developing an appropriate technique for accomplishing this.

The UEL was redefined to enable dual purpose functionality; the user element routine contains code for performing both structural and sensitivity analysis. A flag inside the UEL routine was employed to indicate whether the DSA or the structural analysis procedure should be called. This flag was changed whenever a new increment or step was initiated by ABAQUS; the first increment of every step is reserved for DSA, with the DSA and structural analysis increments alternating strictly for the subsequent increments. Of course, many more calls are made to the analysis procedure for a simple DSA problem: the analysis model is accessed for each iteration of the solver, whereas the DSA procedure doesn't require an iterative solution approach - the discretised DSA formulation is linear in the displacement sensitivities.

Constructing UEL so as to convince the ABAQUS solver that it should regard DSA and structural analysis alike depends crucially on being able to formulate the DSA model in terms of 'pseudo'-stiffness and 'pseudo'-load so as to resemble the discretised kinematic formulation.

Although the DSA procedure does not utilise an iterative solution procedure, it does require a certain minimum number of iterations to prepare the solver for DSA, to successfully implement sensitivity analysis, and then to prepare for the next analysis increment. For the smallest DSA problem, i.e. single design parameter variation, at least *three* iterations are required for the DSA increment.

The DSA procedure is subdivided into the following distinct steps:

i. Import and store the response data for the structural analysis increment. Set up AMATRX and RHS so as to solve for the global load vector.

ii. Solve for the global load vector. Set up the stiffness matrix AMATRX and the internal load vector RHS with the pseudo-stiffness and pseudo internal loads, respectively, in preparation for finding the first sensitivity vector.

iii. Solve for the i^{th} sensitivity vector and set up AMATRX and RHS in preparation for finding the $(i+1)^{th}$ sensitivity vector. This process is repeated $n-1$ times, where n represents the number of design parameters for which response sensitivities are obtained.

iv. Solve for the n^{th} sensitivity vector and set up AMATRX and RHS to produce a zero displacement increment, thereby halting the DSA increment.

A 200 design parameters sensitivity analysis problem therefore requires 202 iterations of the DSA increment. From the DSA increment outline enumerated above, it is apparent that much work during the sensitivity analysis phase is involved with the construction of suitable RHS 'load vectors' for each iteration.

Preventing ABAQUS from unnecessarily subdividing the incremental time steps upon encountering hundreds of DSA iterations requires a careful setting of the ABAQUS solver parameters; ABAQUS provides for this eventuality with the CONTROLS keyword.

A similarly precise calibration of the solver is necessary when analysing a problem likely to yield very small sensitivities: small sensitivity values often cause the DSA increment to terminate prematurely by meeting the displacement convergence criteria, e.g. the DSA increment may halt after obtaining 166, of 200, sensitivity vectors if the response sensitivity to the 166^{th} design parameter is smaller than the solver's displacement tolerance.

For the purposes of performing DSA in ABAQUS, the use of external property and displacement files becomes essential. The property files are used to separately store

information important to the structural analysis and DSA procedures. The UEL routine keeps track of the correct total and incremental displacements, as well as the virtual displacements contributed by the various sensitivities and the global load vector.

Employing the same variable array to solve for displacement, displacement sensitivity and global loads results in a loss of significance for small sensitivity values. This effect is noticeable in the sensitivity results for small load cases by manifesting as a divergence in FDM and DSA estimates. The nature of the DSA implementation in ABAQUS furthermore imposes a theoretical limit on the magnitude of the largest load cases which can be dealt with by the analysis procedure - structural load cases in excess of 1000 kN have been accommodated successfully.

The DSA procedure incorporated into UEL can be represented algorithmically as illustrated in Fig.[5.2].

Structural Optimisation

The PLBA structural optimisation routine is not integrated into ABAQUS, but works in conjunction with ABAQUS as a separate executable module:

- ABAQUS completes a full analysis - alternating between structural and sensitivity analysis - based on a given structural design and fixed set of material parameters.
- On completion of the ABAQUS analysis the optimisation module is called. The optimisation routine utilises the structural response and sensitivity values generated by the preceding analysis to estimate a more optimal set of design parameters.
- The structure configuration and material parameters in the property files and other data files are updated accordingly. Subject to the optimality convergence criterion **not** being met, a new analysis is initiated.

The optimisation cycle is implemented as a operating system script file: in order to allow ABAQUS to smoothly integrate with the optimisation sequence, the standard ABAQUS script files was rewritten.

In addition to the property files utilised by the analysis and DSA module, data files were introduced to store the response and sensitivity information generated by the analysis/DSA module as well as the design parameter variations generated by the optimisation module.

The four modules or elements of the optimisation cycle may be enumerated as follows:

1. The ABAQUS 'PRE' executable processes the information in the input deck and various input files and assimilates the data, written to a data file, into a form accessible by the ABAQUS analysis/DSA module.

2. The ABAQUS analysis/DSA module accesses information in the 'PRE' data file and additional, external property files. The response and sensitivity vectors are calculated and the property and sensitivity information files are updated accordingly.

3. The optimisation module inputs information from the sensitivity information file, performs an optimisation and writes the improved design parameters to the optimisation information file. For the purposes of the research presented here, the objective and constraint functions, and their gradient formulae, were included in the optimisation module. Ideally the optimisation procedure would be made more general by including the application specific details in a separate source file.

4. The design update module reads the optimisation information file and tests for convergence of the design parameters to within tolerance. If the convergence check fails, the property and node definition input files are updated. In a similar fashion to the optimisation module, the design update module is specific to the problem being investigated.

The optimisation cycle is graphically illustrated in Fig.[5.3] by means of a flowchart.

```
Start: UEL is called
        Import:  (From property files) Property, solution variables
                 (From property files) Element counter
                 Element information from ABAQUS

        If: First iteration, first increment, first step, first element ?
        {
                Set: Procedure flag to DSA
        }

        If: New increment or new step; old iter. value > 1
        {
                If: First element and procedure flag is set to ANALYSIS
                {
                        Set: Procedure flag to DSA
                }
                If: First element and procedure flag is set to DSA
                {
                        Set: Procedure flag to ANALYSIS
                }
        }

        If: Procedure flag is set to ANALYSIS
        {
                Import :  (From property files) Total and virtual displacement
                Set:      Construct AMATRX and RHS
        }

        If: Procedure flag is set to DSA
        {
                If: First iteration
                {
                        Export: (To property files) Response variables
                        Set:    Construct AMATRX and RHS to find global load
                }

                If: Iteration NOT first and NOT last
                {
                        Import:  (From property files) Old and virtual displacement
                        Export:  (To property files)   New displacement

                        If: First sensitivity iteration
                        {
                                Determine: Global load
                                Set:       Construct AMATRX and RHS to find first
                                           sensitivity vector
                                Export:    (To property files) Global load and virtual
                                           displacement
                        }
                        Else:
                        {
                                Import:    (From property files) Global load
                                Determine: ith sensitivity vector
                                Set:       Construct AMATRX and RHS to find (i+1)th
                                           sensitivity vector
                                Export:    (To property files) Virtual displacement
                        }
                }

                If: Last sensitivity iteration
                {
                        Import:    (From property files) Old and virtual displacement
                        Determine: Last sensitivity vector
                        Set:       Construct AMATRX and RHS to produce zero
                                   displacement increment.
                        Export:    (To property files)  Virtual displacement
                }
        }

        Export: (To property files) New property, solution variables

        Return: AMATRX and RHS
End: Exit UEL
```

Figure 5.2: Implementing DSA into ABAQUS.

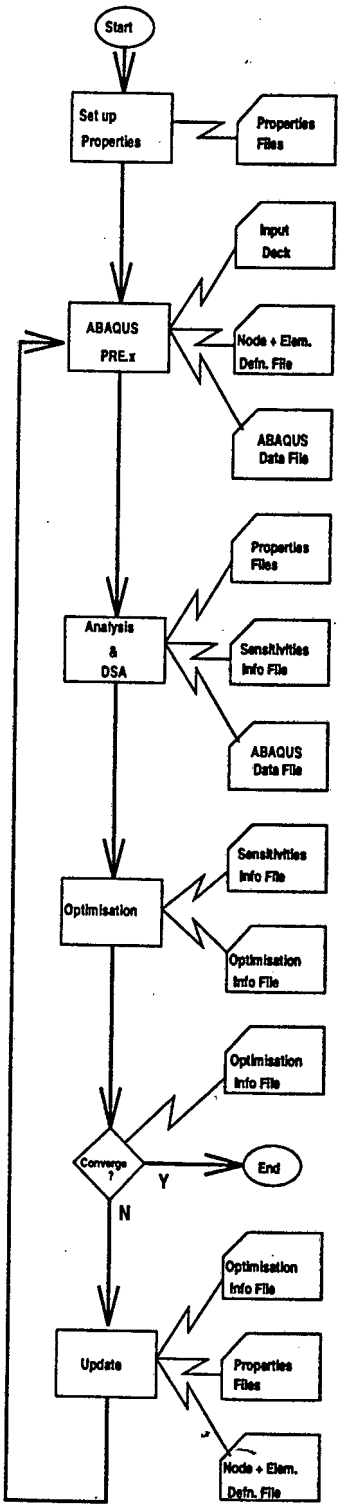

Figure 5.3: The optimisation cycle.

Chapter 6

Numerical Results

6.1 The 3-bar truss

Introduction

The 3-bar truss, due to its geometric simplicity, is generally used as a benchmark for testing different design sensitivity formulations; the structure investigated here is similar to examples in [31] and [32]. The results presented in this section are intended to demonstrate

i. The implementation of *single*-parameter DSA in ABAQUS.

ii. The performance of the 'intuitive' approach to *non-shape* displacement DSA.

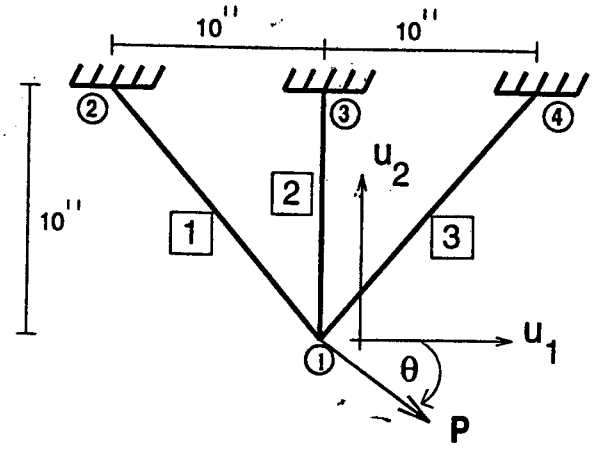

Figure 6.1.1: 3-bar truss configuration.

Material and structural design parameters, as well as loading and boundary conditions, are listed in Table[6.1.1].

Results Summary

The following results were produced for the 3-bar truss structure:

1. Graphical results for a representative loading and deformation of the 3-bar truss is presented in Fig.[6.1.2].

2. Tables[6.1.2-6.1.3][1] present comparative results, verifying the design sensitivity and element formulations, for physically realistic values of the design parameters $\mathbf{b}$ and applied load P, i.e. the values were chosen so as to produce element strain of less than 5%.

3. A selective comparison of the FDM and DSA procedures in estimating the displacement sensitivities $\frac{du_i}{db_j}$ over a range of design parameter values $\mathbf{b}$, and applied loads P, is presented in Figs.[6.1.3-6.1.6].

4. Figs.[6.1.7-6.1.8] similarly provide comparisons between the kinematically nonlinear UL, ABAQUS linear and ABAQUS nonlinear element formulations, for a range of design parameters and applied loads.

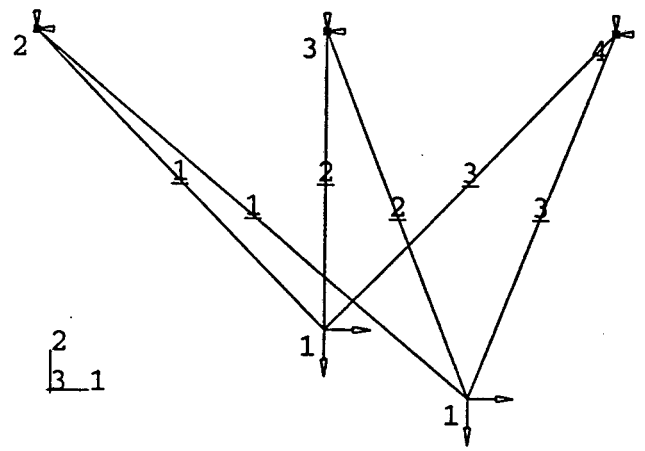

Figure 6.1.2: Initial and Deformed truss structure.

[1]

- The CPU time for UL includes both structural and sensitivity analysis phases. All simulations were performed on an IBM RS/6000 370 workstation.

  NL = Nonlinear kinematic formulation
- LIN = Linear kinematic formulation
  UL = Updated Lagrange NL formulation

Physical properties	
- Young's modulus	: E = 10000 ksi
- Element cross-section	: b_i = A = 0.01 in^2, $i = 1 \ldots 3$
- Structure proportions	: cf. Fig.[6.1.1]
Loads and Constraints	
- Load	: P acts at an angle $\theta = 45°$ below the horizontal at node point 1, as illustrated in Fig.[6.1.1]
- Constraint	: Node points 2, 3 and 4 are fixed.
Analysis procedure	
- UL kinematically nonlinear	
DSA procedure	

- Sensitivities calculated with regard to non-shape cross-sectional design parameters **b** utilising a *displacement-based* 'intuitive' DSA approach.
- Calculate $\frac{du_i^{(j)}}{d\mathbf{b}}$ in order to obtain the objective functional sensitivity $\nabla_{\mathbf{b}}\Psi_i^{(j)}$, where $\Psi_i^{(j)} = \left[\left(\frac{u_i^{(j)}}{0.005}\right)^2 - 1\right]$, so that

$$\nabla_{\mathbf{b}}\Psi_i^{(j)} \equiv \frac{d\Psi_i^{(j)}}{d\mathbf{b}} = \frac{\partial\Psi_i^{(j)}}{\partial u_i^{(j)}} \cdot \frac{du_i^{(j)}}{d\mathbf{b}} + \frac{\partial\Psi_i^{(j)}}{\partial \mathbf{b}}$$
$$= \left(80000\, u_i^{(j)}\right)\left(\frac{du_i^{(j)}}{d\mathbf{b}}\right)$$

with j $\equiv$ node number and i $\equiv x$ or y

Table 6.1.1: Analysis data.

Results

For a particular selection of design parameter values, **b**, and applied load P, Table[6.1.2] is intended to provide a comparison of the functional sensitivity vectors $\frac{d\Psi}{d\mathbf{b}}$ generated by the DSA and FDM procedures. Table[6.1.3] similarly serves to investigate the relative performance of the UL analysis procedure employed in this section. The results presented in Tables[6.1.2-6.1.3] were obtained for physically realistic strain response values of 1.3%-3.9% - i.e. the strain is sufficiently small for the UL procedure to be viable - and consequently a better than 97% DSA-FDM correspondence is obtained in most instances.

	$\frac{d\Psi_x^{(1)}}{db_1}$	$\frac{d\Psi_x^{(1)}}{db_2}$	$\frac{d\Psi_x^{(1)}}{db_3}$	$\frac{d\Psi_y^{(1)}}{db_1}$	$\frac{d\Psi_y^{(1)}}{db_2}$	$\frac{d\Psi_y^{(1)}}{db_3}$
DSA	-227880.7	313579.5	-292793.6	-53200.9	-217816.8	130878.9
FDM	-233476.1	299964.7	-298593.7	-56190.6	-215479.2	133479.9
DSA/FDM	97.6%	104.5%	98.1%	94.7%	101.1%	98.1%
$b_1 = 0.1$ in^2 , $b_2 = 0.01$ in^2 , $b_3 = 0.01$ in^2 , P = 40 kips , E = 10^4 ksi						

Table 6.1.2: DSA vs. FDM - Comparing sensitivities at node **1**

Disp.: Node 1	UL	ABAQUS NL	ABAQUS LIN	UL/NL
u_1	0.5389	0.5392	0.5432	99.9%
u_2	-0.2656	-0.2666	-0.2250	99.6%
CPU secs.	2.23	0.25	0.17	
$b_1 = 0.1$ in^2 , $b_2 = 0.01$ in^2 , $b_3 = 0.01$ in^2 , P = 40 kips , E = 10^4 ksi				

Table 6.1.3: Verifying the UL element formulation

The performance of the 'intuitive' DSA approach is compared to that of the FDM in Figs.[6.1.3-6.1.6] for a wide range of design parameter, b, and load, P, values. In most of the figures a distinctive divergence of the FDM and DSA sensitivity estimates are noted for large deformation accompanied by large strain.

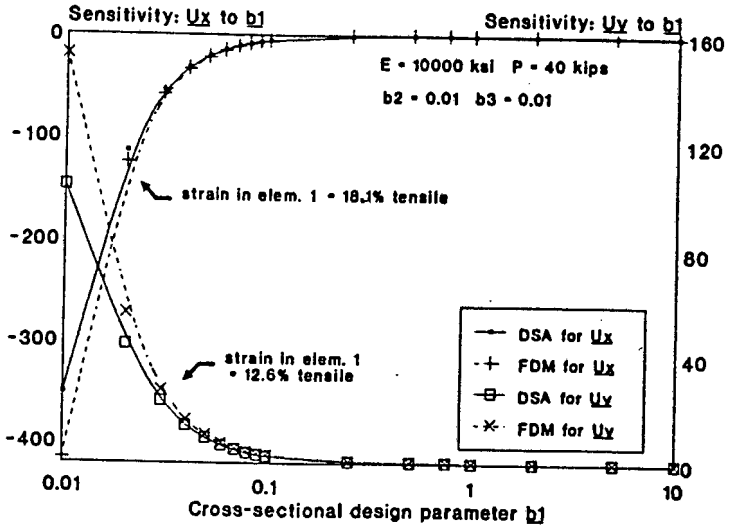

Figure 6.1.3: Displacement sensitivity $\frac{du_1}{db_1}$ vs. design parameter b_1.

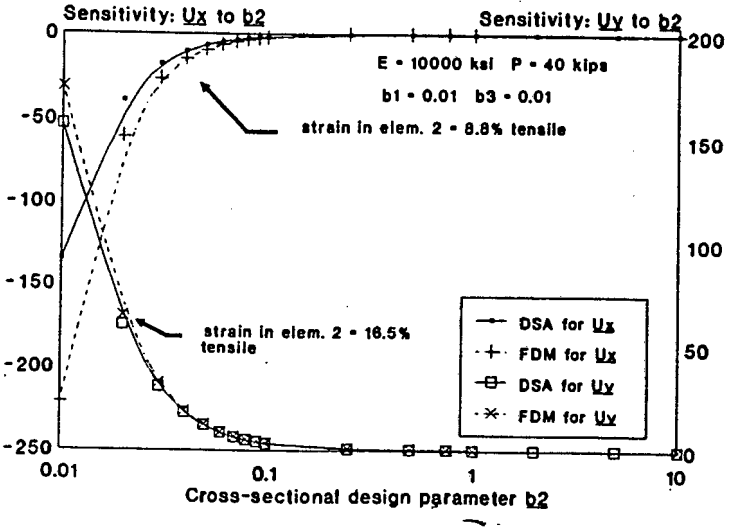

Figure 6.1.4: Displacement sensitivity $\frac{du_1}{db_2}$ vs. design parameter b_2.

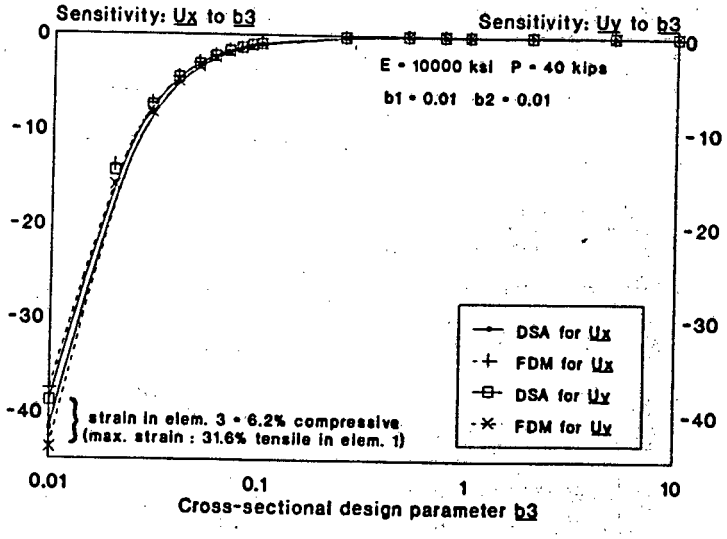

Figure 6.1.5: Displacement sensitivity $\frac{du_1}{db_3}$ vs. design parameter b_3.

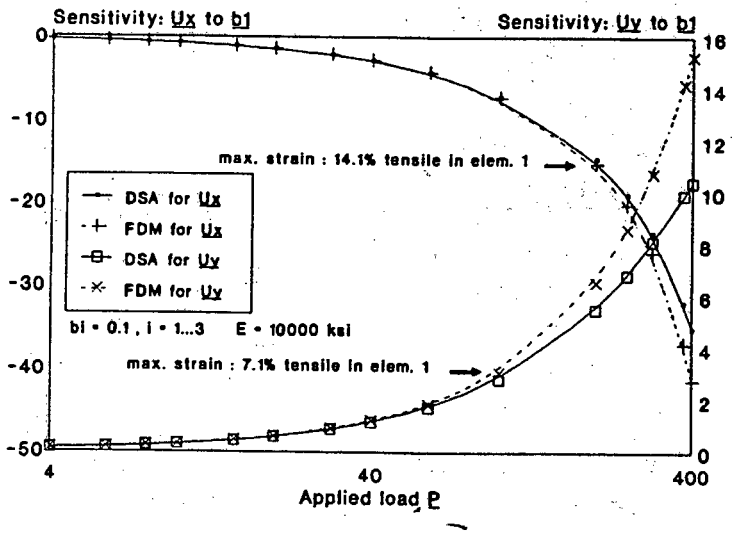

Figure 6.1.6: Displacement sensitivity $\frac{du_1}{db_1}$ vs. applied load P.

In verifying the relative performance of the UL analysis procedure, cf. Figs.[6.1.7-6.1.8], for the same range of design parameter b_2 and load values employed in the sensitivity comparisons, a similar trend of decreasing accuracy with increasing strain is noted.

As illustrated in Fig.[6.1.7], the ABAQUS linear bar element formulation fails inexplicably for the entire range of strain values employed in this particular applications. Several modifications were made to the problem in an attempt to obtain a sensible response from the linear element, without success.

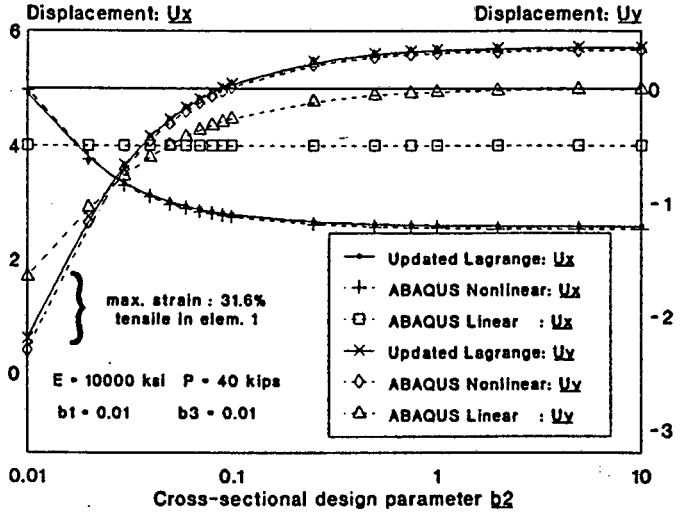

Figure 6.1.7: Displacement u_1 vs. design parameter b_2.

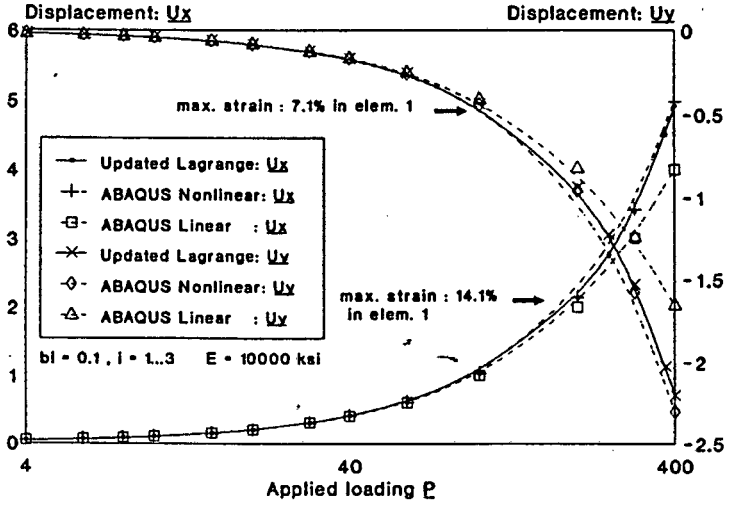

Figure 6.1.8: Displacement u_1 vs. applied load P.

Results discussion

- The marked increase in computational time for the user UL element formulation, noted in Table[6.1.3], is largely due to the inclusion of the sensitivity analysis procedure in the ABAQUS user element routine UEL. For *multi*-parameter DSA, however, the computational time increases at a less than linear rate with respect to the number of design parameters, as is evident from Table[6.2.2] in the next section. Computational costs for truss-like structures remain well within reason.

- The notable divergence of the FDM and DSA estimates for *large* strain, or rather, the lack of such divergence for large deformation accompanied by *small* strain in Figs.[6.1.4-6.1.5], is directly attributable to the decreasing accuracy of the UL formulation for large strain. This results from the fact that the 'intuitive' DSA approach depends on the stiffness matrix produced by the UL analysis procedure and the large strain performance of the UL, hence, detrimentally influences the sensitivity analysis routine. This issue is further underscored by results presented in the ensuing sections.

- Of interest is the y-direction displacement behaviour of nodal point **1** for variation in the cross-sectional design parameter b_2, cf. Figs.[6.1.8]: for increasing values of b_2, element **2** starts behaving like a rigid body and the truss tends to perform more like a pendulum and less like a deformable body, hence the transition from negative to positive y-displacement.

6.2 The 10-bar truss

Introduction

Extending the application of the ABAQUS-integrated DSA implementation to the 10-bar truss problem, cf. Fig.[6.2.1], the aims of this section are

i. primarily to demonstrate the feasibility of multi-parameter DSA with ABAQUS.

ii. to verify the performance of the displacement-based 'intuitive' DSA approach for the more complex 10-bar truss structure.

The truss structure investigated here is broadly based on similar examples in [5] and [32].

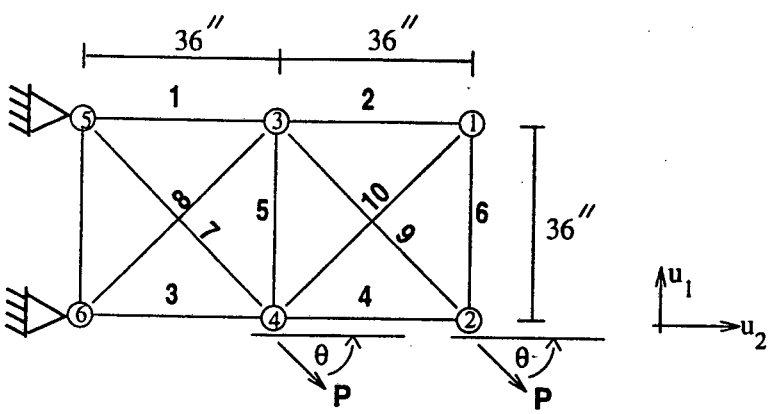

Figure 6.2.1: 10-bar truss configuration.

Details pertaining to the material properties, loading conditions and the DSA procedure are summarised in Table[6.2.1].

Results Summary

The following results were produced for the 10-bar truss structure:

1. Fig.[6.2.2] graphically illustrates a typical structural deformation for a representative loading condition.
2. Table[6.2.2] provides a comparison of displacement estimates u_x, u_y at node **1** for the loading illustrated in Fig.[6.2.2].
3. In Table[6.2.3] a comparison of FDM and DSA displacement sensitivities $\frac{\partial u_1}{\partial b_i}$ is presented.
4. Figs.[6.2.3-6.2.4] contain a comparative evaluation of the DSA and FDM displacement sensitivities $\frac{\partial u_1}{\partial b_1}$ for a range of values of b_1, and P, respectively.
5. Figs.[6.2.5-6.2.8] conclude with a verification of the UL analysis procedure: the displacement $\mathbf{u} \equiv \mathbf{u}_1$ at node **1** is monitored for a range of values of the cross-sectional design parameter b_1, and load P.

Results

The UL kinematically nonlinear formulation is used here, as with the 3 and 200-bar truss structures, largely due to its compatibility with the relatively straightforward 'intuitive' DSA approach. As a consequence the loading condition is limited to physically realistic scenarios, i.e. strain $< 5\%$. Fig.[6.2.2] illustrates a typical deformation mode.

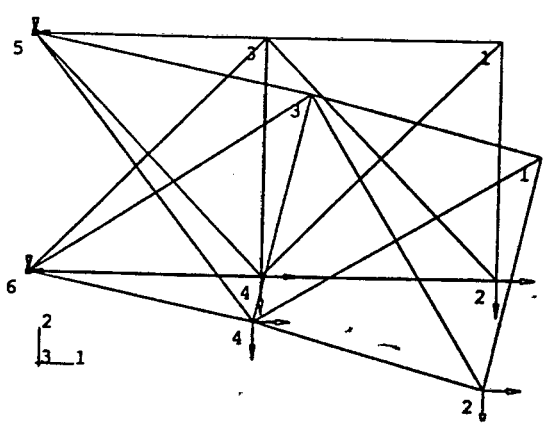

Figure 6.2.2: 10-bar truss structure loading and deformation.

Physical properties	
- Young's modulus	: E = 10000 ksi
- Element cross-section	: $b_i = A = 0.1$ in^2 , $i = 1 \ldots 10$
- Structure proportions	: cf. Fig.[6.2.1]
Loads and Constraints	
- Load	: P acts at an angle $\theta = 45^o$ below the horizontal at node points 4 and 2, as illustrated in Fig.[6.2.1]
- Constraint	: Node points 5 and 6 are fixed.
Analysis procedure	
- UL kinematically nonlinear	
DSA procedure	

- Sensitivities are calculated with regard to non-shape cross-sectional design parameters b utilising a *displacement-based* 'intuitive' DSA approach.
- Calculate $\dfrac{du_i^{(j)}}{d\mathrm{b}}$ in order to obtain the objective functional sensitivity $\nabla_{\mathrm{b}}\Psi_i^{(j)}$, where $\Psi_i^{(j)} = \left[\left(\dfrac{u_i^{(j)}}{2}\right)^2 - 1\right]$, so that

$$\nabla_{\mathrm{b}}\Psi_i^{(j)} \equiv \frac{d\Psi_i^{(j)}}{d\mathrm{b}} = \frac{\partial\Psi_i^{(j)}}{\partial u_i^{(j)}} \cdot \frac{du_i^{(j)}}{d\mathrm{b}} + \frac{\partial\Psi_i^{(j)}}{\partial \mathrm{b}} = \frac{u_i^{(j)}}{2}\left(\frac{du_i^{(j)}}{d\mathrm{b}}\right)$$

with j $\equiv$ node number and i $\equiv x$ or y

Table 6.2.1: Analysis data.

Table[6.2.2] supports Fig.[6.2.2] in numerically comparing displacement values at node 1 for the Total (TL) and Updated Lagrange (UL) procedures, employed here for analysing the 10-bar truss, with the ABAQUS linear and nonlinear C1D2 element formulation. The table clearly demonstrates the decreasing accuracy of the UL procedure for increasing values of strain, hence, for large strain problems, the TL is adopted along with the more complex 'rigorous' DSA approach. The table additionally reveals that the computational time increases two to three-fold for the UL and TL user element routines; this increase is directly attributable to the incorporation of DSA into the ABAQUS user element routine UEL.

Disp.: Node 1	TL	UL	ABAQUS NL	ABAQUS LIN	TL/NL	UL/NL
u_x	0.959	1.140	0.956	1.045	100.3%	119.2%
u_y	-3.681	-3.745	-3.442	-3.606	106.9%	108.8%
CPU secs.	2.640	1.920	0.870	0.800	303.4%	220.6%
$b_i = 0.5$ in^2 , $i = 1 \ldots 10$ $\quad$ $P = 100$ kips						

Table 6.2.2: Node 1 displacements u_x, u_y for a representative loading condition.

The incorporation of multi-parameter DSA in ABAQUS is a crucial step towards enabling multiple constraint optimisation. Table[6.2.3] compares the FDM and DSA objective function sensitivity vectors $\frac{\partial \Psi^{(1)}}{\partial \mathbf{b}}$ evaluated at node 1. From the table the satisfactory performance of the DSA procedure for *large* sensitivities is evident, however, for very small sensitivities a notable divergence is observed (cf. b_5).

Figs.[6.2.3-6.2.4] serve to verify the displacement-based 'intuitive' DSA approach. The DSA and FDM displacement sensitivities $\frac{\partial u_1}{\partial b_1}$, and $\frac{\partial u_1}{\partial P}$, are compared for a wide range of variation in the values of the cross-sectional design parameter $b_1 \equiv A$, and the applied load P, respectively. For this particular truss configuration and loading condition, DSA-FDM convergence is achieved for deformations well exceeding physically realistic values, underscoring the robustness of the DSA formulation.

Des. var b_i	$\frac{d\Psi_x^{(1)}}{db_i}$	$\frac{\Delta\Psi_x^{(1)}}{\Delta b_i}$	$\frac{DSA}{FDM}$	$\frac{d\Psi_y^{(1)}}{db_i}$	$\frac{\Delta\Psi_y^{(1)}}{\Delta b_i}$	$\frac{DSA}{FDM}$
b1	-1.361E-1	-1.404E-1	96.9%	-7.629E-1	-7.872E-1	96.9%
b2	-2.553E-2	-2.523E-2	101.0%	-5.331E-2	-5.151E-2	103.5%
b3	-2.173E-3	-2.916E-3	74.5%	-1.152E-1	-1.216E-1	94.7%
b4	2.362E-3	2.916E-3	80.9%	4.055E-2	4.383E-2	92.5%
b5	-7.068E-5	-3.246E-5	217.7%	2.518E-5	3.653E-4	68.9%
b6	2.664E-3	3.132E-3	85.1%	4.324E-2	4.566E-2	94.7%
b7	-3.399E-2	-3.769E-2	90.2%	-5.417E-1	-5.783E-1	93.7%
b8	2.013E-2	1.815E-2	110.9%	-2.870E-1	-2.988E-1	96.0%
b9	-1.629E-2	-1.847E-2	88.2%	-2.641E-1	-2.779E-1	95.0%
b10	8.038E-3	7.561E-3	106.3%	-1.421E-1	-1.410E-1	100.8%
$b_i = 0.5$ in^2 , $i = 1 \ldots 10$				$P = 40$ kips		

Table 6.2.3: DSA vs. FDM - Comparing sensitivities $\frac{\partial u_1}{\partial b_i}$.

The large strain behaviour, observed in Fig.[6.2.3] for the variation in b_1, is particularly illuminating - the FDM/DSA sensitivity response can be separated into three categories:

i. The *large* strain region, for very small values of b_1, where $\left|\frac{\partial u_1}{\partial b_1}\right|_{DSA} \gg \left|\frac{\partial u_1}{\partial b_1}\right|_{FDM}$.

ii. The *small* sensitivity domain where

$$\left|\frac{\partial u_1}{\partial b_1}\right|_{FDM} \text{ and } \left|\frac{\partial u_1}{\partial b_1}\right|_{DSA} < 10^{-4}$$

but often $\left|\frac{\partial u_1}{\partial b_1}\right|_{DSA}\left|\frac{\partial u_1}{\partial b_1}\right|^{-1}_{FDM} \gg 1$ (or $\ll 1$).

iii. The sensitivity domain, excluding those regions listed in the preceding categories, for which

$$1 \geq \left|\frac{\partial u_1}{\partial b_1}\right|_{DSA} \text{ and } \left|\frac{\partial u_1}{\partial b_1}\right|_{FDM} \geq 10^{-2}$$

and usually $\left|\frac{\partial u_1}{\partial b_1}\right|_{DSA}\left|\frac{\partial u_1}{\partial b_1}\right|^{-1}_{FDM} \approx 1$

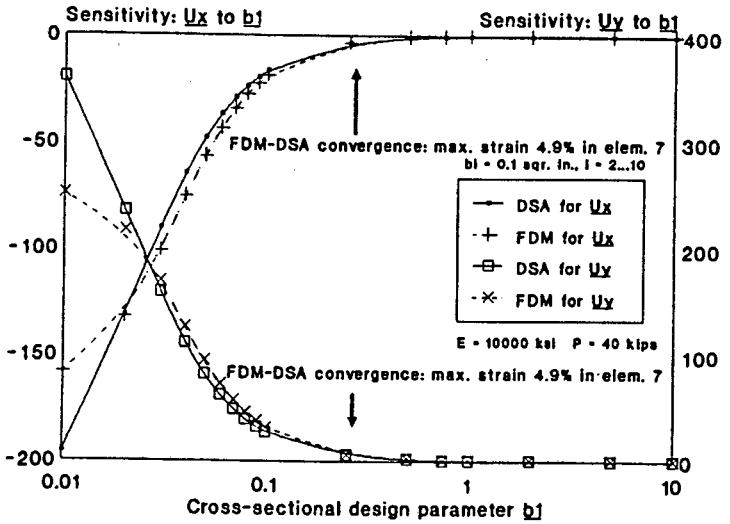

Figure 6.2.3: DSA and FDM estimates $\frac{du_1}{db_1}$ vs. b_1

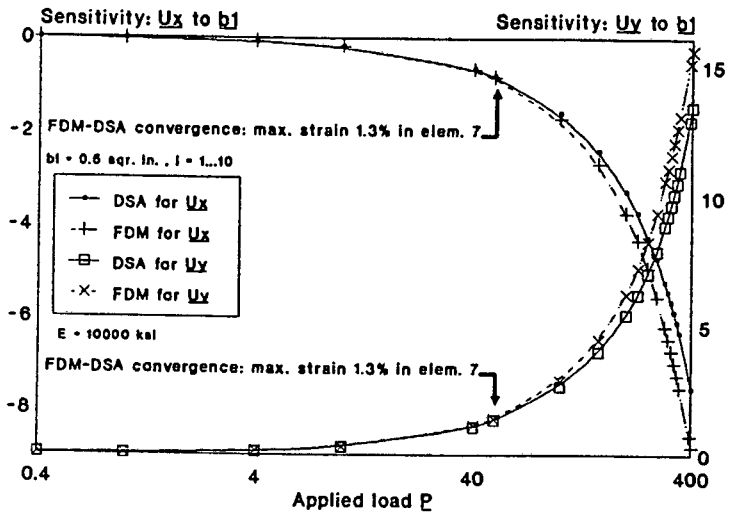

Figure 6.2.4: DSA and FDM estimates $\frac{du_1}{db_1}$ vs. P

The displacement response $\mathbf{u} \equiv \mathbf{u}_1$, at node point **1**, is compared in Figs.[6.2.5-6.2.8] for various element formulations over the same range of values b_1 and P used in Figs.[6.2.3-6.2.4]. The comparison serves to:

i. Underscore the relationship between sensitivity response and strain.

ii. Confirm the UL analysis results and strain behaviour for large structural deformation of the 10-bar truss.

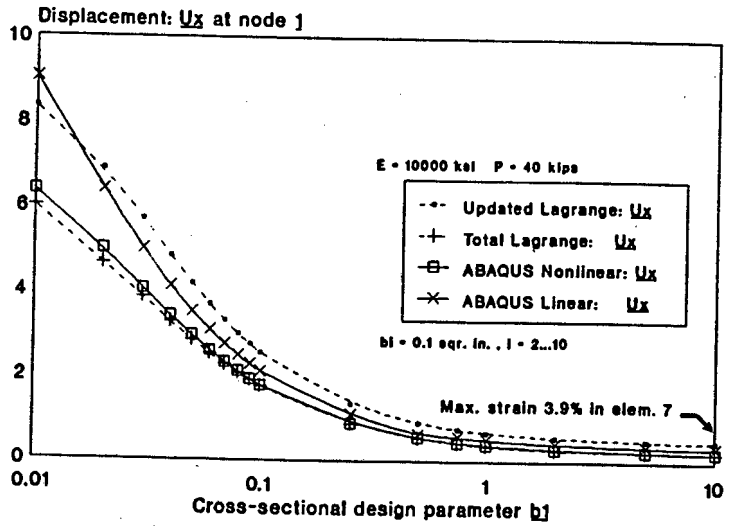

Figure 6.2.5: Node 1 displacement u_x vs. b_1

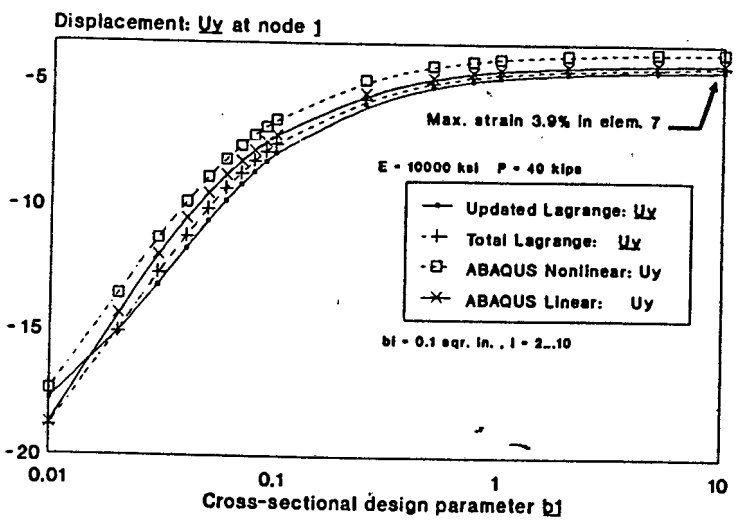

Figure 6.2.6: Node 1 displacement u_y vs. b_1

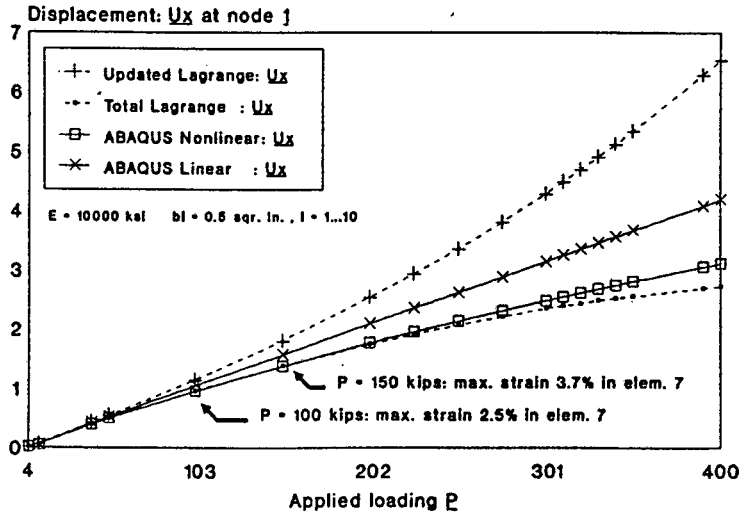

Figure 6.2.7: Node 1 displacement u_x vs. P

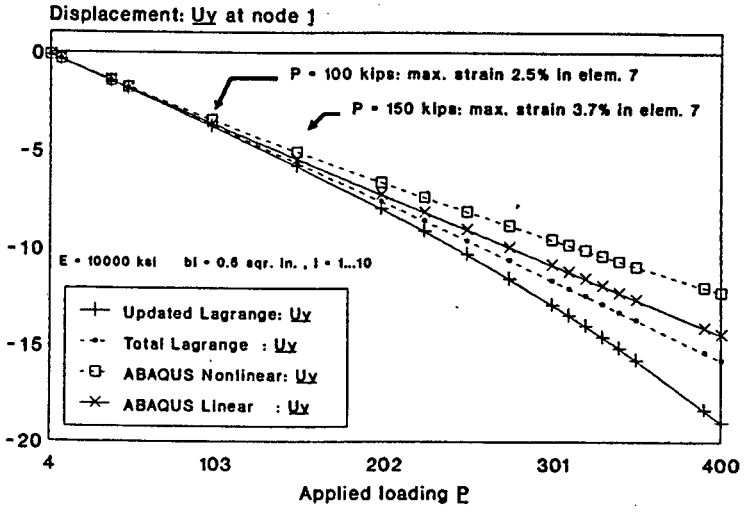

Figure 6.2.8: Node 1 displacement u_y vs. P

Results discussion

- For very small sensitivity response values ($< 10^{-4}$) numerical errors, largely attributable to a loss of significance in the ABAQUS solver (which in the particular DSA implementation employed here is used to resolve sensitivities of order 10^{-4} amid numerical values often exceeding order 10^{4}), cause inaccuracies in the DSA sensitivity estimates, cf. b_5 in Table[6.2.3]. Due to the relatively negligible magnitudes of these sensitivities, such inaccuracies have no observable negative influence and are generally disregarded.

- The divergence between FDM and DSA sensitivity response estimates, particularly noticeable in Fig.[6.2.3], is a result of the tendency of the UL procedure to overestimate structural deformation for large strain (cf. Figs.[6.2.5-6.2.8]) and, hence, adversely affects the stiffness matrix on which the 'intuitive' DSA approach is based; this causes the DSA procedure to become progressively more inaccurate. The TL formulation, used in conjunction with the 'rigorous' DSA approach, in most cases proves to be much more effectual for large-strain deformation cases.

- The load magnitude and orientation, as well as material parameters, for which displacement results are presented in Figs.[6.2.5-6.2.8], were chosen so as to maximise the cumulative strain effect in the structure. This effect is clearly visible in the divergence of the UL procedure with respect to the other element formulations. The aim in doing this is to demonstrate the non-dependence (on the element formulation) of the functional accuracy of the 'intuitive' DSA approach; i.e. even in instances where the reponse variables are inaccurate, the convergence of FDM-DSA results, based on these variables, is nevertheless high in most cases, cf. Figs.[6.2.3-6.2.4].

- Failure of the UL element formulation for very large strain values is apparent in Figs.[6.2.5-6.2.6] for $b_1 \approx 0.01$.

6.3 The 200-bar truss

Introduction

The results presented in this section were generated for a 200-bar truss structure Fig.[6.3.1] based on the example investigated in [5] and [32].

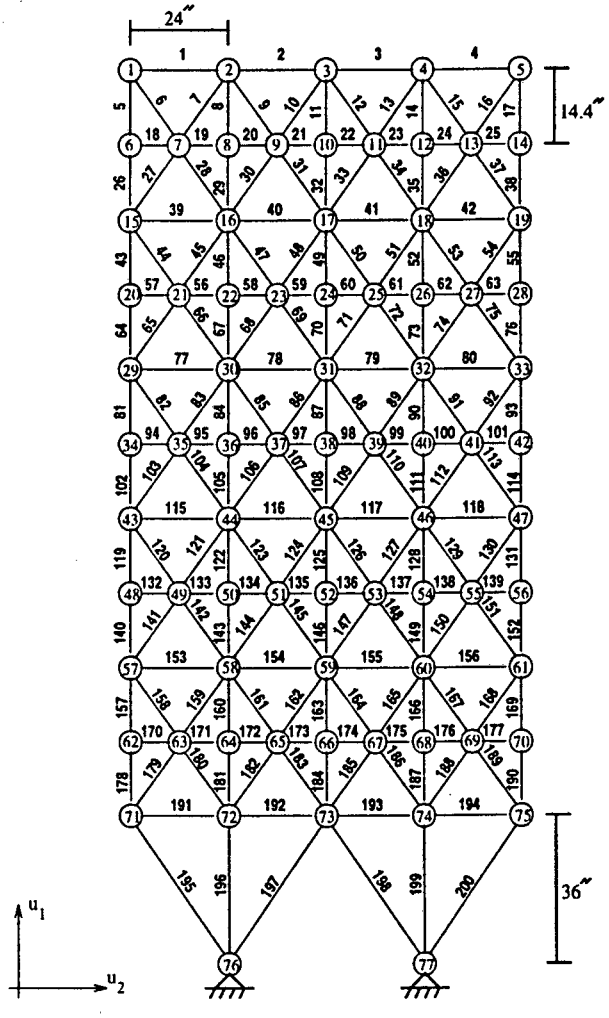

Figure 6.3.1: 200-bar truss configuration.

The elements in the truss structure are apportioned into 29 groups, each of which is assigned specific physical properties and loading conditions [5]; refer to Table[6.3.1].

The physical properties of the truss structure, the loading and boundary conditions imposed, as well as the sensitivity analysis procedure employed, are summarised in Table[6.3.2].

The objective of this section is two-fold:

1. To demonstrate the feasibility of extending the DSA procedure, utilised in the previous results section, to accommodate *generalised* objective and constraint functionals, i.e. functionals $\Psi \equiv \Psi(\mathbf{u}, \boldsymbol{\varepsilon}, \boldsymbol{\sigma})$, dependent on a range of response variables.

2. To underline the capacity of the DSA procedure to perform multiple parameter sensitivity analysis, as first demonstrated in the 10-bar results section. Consistently selecting the bar element cross-section as the *non-shape* design parameter, the sensitivity of displacement $\mathbf{u}$ at node **1** is calculated subject to variation in *all* 200 bar element's cross-sections, thus producing a 200×2 sensitivity vector $\frac{\partial \mathbf{u}}{\partial \mathbf{b}}$. This result is crucial in illustrating the value of DSA, and its stable implementation into ABAQUS, in enabling the implementation of complex, multi-parameter optimisation.

   Additionally, in keeping with the approach adopted in [32], the DSA procedure is complemented by a routine which identifies the **maximum** stress element for each of 29 element groups (cf. Table[6.3.1]) and performs stress sensitivity calculations exclusively for these 29 elements; a 200×29 stress sensitivity vector is obtained.

Results Summary

The following results are presented in this section:

1. Graphical results for a representative loading and deformation of the 200-bar truss are presented in Fig.[6.3.2].

2. Table[6.3.3] presents a comparative results sampling, verifying the sensitivity formulation for physically realistic values of $\mathbf{b}$ and applied loads P_x, P_y.

3. Table[6.3.4] contains the results of a 200 parameter multivariate DSA performed for the displacement $\mathbf{u}$ at node point **1**.

4. In Figs.[6.3.3-6.3.4] a linear regression of FDM vs. DSA results, for the sensitivities $\frac{\partial \mathbf{u}_1}{\partial b_i}$, is performed as a verification of the DSA displacement sensitivities presented in Table[6.3.4]; the design parameters employed in the comparison

Group number	Elements
1	1-4
2	5, 8, 11, 14, 17
3	19-24
4	18, 25, 56, 63, 94, 101, 132, 139, 170, 177
5	26, 29, 32, 35, 38
6	6, 7, 9, 10, 12, 13, 15, 16, 27, 28, 30, 31, 33, 34, 36, 37
7	39-42
8	43, 46, 49, 52, 55
9	57-62
10	64, 67, 70, 73, 76
11	44, 45, 47, 48, 50, 51, 53, 54, 65, 66, 68, 69, 71, 72, 74, 75
12	77-80
13	81, 84, 87, 90, 93
14	95-100
15	102, 105, 108, 111, 114
16	82, 83, 85, 86, 88, 89, 91, 92, 103, 104, 106, 107, 109, 110, 112, 113
17	115-118
18	119, 122, 125, 128, 131
19	133-138
20	140, 143, 146, 149, 152
21	120, 121, 123, 124, 126, 127, 129, 130, 141, 142, 144, 145, 147, 148, 150, 151
22	153-156
23	157, 160, 163, 166, 169
24	171-176
25	178, 181, 184, 187, 190
26	158, 159, 161, 162, 164, 165, 167, 168, 179, 180, 182, 183, 185, 186, 188, 189
27	191-194
28	195, 197, 198, 200
29	196, 199

Table 6.3.1: Grouping information for the two-hundred bar truss.

Physical properties	
- Young's modulus	: E = 10000 ksi
- Element cross-section	
groups 1-12, 14, 16, 17, 19, 21, 22, 24, 26	: A = 2.24 in^2
groups 13, 15, 18, 20, 23, 25	: A = 7.07 in^2
groups 27-29	: A = 14.14 in^2
- Structure proportions	: cf. Fig.[6.3.1]
Loads and Constraints ($P = P_x = P_y$)	
- Load 1	: P_x acting in the positive x-dirn. at nodes 1, 6, 15, 20, 29, 34, 43, 48, 57, 62, 71
- Load 2	: P_y acting in the negative x-dirn. at nodes 1-6, 8, 10, 12, 14-20, 22, 24, ... , 71-75
- Constraint	: Nodes 76, 77, are fixed.
Analysis procedure	
- UL kinematically nonlinear	
DSA procedure	

- Sensitivities calculated with regard to non-shape cross-sectional design parameters b utilising a *stress-based* 'intuitive' DSA approach.
- Calculate $\frac{\partial \sigma_{11}}{\partial \mathrm{b}}$ in order to obtain the objective functional sensitivity $\frac{\partial \Psi_j}{\partial \mathrm{b}}$, where $\Psi_j = \left[\left(\frac{\sigma_{11}}{200}\right)^2 - 1\right]$, so that

$$\nabla_b \Psi_j = \frac{d\Psi_j}{d\mathrm{b}} = \frac{d\Psi_j}{d\sigma_{11}} \left(\left[\frac{\partial \sigma_{11}}{\partial \mathrm{u}}\right]^{\mathsf{T}} \cdot \frac{d\mathrm{u}}{d\mathrm{b}} + \frac{\partial \sigma_{11}}{\partial \mathrm{b}} \right) + \frac{\partial \Psi_j}{\partial b}$$
$$= \frac{\sigma_{11}}{20000} \left(\frac{\partial \sigma_{11}}{\partial \mathrm{u}}\right)^{\mathsf{T}} \cdot \left(\frac{d\mathrm{u}}{d\mathrm{b}}\right)$$

with j $\equiv$ element for which σ_{11} is measured.

Table 6.3.2: Analysis data.

are b_i for $i = 11, 32, 49, 70, 87, 108, 125, 146, 163, 170\text{-}177, 184, 200$. The loads P_x, P_y are a uniform 200 kips and the element cross-sections are as defined in Table[6.3.2].

5. Figs.[6.3.5-6.3.6] compares the FDM and DSA generated sensitivities of the stress-based objective functional Ψ_{199}, chosen as $\frac{d\Psi_{192}}{db_{200}}$ for simplicity, subject to variation in the design parameter b_{200} and the load magnitudes P_x, P_y, respectively.

6. In conclusion Figs.[6.3.7-6.3.8] present the comparative values of stress σ_{11} in element 199 produced by the UL procedure implemented here, as well as the ABAQUS kinematically linear and nonlinear bar elements, subject to variation in the design parameter b_{200} and load magnitudes across the same range as used in Figs.[6.3.5-6.3.6].

Results

Most results were generated from physical parameters and loading conditions selected to produce physically realistic values for local strains **not** exceeding 5%. The UL procedure, employed in this section for its compatibility with the more straightforward 'intuitive' DSA approach, is less accurate than the TL procedure for localised strain levels in excess of 5%. A typical deformation, for $P = 200$ kips, is presented in Fig.[6.3.2] below.

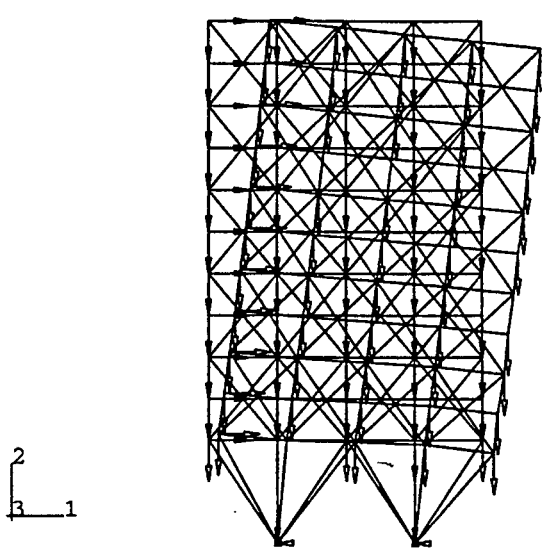

Figure 6.3.2: Truss structure loading and deformation.

In Table[6.3.3] the comparative FDM and DSA stress sensitivities $\frac{\partial \sigma_{11}}{\partial b_{200}}$ and objective functional sensitivities $\frac{d\Psi_{199}}{db_{200}}$, for variation in design parameter b_{200}, are presented for elem. 199, the *maximum* strain element in the truss, as a sampling of the 200 × 29 stress sensitivity vector generated by the implementation used here.

Physical Data	$P_x = 200$ kips	$P_y = 200$ kips	$b_{200} = 0.1414$ in^2
UL Analysis	$\sigma_{11} = -568.077$ ksi	$u_{x\|_{74}} = 1.581$ in	$u_{y\|_{74}} = -2.025$ in
Sens. procedure	$\frac{\partial \sigma_{11}}{\partial b_{200}}$	$\frac{d\Psi_{199}}{db_{200}}$	FDM/DSA
FDM	93.505 ksi	-2.656	
DSA	89.616 ksi	-2.545	104%

Table 6.3.3: Comparative results sample.

With reference to the introduction of this section, implementing multiple parameter DSA is crucial for large scale structural optimisation, as well as being non-trivial in its implementation into ABAQUS; Table[6.3.4] presents the 200 × 2 displacement sensivity vector $\frac{\partial \mathbf{u}}{\partial \mathbf{b}}$ at node point **1** generated by the DSA procedure. In Figs.[6.3.3-6.3.4] a linear regression is performed for the FDM vs. DSA sensitivities generated for the element selection listed in the results summary.

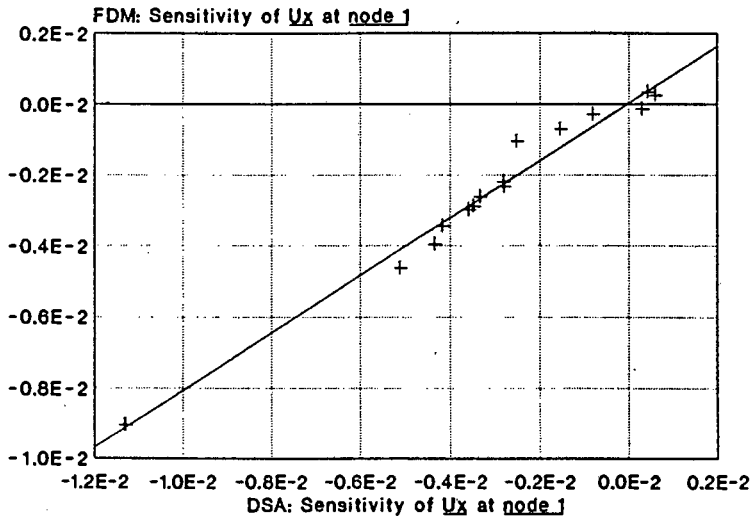

Figure 6.3.3: Linear regression of FDM vs. DSA results for $\frac{du_x^{(1)}}{db_{200}}$.

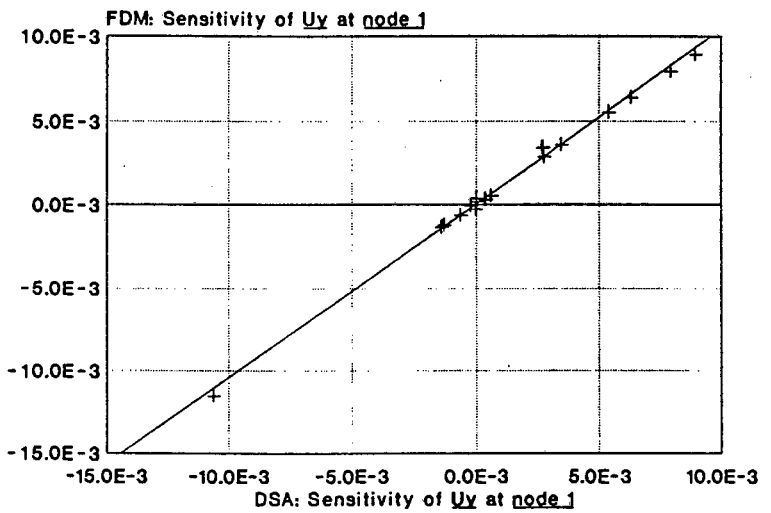

Figure 6.3.4: Linear regression of FDM vs. DSA results for $\frac{du_y^{(1)}}{db_{200}}$.

In keeping with the approach adopted in the preceding results sections, Figs.[6.3.5-6.3.6] and Figs.[6.3.7-6.3.8] respectively verify the stress-based DSA (vs. the FDM) and UL analysis (vs. ABAQUS) procedures for variation in the loadings P_x and P_y and the design parameter b_{200}. The *maximum* stress element 199 is monitored in both the DSA and UL analysis procedures, and the elem. 200 cross-section b_{200} is used consistently as a representative design parameter.

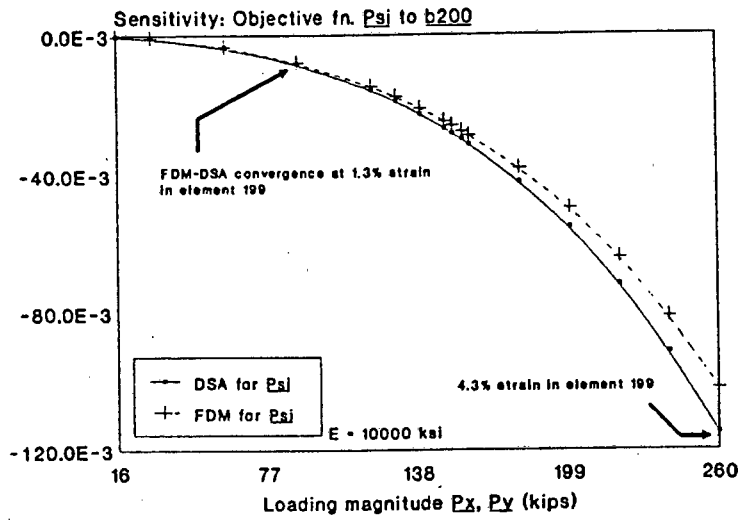

Figure 6.3.5: FDM and DSA sensitivities $\frac{d\Psi_{199}}{db_{200}}$ for variation in P_x, P_y

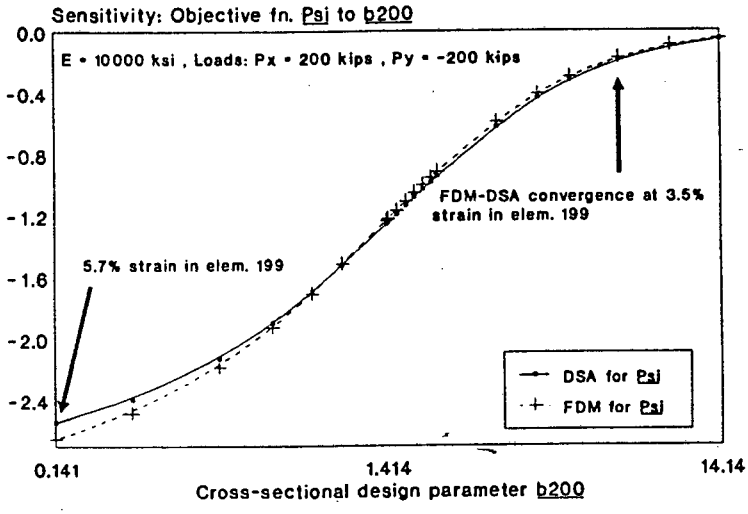

Figure 6.3.6: FDM and DSA sensitivities $\frac{d\Psi_{199}}{db_{200}}$ for variation in b_{200}

	DU_DB(1)	DU_DB(2)		DU_DB(1)	DU_DB(2)		DU_DB(1)	DU_DB(2)		DU_DB(1)	DU_DB(2)
1	-0.414E-01	-0.975E-02	2	-0.330E-02	-0.130E-02	3	0.457E-02	0.220E-02	4	0.148E-02	0.632E-03
5	0.393E-02	0.119E-01	6	-0.203E-01	0.254E-01	7	0.127E-02	-0.688E-05	8	0.368E-03	0.451E-03
9	-0.186E-01	-0.291E-02	10	-0.135E-02	-0.418E-03	11	-0.819E-03	0.122E-04	12	-0.712E-02	-0.264E-02
13	0.100E-02	0.382E-03	14	-0.418E-02	-0.824E-03	15	-0.352E-03	-0.411E-03	16	0.249E-02	0.967E-03
17	-0.345E-02	-0.133E-02	18	-0.421E-03	0.100E-02	19	-0.419E-02	0.971E-03	20	-0.530E-02	0.100E-02
21	-0.111E-03	-0.111E-04	22	-0.726E-03	-0.844E-04	23	0.517E-03	0.108E-03	24	0.479E-03	0.104E-03
25	-0.301E-04	-0.666E-05	26	0.190E-01	0.538E-01	27	-0.628E-02	-0.403E-03	28	-0.193E-01	0.369E-01
29	0.207E-02	0.236E-02	30	-0.118E-01	-0.117E-02	31	-0.303E-01	-0.940E-03	32	-0.252E-02	0.211E-05
33	-0.404E-02	-0.109E-02	34	-0.143E-01	-0.396E-02	35	-0.101E-01	-0.200E-02	36	0.546E-02	0.174E-02
37	-0.685E-03	-0.349E-03	38	-0.819E-02	-0.311E-02	39	-0.509E-02	-0.677E-02	40	-0.201E-02	0.681E-03
41	0.756E-03	-0.239E-03	42	0.153E-02	-0.449E-03	43	0.167E-01	0.228E-01	44	0.118E-02	0.270E-01
45	-0.130E-02	-0.430E-03	46	0.525E-02	0.140E-01	47	-0.424E-01	0.200E-01	48	-0.740E-02	-0.102E-02
49	-0.113E-01	0.264E-02	50	-0.460E-01	-0.266E-02	51	0.565E-02	0.129E-02	52	-0.280E-01	-0.474E-02
53	-0.210E-01	-0.585E-02	54	0.727E-02	0.184E-02	55	-0.363E-01	-0.133E-01	56	-0.529E-04	0.889E-03
57	-0.877E-03	0.284E-05	58	-0.809E-03	0.808E-04	59	-0.115E-04	0.575E-04	60	-0.998E-05	0.738E-04
61	-0.432E-03	-0.306E-03	62	-0.750E-04	-0.221E-03	63	-0.123E-05	0.898E-07	64	0.404E-01	0.537E-01
65	-0.117E-01	-0.342E-02	66	0.452E-02	0.351E-01	67	0.513E-02	0.139E-01	68	-0.209E-01	-0.392E-02
69	-0.530E-01	0.203E-01	70	-0.113E-01	0.269E-02	71	-0.257E-02	-0.435E-03	72	-0.559E-01	-0.138E-02
73	-0.409E-01	-0.684E-02	74	0.107E-01	0.161E-02	75	-0.187E-01	-0.403E-02	76	-0.515E-01	-0.187E-01
77	-0.667E-02	-0.468E-02	78	-0.154E-03	-0.194E-03	79	-0.115E-02	-0.703E-03	80	-0.179E-02	-0.155E-02
81	0.496E-02	0.375E-02	82	-0.102E-01	0.673E-02	83	-0.164E-01	-0.306E-02	84	0.354E-02	0.337E-02
85	-0.492E-01	0.146E-01	86	-0.373E-01	-0.154E-02	87	-0.281E-02	0.273E-02	88	-0.527E-01	0.436E-02
89	-0.230E-01	-0.157E-02	90	-0.174E-01	-0.130E-02	91	-0.170E-01	-0.720E-03	92	-0.520E-02	-0.564E-03
93	-0.189E-01	-0.482E-02	94	0.290E-03	0.721E-03	95	-0.994E-03	-0.676E-03	96	-0.155E-02	-0.748E-03
97	-0.104E-03	0.313E-04	98	0.603E-05	0.902E-05	99	-0.986E-03	-0.135E-03	100	-0.512E-03	-0.109E-03
101	0.514E-05	-0.112E-04	102	0.922E-02	0.690E-02	103	-0.269E-01	-0.201E-02	104	-0.869E-02	0.128E-01
105	0.557E-02	0.534E-02	106	-0.634E-01	-0.501E-02	107	-0.702E-01	0.136E-01	108	-0.359E-02	0.343E-02
109	-0.372E-01	-0.319E-02	110	-0.662E-01	0.348E-02	111	-0.203E-01	-0.150E-02	112	0.147E-02	0.110E-03
113	-0.120E-01	-0.816E-04	114	-0.222E-01	-0.564E-02	115	-0.861E-02	-0.368E-02	116	-0.206E-03	-0.198E-03
117	-0.263E-02	0.276E-03	118	-0.111E-02	-0.300E-03	119	0.474E-02	0.234E-02	120	-0.114E-01	0.986E-02
121	-0.298E-01	-0.493E-02	122	0.674E-02	0.372E-02	123	-0.885E-01	0.140E-01	124	-0.644E-01	-0.454E-02
125	-0.349E-02	0.539E-02	126	-0.103	0.504E-02	127	-0.351E-01	-0.169E-02	128	-0.428E-01	-0.172E-02
129	-0.225E-01	0.112E-02	130	-0.958E-03	0.414E-05	131	-0.361E-01	-0.644E-02	132	0.377E-03	0.473E-03
133	-0.184E-02	-0.851E-03	134	-0.244E-02	-0.918E-03	135	-0.211E-03	0.335E-03	136	0.574E-04	0.226E-03
137	-0.223E-02	0.142E-03	138	-0.217E-02	0.392E-04	139	-0.178E-03	-0.505E-04	140	0.107E-01	0.526E-02
141	-0.365E-01	-0.266E-02	142	-0.419E-02	0.171E-01	143	0.104E-01	0.578E-02	144	-0.108	-0.882E-02
145	-0.128	0.129E-01	146	-0.417E-02	0.630E-02	147	-0.541E-01	-0.377E-02	148	-0.127	0.266E-02
149	-0.472E-01	-0.188E-02	150	0.512E-02	-0.388E-03	151	-0.102E-01	0.109E-02	152	-0.406E-01	-0.722E-02
153	-0.171E-01	-0.545E-02	154	0.516E-03	0.430E-03	155	-0.102E-01	0.530E-03	156	-0.916E-02	-0.918E-03
157	0.114E-02	0.417E-03	158	0.204E-02	0.114E-01	159	-0.444E-01	-0.627E-02	160	0.551E-02	0.201E-02
161	-0.161	0.150E-01	162	-0.971E-01	-0.785E-02	163	-0.282E-02	0.794E-02	164	-0.201	0.312E-02
165	-0.633E-01	-0.323E-02	166	-0.106	-0.512E-02	167	-0.245E-01	0.296E-02	168	0.350E-02	-0.227E-03
169	-0.616E-01	-0.770E-02	170	0.418E-03	0.341E-03	171	-0.434E-02	-0.128E-02	172	-0.510E-02	-0.139E-02
173	0.285E-03	0.602E-03	174	0.599E-03	0.384E-03	175	-0.633E-02	-0.942E-05	176	-0.103E-01	-0.619E-03
177	-0.155E-02	-0.229E-03	178	0.844E-02	0.305E-02	179	-0.380E-01	-0.207E-02	180	0.189E-01	0.185E-01
181	0.117E-01	0.430E-02	182	-0.170	-0.149E-01	183	-0.246	0.106E-01	184	-0.335E-02	0.895E-02
185	-0.103	-0.715E-02	186	-0.266	-0.248E-02	187	-0.113	-0.539E-02	188	-0.847E-02	-0.420E-02
189	-0.114E-02	0.225E-02	190	-0.664E-01	-0.828E-02	191	-0.423E-02	-0.117E-02	192	-0.181E-01	-0.351E-02
193	-0.413E-01	-0.176E-02	194	-0.255E-01	-0.185E-02	195	0.778E-02	0.249E-02	196	0.670E-02	0.220E-02
197	-0.186	-0.286E-01	198	-0.354	-0.209E-01	199	-0.144	-0.706E-02	200	-0.114	-0.106E-01

Table 6.3.4: 200 parameter multivariate DSA.

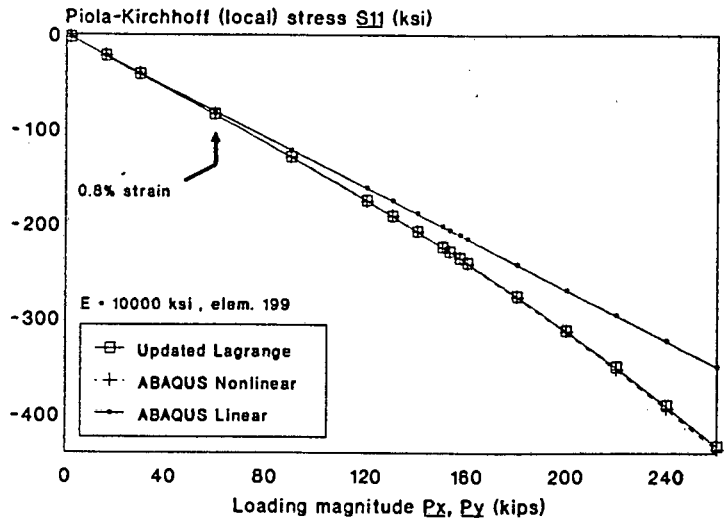

Figure 6.3.7: Comparative stress results for variation in loads P_x, P_y.

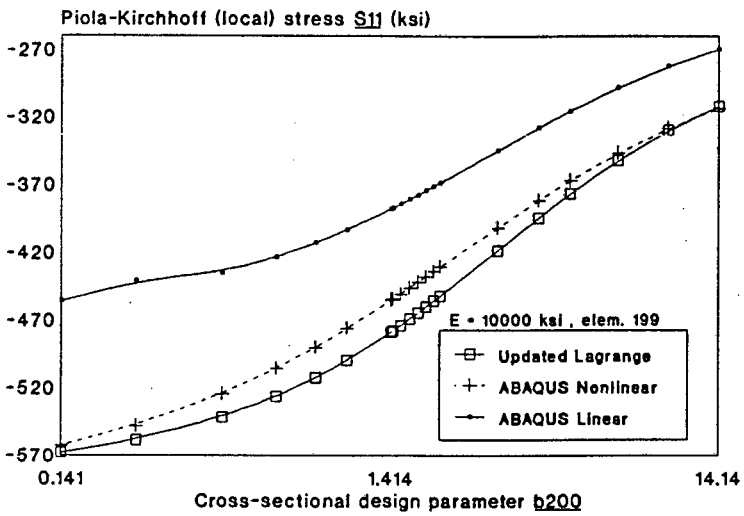

Figure 6.3.8: Comparative stress results for variation in b_{200}.

Results Discussion

- The linear regression in Figs.[6.3.3-6.3.4] confirms the displacement-based 'intuitive' DSA results presented in Table[6.3.4], in comparison with the FDM, for a selection of design parameters. The FDM and DSA results compare very well for the majority of paremeter sensitivities investigated; ie. FDM-DSA correspondence greater than 97% for realistic loading and deformation cases ($< 5\%$ strain).

Notable exceptions tend to occur for

1. Elements under large strain ($> 5\%$).
2. Very small values of sensitivity $\frac{\partial u_1}{\partial b_i}$ ($< 1.0E-3$).

as was observed and commented upon in section (6.2).

- The deviation in the DSA results in case (1) are attributable to the failure of the UL procedure for large strain, whereas case (2) is the result of numerical errors that occur due to a loss of significant numbers in the ABAQUS solver. The latter problem is largely irrelevant due to the negligible size of the sensitivities; in the former case, for large strains, a TL analysis procedure, in conjunction with the 'rigorous' DSA approach, is adopted to avoid inaccuracies.

- Figs.[6.3.5-6.3.6] present comparisons of the ('intuitive' approach) DSA vs. FDM sensitivities of the stress-based objective function, $\frac{d\Psi_{199}}{db_{200}}$, for a range of loads P_x, P_y and values of b_{200}, respectively.

  In Fig.[6.3.5], the DSA and FDM results predictably diverge for large values of strain. On the other hand, better than 99% correspondence is attained for strains of less than 1.3%.

  The sigmoidal behaviour of the object function sensitivity, especially for small values of the design parameter b_{200}, is an accurate reflection of the actual physical behaviour of the truss: variations in the cross-sectional values b_{200}, for small values of b_{200}, result in roughly the **same** stress sensitivity response over a wide range of values b_{200}; i.e., Ψ_{199} becomes **more** sensitive to the *other* design parameters b_i as b_200 is decreased beyond a certain limit.

- Figs.[6.3.7-6.3.8] verifies the UL kinematically nonlinear element formulation employed here over the same range of variation in the loads P_x, P_y and design parameter b_{200}, as employed in Figs.[6.3.5-6.3.6].

Conclusion

The results presented above demonstrate

- the suitability of the model in performing DSA for *generalised* objective and constraint functionals.

- that DSA can be successfully implemented in a commercial FE code, viz. ABAQUS, to conduct large parameter systems sensitivity analyses.

6.4 The 25-bar pylon truss

Introduction

The pylon truss structure investigated here is representative of a whole range of 3D structural problems commonly encountered in industry. Three dimensional structural optimisation problems frequently arise in fields as diverse as electrification and off-shore oil production [22].

The results presented in this section seek to demonstrate the following two vital extensions to the subject matter of the preceding results sections:

i. The implementation of the 'rigorous' displacement-based *non-shape* DSA approach utilising the TL analysis formulation for **large** strain problems.

ii. The implementation of a **shape** (geometric) DSA procedure, employing the 'rigorous' sensitivity analysis approach.

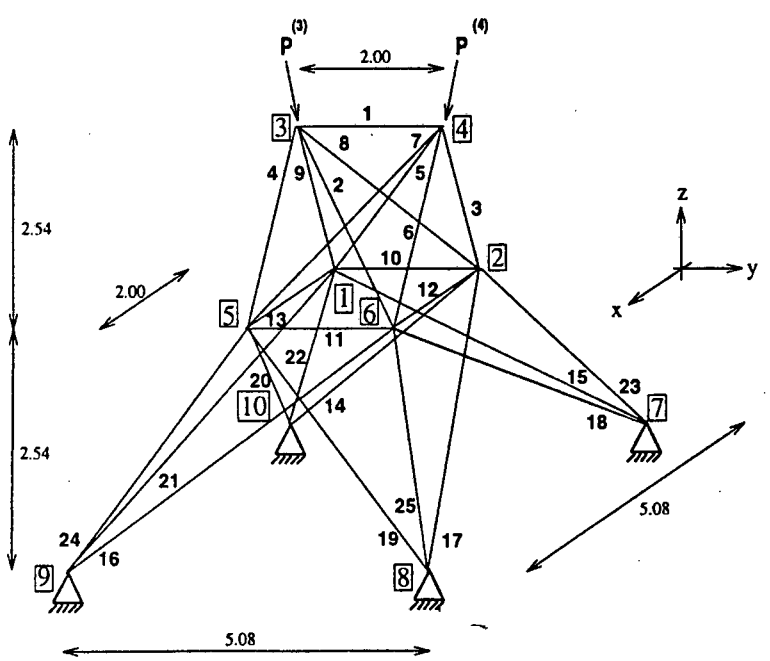

Figure 6.4.1: 25-bar pylon configuration.

The particular functional sensitivity vector formulations for the two cases above, as well as information pertaining to the structural design and loading of the pylon, are summarised in Table[6.4.1].

Results Summary

The results section is divided into two parts, respectively verifying the two DSA enhancements listed above:

1. Graphical results for a representative loading and deformation of the pylon truss structure is presented in Fig.[6.4.2].

2. Fig.[6.4.3] provides a diagrammatic distinction between the **shape** and *non-shape* DSA approaches adopted in the investigation of the pylon's structural behaviour; that is, giving physical meaning to the material and geometric design parameters, b_4 and h, respectively.

3. Table[6.4.2] contains comparative FDM and DSA functional sensitivities, $\frac{d\Psi^{(3)}}{dh}$ and $\frac{d\Psi^{(3)}}{db_4}$, for representative loading P_z and design parameter h values.

4. In Figs.[6.4.4-6.4.9] the displacement responses, in the y and z directions at node point **3**, of the TL, UL, ABAQUS linear and ABAQUS nonlinear formulations are compared for variation in the *non-shape* design parameter, b_4, the *shape* design parameter , h, and the vertical load, P_z, respectively.

5. A comparison of the sensitivity estimates, $\frac{d\Psi_y^{(3)}}{db_4}$ and $\frac{d\Psi_z^{(3)}}{db_4}$, produced by 'intuitive' (with UL) and 'rigorous' (with TL) DSA implementations, as well as the FDM, for variation in b_4 and P_z, is presented in Figs.[6.4.10-6.4.13].

6. In introducing the **shape** DSA formulation results, Figs.[6.4.14] presents the functional sensitivity $\frac{d\Psi_z^{(3)}}{dh}$ for a limited selection of structural configurations.

7. Figs.[6.4.15-6.4.16] compares the FDM and 'rigorous' **shape** DSA functional sensitivity estimates , $\frac{d\Psi_y^{(3)}}{dh}$ and $\frac{d\Psi_z^{(3)}}{dh}$, for a range of *geometric* design parameter values h and loads P_z.

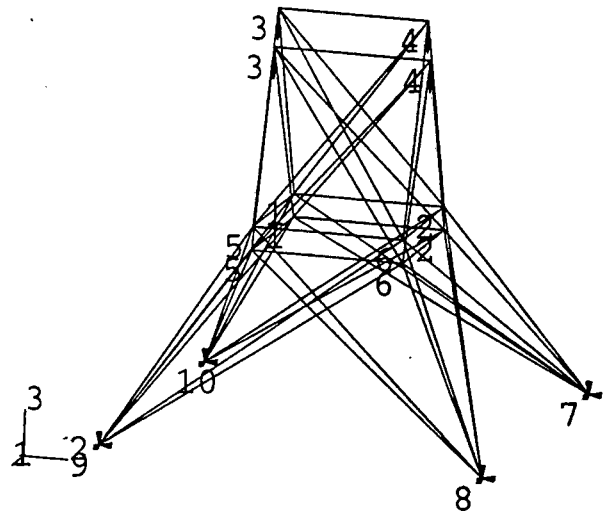

Figure 6.4.2: Initial and Deformed truss structure.

Results

The diagrams in Fig.[6.4.3] lend physical meaning to the sample *shape*, h, and *non-shape*, b_4, design parameters employed in the sensitivity analysis of the 25-bar pylon structure.

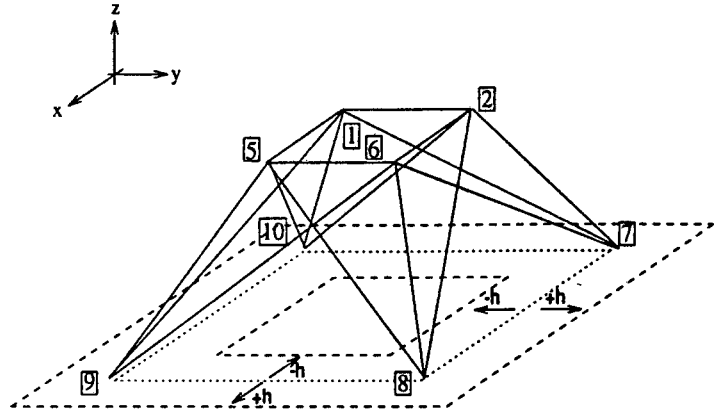

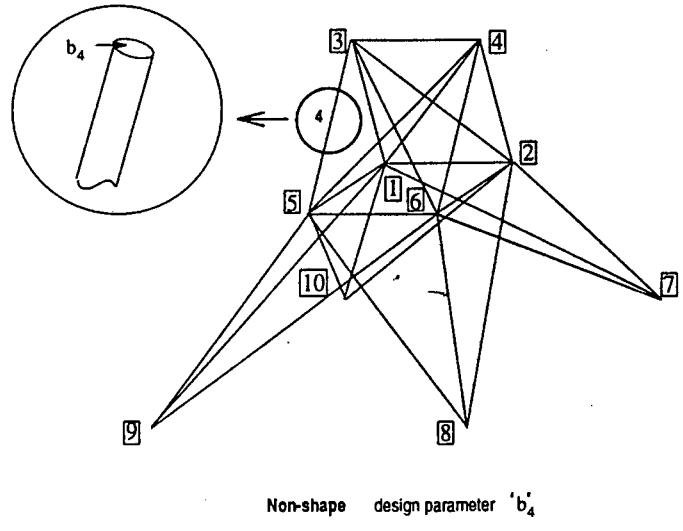

Figure 6.4.3: Shape and Non-shape design parameters.

Physical properties	
- Young's modulus	: $E = 6.9 \times 10^7$ kPa
- Element cross-section	: $b_i = A = 3.225 \times 10^{-4}$ m^2 , $i = 1 \ldots 25$
- Structure proportions	: cf. Fig.[6.4.1]
Loads and Constraints	
- Load	: Node point 3 — $P^{(3)} = (\ 1.92,\ 19.2,\ -P_z\ )$ Node point 4 — $P^{(4)} = (-1.92,\ -19.2,\ -P_z\ )$ where $P_z = 240$ kN, as illustrated in Fig.[6.4.1].
- Constraint	: Node points 7, 8, 9 and 10 are fixed.
Analysis procedure	
- TL and UL kinematically nonlinear	
DSA procedure	

- Non-shape sensitivities $\nabla_{\mathbf{b}}\Psi_i^{(j)}$ calculated w.r.t. cross-sectional design parameters $\mathbf{b}$, utilising a *displacement-based* 'rigorous' DSA approach.
- Calculate $\dfrac{du_i^{(j)}}{d\mathbf{b}}$ in order to obtain the objective functional sensitivity $\nabla_{\mathbf{b}}\Psi_i^{(j)}$, where $\Psi_i^{(j)} = \left(u_i^{(j)}\right)^2 - 1$, so that

$$\nabla_{\mathbf{b}}\Psi_i^{(j)} \equiv \frac{d\Psi_i^{(j)}}{d\mathbf{b}} = \frac{\partial\Psi_i^{(j)}}{\partial u_i^{(j)}} \cdot \frac{du_i^{(j)}}{d\mathbf{b}} + \frac{\partial\Psi_i^{(j)}}{\partial \mathbf{b}} = \left(2\,u_i^{(j)}\right)\left(\frac{du_i^{(j)}}{d\mathbf{b}}\right)$$

- Shape DSA sensitivities $\nabla_h\Psi_i^{(j)}$ calculated with regard to the *geometric* design parameter h, also utilising the 'rigorous' DSA approach.
- The *shape* parameter displacement sensitivities $\dfrac{du_i^{(j)}}{dh}$, and hence the objective functional sensitivities $\nabla_h\Psi_i^{(j)}$, are found in a fashion analogous to the procedure employed for obtaining $\nabla_{\mathbf{b}}\Psi_i^{(j)}$, so that

$$\nabla_h\Psi_i^{(j)} \equiv \frac{d\Psi_i^{(j)}}{dh} = \left(2\,u_i^{(j)}\right)\left(\frac{du_i^{(j)}}{dh}\right)$$

with j $\equiv$ node number and i $\equiv y$ or z

Table 6.4.1: Analysis data.

In order to estimate the relative accuracy of the 'rigorous' DSA approach, used in conjunction with the TL analysis procedure, Table[6.4.2] provides a comparison of FDM and 'rigorous' DSA results for *shape* and *non-shape* functional sensitivities, subject to a representative selection of load and boundary conditions (cf. Fig.[6.4.1]). Additionally, results generated by the 'intuitive' DSA approach have also been included for non-shape sensitivity analysis. As mentioned in chapter 3, shape, or geometric, sensitivity analysis is unfeasible with the 'intuitive' DSA approach, hence the omission of results for DSA_i.

The results predictably indicate a relatively high displacement sensitivity, in node point **3**, to variation in the cross-sectional design parameter b_4 for the given structural configuration; sensitivity to variation in the geometric design parameter h is negligible. An increased shape sensitivity $\frac{d\Psi_i^{(3)}}{dh}$ for large values h is demonstrated in Fig.[6.4.16].

Additionally, from Table[6.4.2] it may be observed that, for the small strain deformation case examined, the DSA_i results perform marginally better than DSA_r relative to the FDM.

	Non-shape		Shape	
	$\frac{d\Psi_y^{(3)}}{db_4}$	$\frac{d\Psi_z^{(3)}}{db_4}$	$\frac{d\Psi_y^{(3)}}{dh}$	$\frac{d\Psi_z^{(3)}}{dh}$
DSA_r	-0.717778E-1	-0.976143	0.544858E-6	0.816130E-3
DSA_i	-0.703918E-1	-0.955257	—	—
FDM	-0.673398E-1	-0.932395	0.510149E-6	0.818099E-3
DSA_r/FDM	106.6%	104.7%	106.8%	99.8%
$b_i = 3.225\times10^{-4}$ m^2 with $i = 1 \ldots 25$, $P_z = 240$ kN , E $= 6.9\times10^7$ kPa $\lvert$ max. $\varepsilon_{xx}\rvert = 0.41\%$ DSA_i : 'intuitive' approach , DSA_r : 'rigorous' approach.				

Table 6.4.2: DSA vs. FDM - Comparing sensitivities at node **3**

The displacement results in Figs.[6.4.4-6.4.9] are generated for variation in the design parameters and loads. The results verify the UL and TL analysis procedures, applied to the pylon truss structure, by comparison with the ABAQUS kinematically nonlinear element formulation. The displacement results are furthermore analysed in order to gain additional insight into the relationship between displacement and functional sensitivity, especially in the case of the 'intuitive' DSA approach.

Due to the tendency of the pylon structure to distribute the load imposed through as many elements as possible, large deformation occurs in conjunction with relatively *small* values of strain. Numerical problems (specifically bifurcation behaviour) prevent imposing material parameters and/or loads which would generate strains in the pylon truss structure in excess of 1%. A comparison of the maximum strain in any element of the pylon structure ($\approx$ 1%) with the maximum strains occuring in the 3-bar truss (cf. Fig.[6.1.3]) enables a proper assessment of the reduced range of behaviour observable for the pylon structure.

Consequently, most displacement results were generated for relatively small values of strain ε_{xx} and, hence, good correspondence between the various nonlinear formulations is maintained. Only for strain values exceeding 3%-4% would divergence of the TL and UL values become more apparent.

Additionally, as will be demonstrated in the case of *non-shape* design parameter sensitivity for *small* strain, any variation between TL and UL based results is more likely to be attributable to numerical error than to inherent characteristics of the formulations.

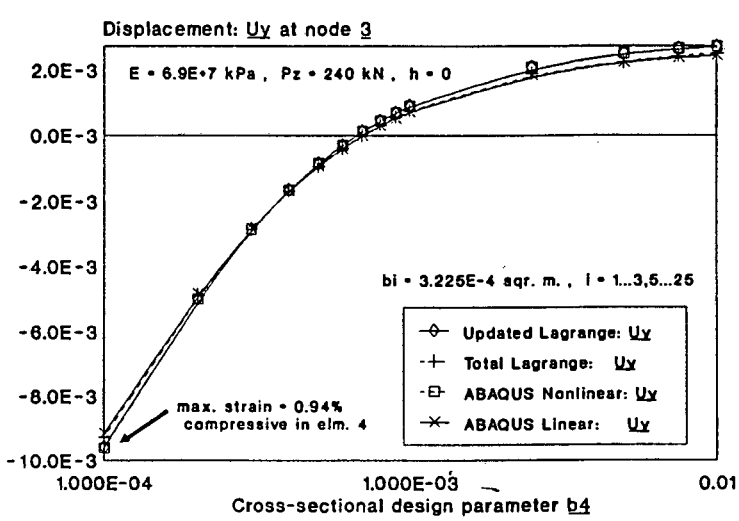

Figure 6.4.4: Displacements $u_y^{(3)}$ vs. cross-section b_4.

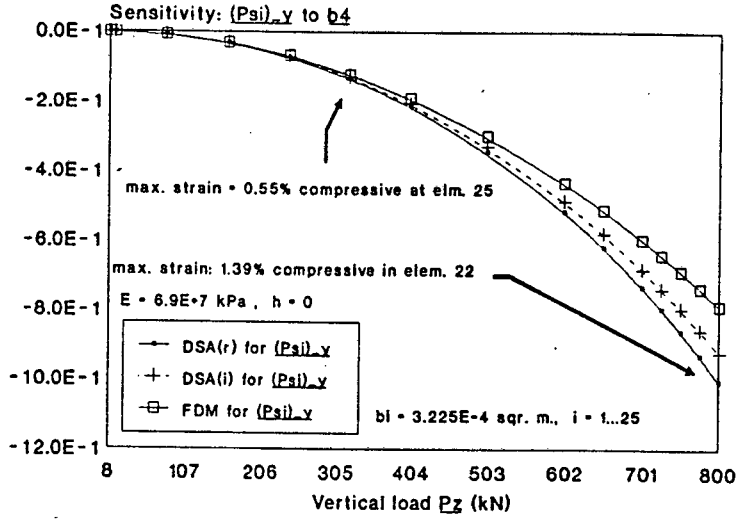

Figure 6.4.12: *Non-shape* sensitivity $\frac{d\Psi_y^{(3)}}{db_4}$ vs. load P_z.

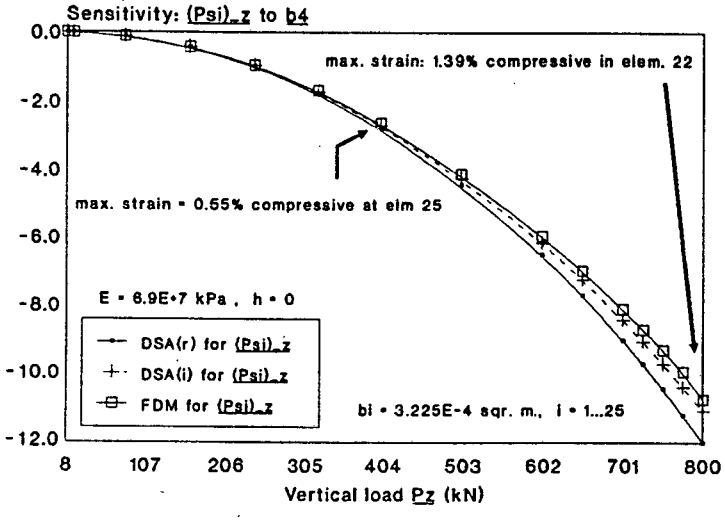

Figure 6.4.13: *Non-shape* sensitivity $\frac{d\Psi_z^{(3)}}{db_4}$ vs. load P_z.

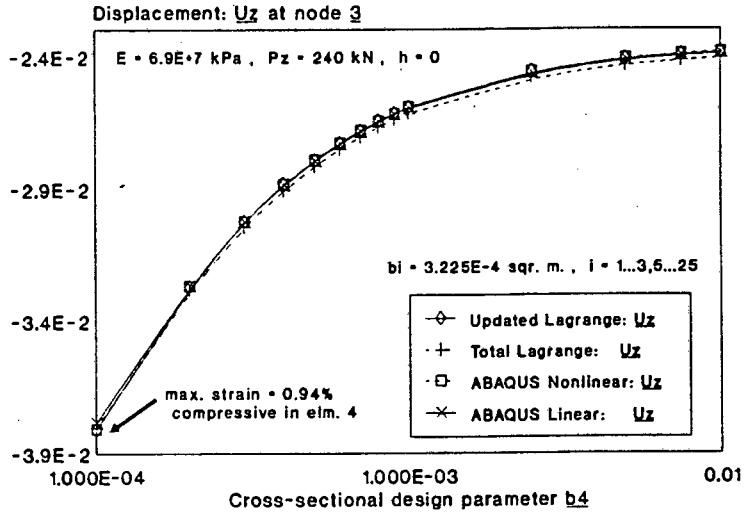

Figure 6.4.5: Displacements $u_z^{(3)}$ vs. cross-section b_4.

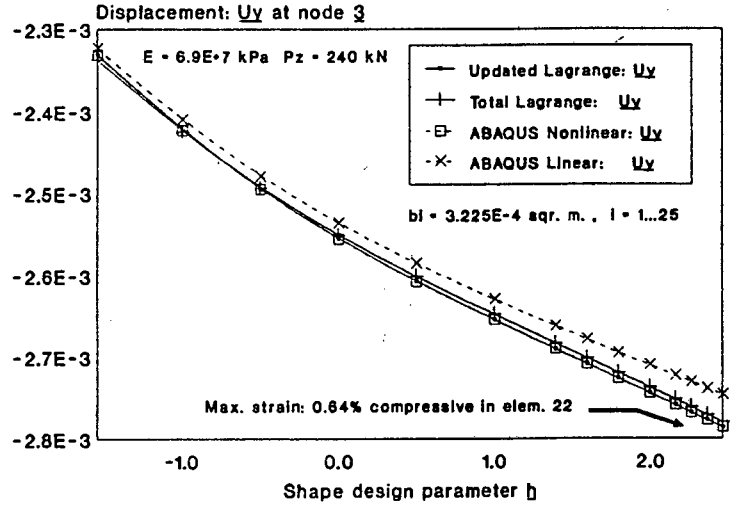

Figure 6.4.6: Displacements $u_y^{(3)}$ vs. *shape* design h.

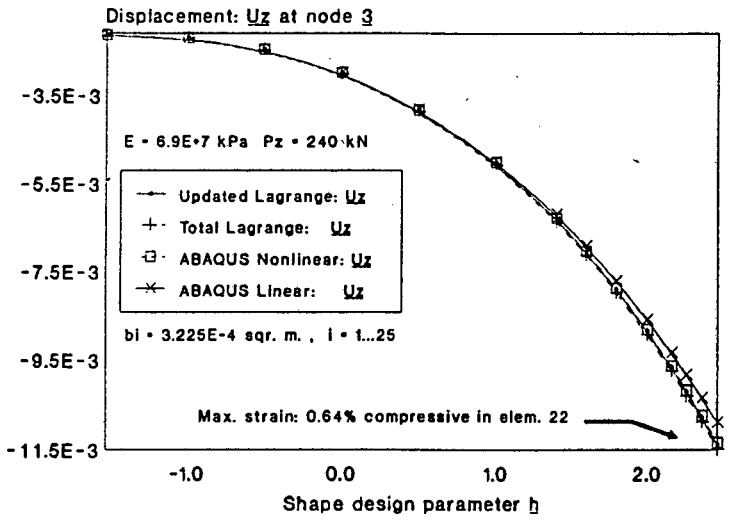

Figure 6.4.7: Displacements $u_z^{(3)}$ vs. *shape* design h.

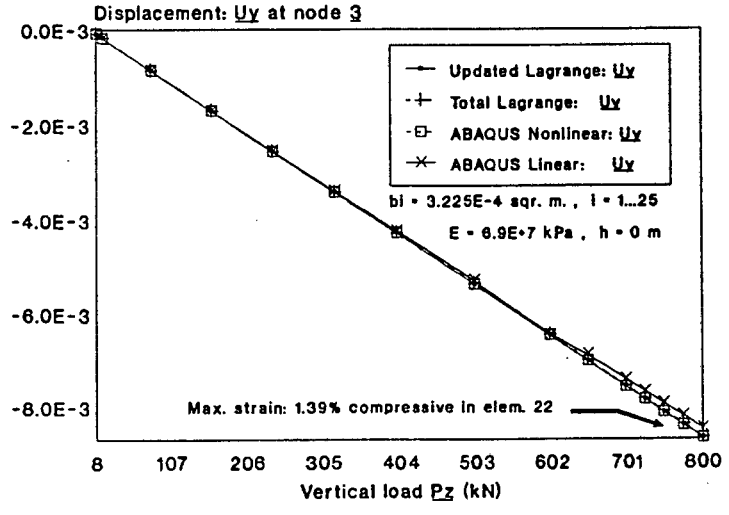

Figure 6.4.8: Displacements $u_y^{(3)}$ vs. load P_z.

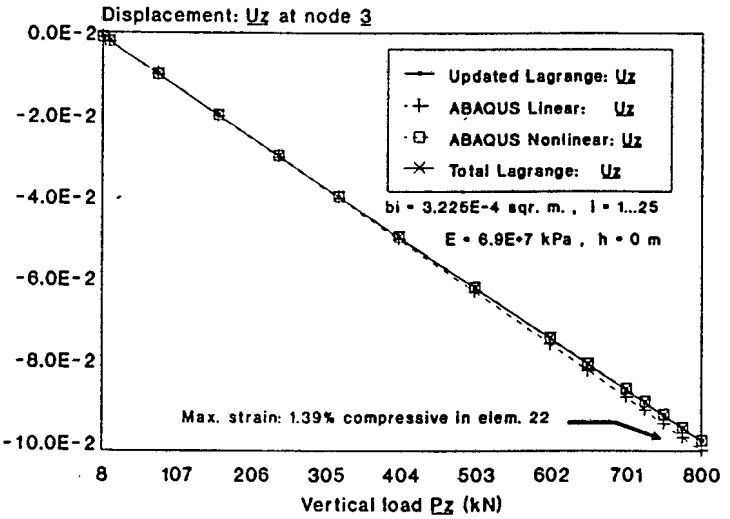

Figure 6.4.9: Displacements $u_z^{(3)}$ vs. load P_z.

The 'rigorous' DSA approach (with TL) is adopted for *shape* sensitivity analysis due to the infeasibility of performing *shape* DSA with the 'intuitive' approach (with UL). For *non-shape* sensitivity analysis of a structure subject to large deformation, however, the main purpose in utilising the 'rigorous' approach stems from the deteriorating accuracy of the UL formulation for large deformation *accompanied* by large strain.

As was the case for the displacement results, the large deformation/*small* strain behaviour of the pylon structure causes convergence of the 'rigorous' and 'intuitive' DSA formulations for a wide range of variation in the cross-sectional design parameter b_4 (cf. Figs.[6.4.10-6.4.11]).

In Figs.[6.4.12-6.4.13], however, distinct divergence between the various sensitivity estimates is clearly observable for relatively *small* strain values ($\approx$ 0.5%). More importantly, the results apparently suggest that the 'intuitive' DSA approach (DSA_i) produces more accurate sensitivity results than the 'rigorous' DSA approach (DSA_r), in direct contradiction to the theory-based expectations. This anomality is discussed towards the end of the section.

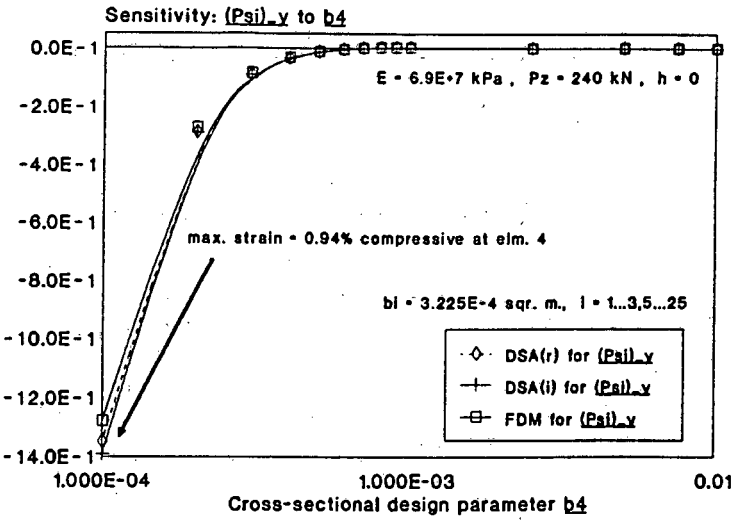

Figure 6.4.10: *Non-shape* sensitivity $\frac{d\Psi_y^{(3)}}{db_4}$ vs. cross-section b_4.

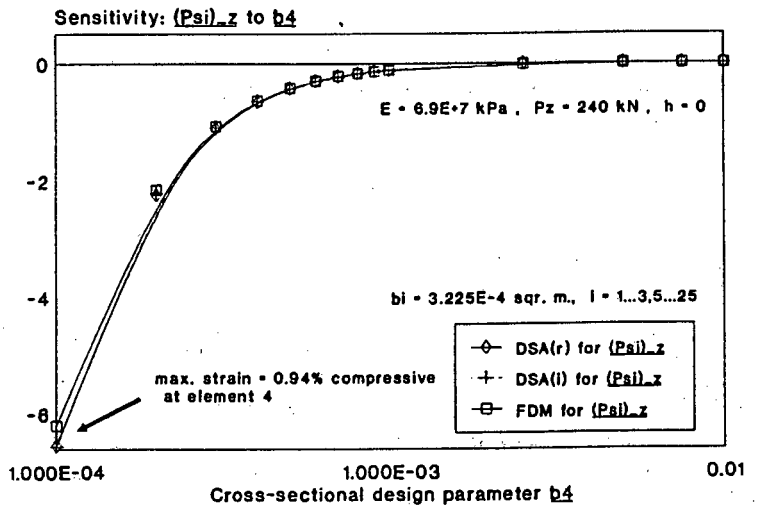

Figure 6.4.11: *Non-shape* sensitivity $\frac{d\Psi_z^{(3)}}{db_4}$ vs. cross-section b_4.

As demonstrated in Table[6.4.2], the structural configuration in Fig.[6.4.1] exhibits negligible sensitivity to variation in h, whereas for an incrementally enlarged pylon base the structure becomes progressively more sensitive to Δh, cf. Fig.[6.4.14].

From the table in Fig.[6.4.14] it is evident that a 400% increase in the pylon base area results in an 18-fold increase in the sensitivity $\frac{d\Psi_z^{(3)}}{dh}$.

h	0.00	1.23	2.46
$\frac{d\Psi_z^{(3)}}{dh}$	0.816E-3	0.377E-2	0.144E-1
$b_i = 3.225\times10^{-4}$ m^2 with $i = 1 \ldots 25$ $P_z = 240$ kN , E $= 6.9\times10^{7}$ kPa			

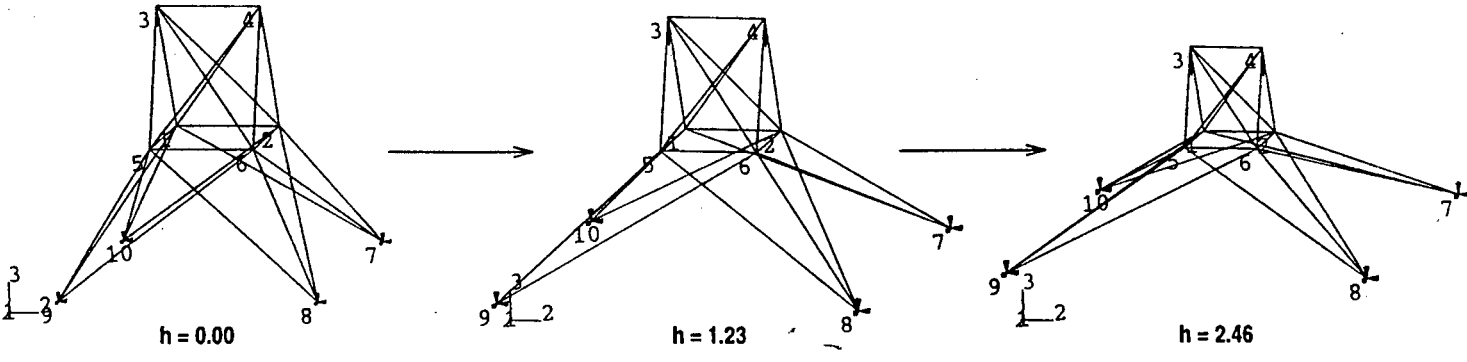

Figure 6.4.14: Structural configuration and *shape* sensitivity $\frac{d\Psi_z^{(3)}}{dh}$.

The results in Figs.[6.4.15-6.4.16] pertain to the second part of the subject matter dealt with in this section, that is the enhancement of the sensitivity formulation so as to deal with *shape* sensitivity analysis. Very close correspondence between the FDM and the *shape* DSA procedures is observed in the results. The close correspondence is at least partially attributable to the greater accuracy of the FDM for small sensitivities, whereas for larger sensitivities divergence between the FDM and the DSA implementations is in no small part due to the increasing inaccuracy of the FDM as a numerical technique.

Figs.[6.4.15-6.4.16] illustrate that for the structural configuration in Fig.[6.4.15] ($h = 0$), the pylon response is markedly insensitive to small variations in the pylon base area, implying a very stable design. Fig.[6.4.14] demonstrates decreasing stability with increasing base area.

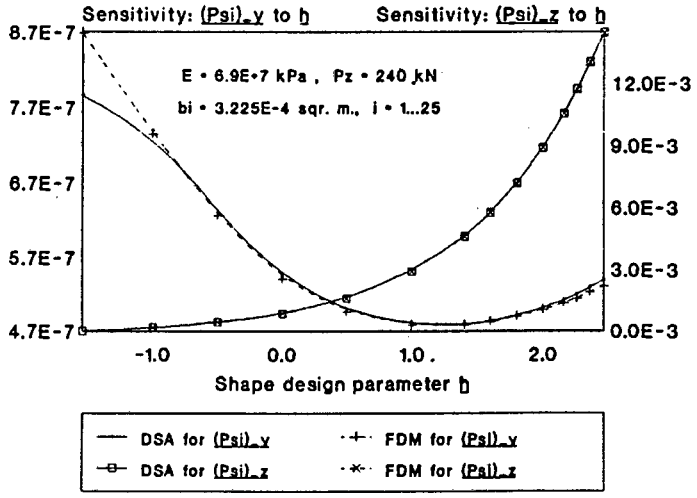

Figure 6.4.15: *Shape* sensitivities $\frac{d\Psi_y^{(3)}}{dh}$, $\frac{d\Psi_z^{(3)}}{dh}$ vs. design parameter h.

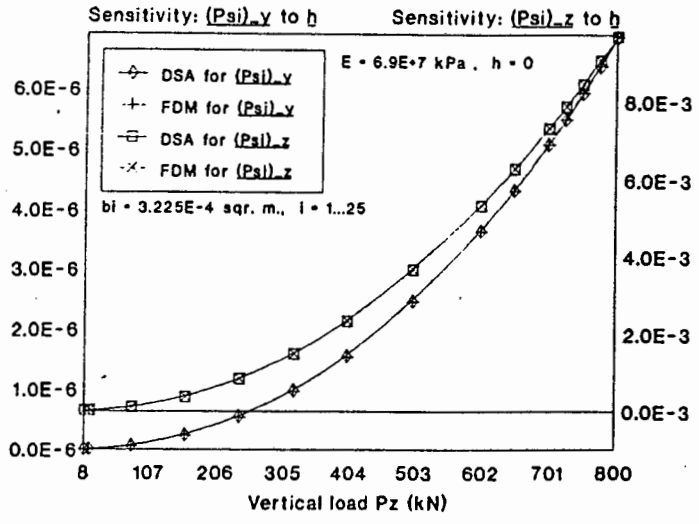

Figure 6.4.16: *Shape* sensitivities $\frac{d\Psi_y^{(3)}}{dh}$, $\frac{d\Psi_z^{(3)}}{dh}$ vs. load P_z.

Results discussion

In the results presented in this section for the structural and sensitivity analyses of the pylon truss structure, the 'rigorous' (TL based) and *shape* DSA procedures were investigated as enhancements to the procedures utilised in the preceding sections.

A comparative analysis of the enhanced procedures verified their correctness and underscored their usefulness viz. the implementations of the preceding sections. In what follows below, certain peculiarities observed in the results are analysed and discussed.

- As mentioned above, due to the tendency of the pylon to deform with minimum strain, clear divergence between the UL and TL based formulations - a result of the UL formulation's inability to accurately model *large* strain behaviour - is not clearly observable. To be more precise: large deformation is accompanied by small strain; attempting to deform the structure sufficiently in order to produce large strains more often leads to numerical instability.

- A consequence of adopting a limited range of strain values to investigate the structural and sensitivity analysis models is the disproportionate impact of numerical errors on the results: the more complex the formulation of a model (eg. TL or DSA_r), the more prone it becomes to machine errors; eg. loss of significance, truncation and rounding. Numerical errors have a negligible impact on the results when assessed over a wide range of strain values, as in the case of the 3-bar truss (cf. Figs.[6.1.3-6.1.4]). For the results presented in Figs.[6.4.4-6.4.5] and Figs.[6.4.12-6.4.13], however, the *small* strain range and numerical errors are responsible for some, usually unapparent, anomalous behaviour; eg. the apparent reduced accuracy of the TL or DSA_r formulations. Over a larger strain range, the intrinsic characteristics of the various models dominate inaccuracies due to numerical error; ie. for large strain, TL-based models outperform UL-based formulations.

6.5 Optimising the 25-bar pylon truss

Introduction

Two distinct PLBA structural optimisation procedures are applied to the 25-bar pylon structure in order to find the optimal values of, respectively, single shape and non-shape design parameters.

The pylon structure is preferred for the purposes of structural optimisation due to its relatively simple design, stable behaviour and general appeal. Pylon and off-shore structures provide ideal practical real-world benchmarks: the designs are standardised and data for these structures, subject to various types of loading conditions, is readily available from the literature.

The results presented here aim

- To verify the successful implementation of the PLBA structural optimisation, thereby concluding one of the main undertakings of this thesis, namely the inclusion of optimisation into an established commercial FEA package.
- To demonstrate the successful application of structural optimisation to shape and non-shape optimal design problems.

Data pertaining to the structural design, material parameters and loading/boundary conditions for the pylon structure are similar to that of section 6.4 (cf. Table[6.4.1]).

Results Summary

Three sets of results are provided in this section:

- The first set of results verifies the performance of the PLBA RQP optimisation routine separately. The optimal spring design problem presented in [26] is investigated. The problem involves four primary inequality constraints and three side-constraints, cf. Table[6.5.1].
- The second set of optimisation results seeks to demonstrate the applicability of ABAQUS to *non-shape* structural optimisation. A single generic cross-sectional design parameter is optimised, cf. Table[6.5.3].
- The final set of optimisation results demonstrates the applicability of ABAQUS to *shape* structural optimisation: a single *shape* design parameter h^2, proportional to the base area of the pylon structure, is optimised, cf. Table[6.5.5].

[2]Refer to Fig.[6.4.1]

Results

The results for each of the three optimisation sets enumerated above are presented in Table[6.5.2], Table[6.5.4] and Table[6.5.6], respectively.

Problem Specification		
- Initial Design	:	d ≡ wire diameter = 1 D ≡ mean coil diameter = 2 n ≡ number active coils = 3
- Design Parameters	:	d, D, n
- Cost Function (minimise)	:	$f = (n+2)\,Dd^2$
- Constraint Functions	:	$g_1 = 1 - \frac{D^3 n}{71875d^4} \leq 0$ $g_2 = \frac{(4D^2 - dD)}{(12566(Dd^3 - d^4))} + \frac{1}{(5108d^2)} - 1 \leq 0$ $g_3 = 1 - \frac{140.45d}{(D^2 n)} \leq 0$ $g_4 = \frac{(D+d)}{1.5} - 1 \leq 0$ $g_5 = 0.05 - d \leq 0$ $g_6 = 0.05 - D \leq 0$ $g_7 = 1 - n \leq 0$

Table 6.5.1: Spring optimisation: verifying the PLBA procedure.

Results					
Final Cost	Final Design				
f	d	D	n	NI	NF
0.0128	0.0538	0.409	10.7	46	254

Table 6.5.2: Spring optimisation: verifying the PLBA procedure.

Problem Specification		
- Design and Loads	:	cf. Table[6.4.1]
- Design Parameter Definition	:	cf. Fig[6.4.3]
- DSA Procedure	:	'Rigorous' Non-shape sensitivity
- Cost Function	:	$f = \sum_{i=1}^{NEL} L^{(i)} A^{(i)}$, total pylon volume
(minimise)		
- Constraint Functions	:	$g_1 = \left(\frac{u_z^{(3)}}{2.5 \times 10^{-2}} \right)^2 - 1 \leq 0$
		$g_2 = \left(\frac{u_y^{(3)}}{2.0 \times 10^{-3}} \right)^2 - 1 \leq 0$

Table 6.5.3: Optimising the pylon truss w.r.t. cross-section b_4.

Results						
	Initial Design	Initial Cost	Final Design	Final Cost	NI	NF
1	1.000×10^{-4} m^2	3.00×10^{-2} m^3	6.239×10^{-3} m^2	4.68×10^{-2} m^3	64	159
2	3.225×10^{-4} m^2	3.06×10^{-2} m^3	5.914×10^{-3} m^2	4.59×10^{-2} m^3	51	127
3	1.000×10^{-3} m^2	3.25×10^{-2} m^3	5.830×10^{-3} m^2	4.56×10^{-2} m^3	27	71

Table 6.5.4: Optimising the pylon truss w.r.t. cross-section b_4.

Problem Specification		
- Design and Loads	:	cf. Table[6.4.1], with $\boldsymbol{P}^{(4)}$= (-1.92, 0.0, -240 kN)
- Design Parameter Definition	:	cf. Fig[6.4.3]
- DSA Procedure	:	'Rigorous' Shape sensitivity
- Cost Function (minimise)	:	$f = \left(\frac{u_y^{(5)}}{1.0\times10^{-4}}\right)^2 - 1 \leq 0$
- Constraint Function	:	$g_1 = \left(\frac{u_z^{(3)}}{5.0\times10^{-3}}\right)^2 - 1 \leq 0$

Table 6.5.5: Optimising the pylon truss w.r.t. base area index h.

Results						
	Initial Design	Initial Cost	Final Design	Final Cost	NI	NF
1	-0.025	2.33×10^{-3} m^3	0.482	9.72×10^{-5} m^3	22	39
2	0.000	7.31×10^{-4} m^3	0.493	9.86×10^{-5} m^3	20	33
3	0.025	1.92×10^{-4} m^3	0.485	1.14×10^{-4} m^3	17	26

Table 6.5.6: Optimising the pylon truss w.r.t. base area index h.

Results discussion

This section largely represents the culmination, or verification, of the research effort undertaken in this thesis.

In most cases the rates of convergence were comparable to those presented in the literature for similar problems. For both *shape* and *non-shape* structural optimisation relatively stable structural configurations were selected as initial designs - the PLBA optimisation procedure was *not* subjected to extreme scenarios comparable to what was used to test the structural and sensitivity analysis models. This approach is justified as the primary focus of this research is concentrated on sensitivity analysis. Investigating the overall robustness of the optimisation model is a future undertaking.

The results presented here are not directly comparable to similar examples investigated by other authors, e.g. Haug and Arora[15]. This is largely a consequence of the fact that the results presented here are based on an analysis model which neglects the effect of body force, or self-weight, on the structure.

Various minor difficulties were encountered during the implementation of the different sets of optimisation problems:

- Occasionally, especially for *shape* optimisation, the design sensitivity coefficients (DSC) in a particular sensitivity vector became sufficiently small to force termination of the DSA procedure, thereby providing the optimisation module with spurious results.
- An initially unrobust line search routine, applied to the descent function, on occasion exhibited instability thereby adversely affecting the optimisation procedure.
- Substantial overhead code in the SIMPLEX procedure, used to solve the linearised QP problem, resulted in a noticeable decrease in computational efficiency.

An important component of future research will entail a further refinement of the optimisation procedures employed.

Chapter 7

Conclusion

7.1 Research Achievements

The numerical results presented in Chapter 6 verified the successful completion of the primary objectives of this thesis[1]. To extrapolate from Chapter 6, the achievements of this work can be summarised as follows:

I. The formulation of design sensitivity analysis (DSA), specifically the direct differentiation method (DDM), in 'pseudo'-element form, thereby theoretically enabling the incorporation of sensitivity analysis in **any** established finite element analysis (FEA) code.

II. The implementation into ABAQUS of a range of different DSA procedures, specifically:

   (1) The 'intuitive' non-shape DSA approach, *here* utilising the UL kinematic model.

   (2) The 'rigorous' non-shape DSA approach, utilising the TL kinematic model.

   (3) Shape design sensitivity analysis.

   Additionally, results were presented to demonstrate:

   - Multi-parameter DSA (cf. Section 6.3_Table[6.3.4]).
   - The feasibility of non-displacement based functional sensitivity analysis (cf. Section 6.3 Table[6.3.3], Figs.[6.3.5-6.3.6]).
   - The influence of **large** strain on the behaviour of selected DSA formulations (cf. Section 6.1).

[1] Refer to Summary.

III. The implementation of structural optimisation in conjunction with an established commercial FEA code, for instance ABAQUS, which enables the structural optimisation of problems too complex to be attempted by small scale, focussed optimisation routines.

7.2 Results Discussion

Many of the observations and comments made for the specific problems implemented and analysed in Chapter 6 may be further *generalised.* In addition, many of the issues or results highlighted in the discussion concluding each results section are worthwhile emphasising.

7.2.1 Design Sensitivity Analysis

Small Strain

The uncertainty, or error margin, of the *small* strain (2-3% max. strain ε_{xx}) shape and non-shape DSA[2] results, as compared to the FDM, is less than 5% for the largest sensitivities[3]. Considering that the accuracy of the FDM fluctuates significantly depending on the specific application, the DSA behaviour may be even better than the comparison suggests. Points of interest in the behaviour of the various formulations for small strain are:

- The results obtained indicate a particularly good comparison between the DSA and FDM results for *shape* sensitivity analysis (cf. Fig.[6.4.15]).
- As a rough rule of thumb, small sensitivities are a characteristic consequence of small strain behaviour[4]. It is important to note that small sensitivities are particularly susceptable to machine error (truncation, rounding) due to peculiarities in the ABAQUS implementation. This occasionally results in a sizeable divergence between the DSA and FDM small strain estimates (cf. Table[6.2.3]). This effect, though noticeable, is generally disregarded due to the negligible size of the sensitivities involved.
- Due to the complexity of the 'rigorous' DSA implementation, machine error dominates for very small strain, occasionally resulting in a noticeable divergence when compared to results produced using the 'intuitive' approach (cf.

[2]'intuitive' or 'rigorous', UL or TL.
[3]Refer to Tables[6.1.2], [6.2.3], [6.3.4], [6.4.2]
[4]Notable exceptions exist.

Figs[6.4.12-6.4.13]). This behaviour is overcome for large strain where the 'intuitive' approach becomes progressively more inaccurate.

Large Strain

Noticeable variation occurs in the performance of the various DSA approaches for large strain, as indicated and discussed in the numerical results section. Additional aspects of the DSA large strain behaviour that should be emphasised are:

- For the purposes of the work presented in this thesis the 'intuitive' DSA approach utilises the Updated Lagrange (UL) formulation[5] and, consequently, exhibits decreasing accuracy for large strain. The TL formulation's accurate performance for large strain is the primary motivation for it being employed, in preference to the UL, in the 'rigorous' DSA approach (cf. Table[6.2.2], Figs.[6.2.7-6.2.8]). Figs.[6.2.5-6.2.6] in Section 6.2 suggest the possible failure of the UL formulation for very large strain.
- A particular shortcoming of the Section 6.4 was the omission of numerical results representing the behaviour of the various DSA procedures for *large* strain. As mentioned previously, this is due to the tendency of the pylon structure to distribute loads efficiently and so deform with minimal strain. Overloading the structure in order to observe large strain behaviour results in numerical instability.

7.2.2 Structural Optimisation

The successful implementation of the PLBA RQP optimisation procedure into a commercial FEA package, viz. ABAQUS, fulfills a fundamental objective of this research in addition to consolidating the various DSA formulations utilised.

Structural optimisation was performed for relatively simple constraint and objective function sets. For these, and a range of additional simulations performed, the optimisation routine enabled a successful investigation of the problem of finding optimal *shape* and *non-shape* design parameters for the 25-bar pylon structure.

Results converge at rate comparable to that presented in the literature for similar constraint and objective function scenarios. Specific assumptions made in this work, eg. neglecting body force in the equilibrium formulation, preclude direct comparison

[5] In this research the 'intuitive' method has consistently been associated with the UL variational formulation and the 'rigorous' approach with the TL. The 'intuitive' formulation can, however, also be used in conjunction with the TL; likewise the UL variational approach could be used in conjunction with the 'rigorous' approach.

with similar examples in the literature. Further research will involve the implementation of additional optimisation models, eg. the truss region method [32], enabling the evaluation of the efficiency of the optimisation procedure employed here.

7.3 Future Research

Wide scope exists for extending the research undertaken in this thesis - the range of topical issues in DSA and structural optimisation are extensive. The main objectives of most research conducted in the field of design sensitivity analysis, particularly when applied to structural optimisation, are increased accuracy and computational speed. Future research effort will be focussed primarily on extending the current research in the following areas:

- The kinematic model may be improved by choosing a more efficient element formulation based on the enhanced assumed strain variational description. This would offer a cost efficient opportunity to implement structural optimisation involving higher order elements. One such possible application allows for material parameter optimisation for sheet metalforming: the interface between ABAQUS, DSA and structural optimisation developed in this thesis enables the utilisation ABAQUS' sophisticated solving, contact and friction procedures for the purposes of structural optimisation.
- A secondary goal involves implementing design sensitivity analysis, and eventually structural optimisation, for a nonlinear material model. Work in this area is fraught with difficulty - even the simplest kinematic hardening procedures are seemingly intractable.

For the sake of comparison various other non-DDM based sensitivity approaches and optimisation procedures could be investigated. For the purposes of this research such a wide approach was considered to be beyond the scope of the objectives set for this thesis.

Bibliography

[1] J.S. Arora, J.E.B. Cardosa - **A Design Sensitivity Analysis Principle and its Implementation into ADINA**, Comp. Structs., 32(3/4):691-705, (1989).

[2] J.S. Arora, J.B. Cardoso - **Variational Principle for Shape Design Sensitivity Analysis**, AIAA J., 30(2):538-547, (1992).

[3] K.-J. Bathe - **Finite Element Procedures in Engineering Analysis**, *Prentice Hall Inc.*, Englewood Cliffs, New Jersey, (1982).

[4] A.D. Belegundu, J.S. Arora - **A Study of Mathematical Programming Methods for Structural Optimisation. Part 1: Theory**, Int. J. Num. Meths. Eng., 21:1583-1599, (1985).

[5] A.D. Belegundu, J.S. Arora - **A Study of Mathematical Programming Methods for Structural Optimisation. Part II: Numerical Results**, Int. J. Num. Meths. Eng., 21:1601-1623, (1985).

[6] M.P. Bendsøe, J. Sokolowski - **Sensitivity Analysis and Optimisation of Elastic-Plastic Structures**, Eng. Optim., 11:31-38, (1987).

[7] M.P. Bendsøe, N. Kikuchi - **Topology and Layout Optimisation of Discrete and Continuum Structures**, Structural Optimisation: Status and Promises, AAIA Series in Progress in Astronautics and Aeronautics, *AIAA*, Washington, DC, (1992).

[8] J.B. Cardoso, J.S Arora - **Variational Method for Design Sensitivity Analysis in Nonlinear Structural Mechanics**, AIAA J., 26(5):595-603, (1988).

[9] J.E. Coster, N. Stander - **Formulation and Performance Assessment of an Optimal Design Tool for Guyed Towers**, Conference Proceedings: FEMSA95 - Finite Elements in South Africa, 1:90-105, (1995).

[10] K. Dems, Z. Mróz - **Variational approach by means of Adjoint Systems to Structural Optimization and Sensitivity Analysis - part I: Variation of Material parameters within a Fixed Domain**, Int. J. Solids. Structs., 19(8):677-692, (1983).

[11] K. Dems, Z. Mróz - **Variational approach to First- and Second-order Sensitivity Analysis**, Int. J. Num. Meth. Eng., 21(4):637-646, (1985).

[12] R.T. Haftka, Z. Mróz - **First- and Second-order Sensitivity Analysis of Linear and Nonlinear Structures**, AIAA J., 24:1187-1192, (1986).

[13] R.T. Haftka - **Second Order Sensitivity derivatives in Structural Analysis**, AIAA J., 20:1765-1766, (1982).

[14] M. Haririan, J.B. Cardosa, J.S. Arora - **Use of ADINA for Design Optimisation of Nonlinear Structures** , Comp. Structs., 26(1/2):123-133, (1987).

[15] E.J. Haug, J.S. Arora - **Applied Optimal Design: Mechanical and Structural Systems**,*John Wiley & Sons*, (1979).

[16] R.B. Haber - **A new Variational Approach to Structural Shape Design Sensitivity Analysis**, in: C.A. Mota Soares, ed., Computer Aided Optimal Design, Series F: Computer and Systems Sciences, *Springer*, New York, 27:573-587, (1987)

[17] T.D. Hien - **Deterministic and Stochastic Sensitivity in Computational Structural Mechanics**, Habilitation Thesis, Institute of Fundamental Technological Research, Polish Academy of Sciences, Warsaw, (1990).

[18] T.D. Hien, M. Kleiber - **Stochastic Structural Design Sensitivity of Static Response**, Comp. Structs., 38:659-667, (1991).

[19] T.D. Hien, M. Kleiber - **Stochastic Design Sensitivity in Structural Dynamics**, Int. J. Num. Meths. Eng., 32:1247-1265, (1991).

[20] S.Y. Jao, J.S. Arora - **Design Optimisation of Non-linear Structures with Rate-dependent and Rate-independent Constitutive Models**, Int. J. Num. Meths. Eng., 36:2805-2823, (1993).

[21] I. Kaneko, G. Maier - **Optimal Design of Plastic Structures under Displacement Constraints**, Comp. Meths. Appl. Mech. Eng., 27:369-391, (1981).

[22] M. Kleiber, T.D. Hien, E. Postek - **Incremental Finite Element Sensitivity Analysis for Nonlinear Mechanics applications**, Int. J. Num. Meths. Eng., 37:3291-3308, (1994).

[23] M. Kleiber - **Shape and Non-Shape Structural Sensitivity Analysis for problems with any Material and Kinematic Nonlinearity**, Comp. Meths. Appl. Mech. Eng., 108:73-97, (1993).

[24] M. Kulkarni, A.K. Noor - **Sensitivity Analysis of the Non-linear Dynamic Viscoplastic Response of 2-D Structures with respect to Material Parameters**, Int. J. Num. Meths. Eng., 38:183-198, (1995).

[25] L.-J. Leu, S. Mukherjee - **Implicit Objective Integration for Sensitivity Analysis in Non-linear Solid Mechanics**, Int. J. Num. Meths. Eng., 37:3843-3868, (1994).

[26] O.K. Lim, J.S. Arora - **An Active Set RQP Algorithm for Engineering Design Optimisation**, Comp. Meths. Appl. Mech. Eng., 57:51-65, (1986).

[27] Z. Mróz - **Variational methods in Sensitivity and Optimal Design**, Eur. J. Mech. A/Solids., 13(4-suppl):115-147, (1994).

[28] M. Ohsaki, J.S. Arora - **Design Sensitivity Analysis of Elastoplastic Structures**, Int. J. Num. Meths. Eng., 37:737-762, (1994).

[29] H. Rodrigues, P. Fernandes - **A Material based Model for Topology Optimisation of Thermoelastic Structures**, Int. J. Num. Meths. Eng., 38:1951-1965, (1995).

[30] D. Ray, K. Pister, E. Polak - **Sensitivity Analysis for hysteretic dynamic systems: theory and application**, Comp. Meths. Appl. Mech. Eng., 14:179-208, (1978).

[31] Y.S. Ryu, M. Haririan, C.C. Wu, J.S. Arora - **Structural Design Sensitivity Analysis of nonlinear response**, Comp. Structs., 21:245-255, (1985).

[32] M. Sunar, A.D. Belegundu - **Trust Region methods for Structural Optimization using Exact Second Order Sensitivity**, Int. J. Num. Meths. Eng., 32:275-293, (1991).

[33] A.J.M. Spencer - **Continuum Mechanics**, *Longman Inc.*, New York, (1980).

[34] P.J. Thanedar, J.S. Arora, C.H. Tseng, O.K. Lim, G.J. Park - **Performance of some SQP Algorithms on Structural Design problems**, Int. J. Num. Meths. Eng., 23:2187-2203, (1986).

[35] J.J. Tsay, J.S. Arora - **Nonlinear Structural Design Sensitivity Analysis for Path-Dependent problems. Part 1: General Theory**, Comp. Meths. Appl. Mech. Eng., 81:183-208, (1990).

[36] C.A. Vidal, R.B. Haber - **Design Sensitivity Analysis for Rate-Independent Elastoplasticity**, Comp. Meths. Appl. Mech. Eng., 107:393-431, (1993).

[37] C.A. Vidal, H.-S. Lee, R.B. Haber - **The Consistent Tangent Operator for Design Sensitivity Analysis of History-Dependent Response**, Comp. Systems. Eng., 2(5/6):509-523, (1991).

[38] L. Wang, R.V. Grandhi - **Structural Reliability Optimisation using an Efficient Safety Index calculation procedure**, Int. J. Num. Meths. Eng., 38:1721-1738, (1995).

[39] K. Washizu - **Variational Methods in Elasticity and Plasticity**, 2nd Ed., *Pergamon Press*, Oxford, (1974).

[40] R.J. Yang, M.E. Botkin - **Comparison between the Variational and Implicit Differentiation approaches to Shape Design Sensitivities**, AIAA J., 24(6):1027-1032, (1986).